

Analysis and Characterization of Electrochemically Decomposed Lignin

Dissertation

zur Erlangung des Grades

des Doktors der Naturwissenschaften

der Naturwissenschaftlich-Technischen Fakultät

der Universität des Saarlandes

von

Tobias Karl-Fridolin Dier

Saarbrücken

2017

Tag des Kolloquiums: 28.07.2017

Dekan: Prof. Dr. G. Kickelbick

Berichterstatter Prof. Dr. D.A. Volmer

..... Prof. Dr. R. Hempelmann

.....

Vorsitz: Prof. Dr. J. Jauch

Akad. Mitarbeiter: Dr. M. Litzenburger

Acknowledgements

At this point I would like to thank and express my deep gratitude to Prof. Dr. Dietrich A. Volmer for providing his scientific skills, the opportunity to work in his laboratories and to perform my research on state-of-the-art instruments, the supervision of the work, his permanent readiness for discussing the results and giving helpful advices to achieve an objective, and especially for his assistance in publishing the results of my research.

A special thanks goes to the working group of Prof. Dr. Dietrich A. Volmer, Saarland University, in particular to Reiner Wintringer, Miriam Müller, Dr. Klaus Hollemeyer and Ignacy Rzagalinski for their input and the discussion on various research-related topics as well as the discussions on everyday topics and therefore making the time as a member of this working group unforgettable in a very positive way.

Furthermore, I would like to thank Prof. Rolf Hempelmann, Dr. Harald Natter, Dan Durneata, Daniel Rauber and Verlainé Fossog from the Institute of Physical Chemistry, Saarland University for their helpful advices, for performing the electrochemical degradation processes and therefore for providing the degraded lignin samples, and the provision of their knowledge in electrochemistry and ionic liquid synthesis.

I appreciate the collaboration with the working group of Prof. Dr. Johann Jauch from the Saarland University, and I want to thank especially himself as well as Eva Feidt and Stefanie Schmidt for their devoted commitment in the synthesis of dimeric lignin standards and the supervision of Thorsten Dreher, Anna Heib, Christopher Scherrer and Ammar Tatlisu, who also participated in the synthesis project and supported the progress of the work and whom I want to thank, too.

I also want to thank Prof. Dr. Holger Militz and Marco Fleckenstein from the Georg-August University, Göttingen, department Wood Biology and Wood Products for a successful and uncomplicated collaboration in the field of wood modification to enhance my knowledge about lignin further and to enable another point of view on the lignin utilization, as well as their warm welcome and exceptional support in their department during my scientific excursion in Göttingen.

Another thanks go to Blandine Boßmann for her support in performing GPC experiments at the working group of Prof. Dr. Gerhard Wenz and assisting in the interpretation of the GPC results.

I also want to express thanks to Dr. Thomas Jahns from Schneider-Planta Chemicals GmbH, Eppelborn, Germany for providing real lignin samples and therefore enabling the possibilities to apply the developed methods on industrial samples.

Acknowledgements

At this point, I also want to mention Günther Berlin and acknowledge him for the preparation of custom-made glassware that were used in the synthesis of the custom-made stationary phases and were necessary for a rapid success in the preparation of a preparative custom-made column.

My warm thanks go to my former colleagues Giuseppe Coviello and Dr. Yuliya Silina, who supported me during that time in a scientific way and contributed to a very good working atmosphere, which I will always appreciate.

Coming to the end, I want to express my warmest thanks to my family and friends, who accompanied me from the beginning of my studies all the way through to this final university degree. All this would have never been possible without your love and support. At this point, I want to explicitly mention my parents and I thank them from the bottom of my heart for their permanent support and their continuous availability in bad times as well as good. Finally, my deepest gratitude goes to Samantha Gauer, my star and everlasting love, for being my anchor; my constant that I could always trust on in my worst and my best times.

Table of Contents

Acknowledgements	iii
Table of Contents	v
I. Zusammenfassung	1
II. Abstract	2
III. Abbreviations	3
IV. Introduction	4
4.1 Complex mixtures and the significance for comprehensive analytical methods.....	4
4.2 Characterization of lignin and degraded lignin.....	5
4.2.1 Fourier-transform infrared spectroscopy.....	5
4.2.2 Nuclear magnetic resonance spectroscopy.....	6
4.2.3 Chromatographic separation.....	8
4.2.4 Mass spectrometry.....	8
4.3 Aim of the thesis.....	12
V. List of Publications	13
Publication 1	14
Publication 2	34
Publication 3	57
VI. Summary and Conclusions	74
VII. References	79
VIII. Curriculum Vitae	87
IX. Scientific Contributions	89

I. Zusammenfassung

Das Ziel dieser Arbeit war die Entwicklung eines analytischen Verfahrens zur Charakterisierung elektrochemisch gespaltenen Lignins. Dabei sollten einerseits die Reaktionsmechanismen der elektrochemischen Prozesse in ionischen Flüssigkeiten aufgeklärt und andererseits wertvolle Substanzklassen für verschiedene Anwendungen (z.B. Energiespeicher oder nachhaltige Grundchemikalien) identifiziert und isoliert werden.

Die Entwicklung einer neuen Datenverarbeitungs- und -visualisierungsmethode, basierend auf hochauflösender Massenspektrometrie, vereinfachte die Interpretation der detektierten m/z Signale erheblich und erlaubte die Formulierung möglicher Reaktionsmechanismen. Das sogenannte „Enhanced Mass Defect Filtering“ ordnete hierbei in x,y-Diagrammen die detektierten m/z Signale nach Art des aromatischen Grundgerüsts der Ligninbausteine (Cumaryl-, Coniferyl- und Sinapylalkohol) entlang der x-Achse und nach Anzahl der CH_2 -Analoge entlang der y-Achse an. So konnten strukturell verwandte Verbindungen schnell identifiziert und klassifiziert werden. Weiterhin ermöglichten geringfügige Modifikationen des „Enhanced Mass Defect Filtering“ die Anwendung dieser Visualisierungsmethode in verwandten Ligninanwendungsbereichen, beispielsweise der Phenol-Formaldehyd Harzsynthese unter Verwendung nachhaltiger, monomerer Lignin-Modellverbindungen.

Die chromatographische Trennung der Ligninabbauprodukte unter Verwendung eigens präparierter, neuartiger stationärer Phasen (immobilisierte Trioctylpropylphosphonium Salze) und High-Performance Liquid Chromatography (HPLC) erweiterte die Charakterisierung der elektrochemischen Prozesse um eine weitere Dimension. Durch die hohe Vielfalt an Wechseleffektmechanismen konnten die Ligninabbauprodukte anhand ihrer chemischen Funktionalität in der Seitenkette aufgetrennt werden.

Die Kombination des Massendefektfilters und der chromatographischen Trennung erlaubten die Evaluierung des elektrochemischen Prozesses. Neben bereits bekannten Oxidationsprozessen, konnten Reduktionsprozesse über detektierbare Reduktionsprodukte formuliert werden.

II. Abstract

The aim of the thesis was the development of an analytical method for the characterization of electrochemically degraded lignin. A further goal was the elucidation of reaction mechanisms for the electrochemical process in ionic liquids and the identification of high value degradation products for application in areas such as energy storage or sustainable base-chemicals.

The development of a high resolution mass spectrometry-based simplification strategy for data visualization enabled rapid classification of measured m/z features and the elucidation of possible reaction mechanisms. The so called “enhanced mass defect filtering” aligned m/z features based on lignin-related aromatic core units (*p*-coumaryl, coniferyl and sinapyl alcohol) along the x-axis and on the number of repeating CH₂-units along the y-axis. As a result, identification and classification of structural related degradation products was readily possible. Minor modifications of the mass defect filter extended its potential for application to other lignin-related applications, in particular in evaluation of phenol formaldehyde resol resin synthesis using monomeric lignin model compounds.

The chromatographic separation of lignin degradation products using custom-made stationary phases (tricoctylpropylphosphonium salts immobilized on porous silica particles) and high-performance liquid chromatography (HPLC) added an additional dimension to the characterization of the electrochemical process. The high diversity of interaction mechanisms allowed rough separation of the degradation products according to the chemical functionality of the side chains.

The combination of the mass defect filtering and chromatographic separation enabled evaluation of the electrochemical process. In addition to well-known oxidation processes, mechanisms for reduction processes were proposed based on the detected reduction products.

III. Abbreviations

¹³ C CP/MAS	¹³ C cross polarization- magic angle spinning		spectrometry
ABTS	2,2'-azinobis-(3- ethylbenzthiazoline-6- sulfonate)	HSQC	heteronuclear single quantum coherence
APCI	atmospheric pressure chemical ionization	IUPAC	International Union of Pure and Applied Chemistry
APPI	atmospheric pressure photoionization	KM	Kendrick mass
CID	collision induced dissociation	KMD	Kendrick mass defect
DI	direct infusion	<i>m/z</i>	mass to charge ratio
e.g.	exempli gratia	MALDI	matrix-assisted laser desorption/ionization
ESI	electrospray ionization	MS	mass spectrometry
FTICR	Fourier-transform ion cyclotron resonance	M _w	weight average molecular mass
FTIR	Fourier-transform infrared	NMR	nuclear magnetic resonance
GC	gas chromatography	O/C	oxygen to carbon ratio
GPC	gel permeation chromatography	PF	phenol-formaldehyde
H/C	hydrogen to carbon ratio	Py-GC/MS	pyrolysis gas chromatography/mass spectrometry
HPLC	high-performance liquid chromatography	RP	reversed phase
HRMS	high resolution mass	SET	single electron transfer
		u	atomic mass units

IV. Introduction

4.1 Complex mixtures and the significance for comprehensive analytical methods

The reserves of valuable fossil resources continuously shrink due to population growth and technical progress. Therefore, the chemical industry has endeavored to develop sustainable processes for reducing the dependency on fossil fuels. Lignin as one of the most abundant renewable biopolymers therefore evolved into a very attractive material for the chemical industry. The molecular components of lignin's polyaromatic structure^{1,2} are very similar to those of fossil fuels. As a result, lignin can be treated as a sustainable precursor for fossil fuels. The development of suitable lignin degradation processes for getting access to valuable chemicals was therefore a main objective of recent studies.³⁻¹⁸ However, the analysis of complex mixtures is a non-trivial scientific problem, since the high variety of occurring analytes requires enhanced analytical strategies to provide meaningful information. The analysis of lignin, or rather degraded lignin is an example for such a complex scientific problem. The difficulty of the sample interpretation already starts in the different composition of the starting material. Lignin's complex biosynthesis^{2,19-22} results in a high variety of incomparable lignin polymers. Furthermore, the embedding of the polymer into the plant cell structure²³ complicates the extraction of lignin. Therefore, lignin fragments received by common extraction techniques significantly differ in molecular size and composition.²⁴⁻³¹ Subsequent lignin degradation processes consequentially results in highly complex samples. The development of comprehensive analytical methods for e.g. understanding reaction mechanisms or elucidating chemical structures of analytes is therefore a primary step for accomplishing the desired objectives. Several analytical techniques have been applied to the analysis and characterization of lignin or its degraded version.³² The information received from each respective analytical method comprised individual partial aspects of the analyzed sample. However, specific disadvantages for each respective method necessitated the usage of multiple analytical methods for a comprehensive analysis of the degraded lignin sample. Therefore, the necessity for developing comprehensive analytical methods providing as much information as possible is evidenced by the partial degraded lignin analysis from the sole usage of previously mentioned analytical techniques and the time-consuming aspect resulting from the usage of multiple ones. Nevertheless, the gathered information from the results of these basic analytical methods evolved as an important starting point and supported the elaboration of desired developments. In the following, recent results of the most frequently used analytical techniques, namely Fourier-transform infrared (FTIR) spectroscopy, nuclear magnetic resonance (NMR) spectroscopy, mass spectrometry (MS) and chromatographic separation were considered and summarized.

4.2 Characterization of lignin and degraded lignin

Depending on the specific analytical problem, especially in the case of lignin analysis, the used analytical technique provided significant information about structure,³³ sample composition³⁴ or chemical alteration of the sample after treatment^{35,36}. However, not every available analytical technique is suitable for every appearing problem in the field of lignin analysis.

4.2.1 Fourier-transform infrared spectroscopy

The molecular components of (degraded) lignin were, of course, able to change their quantized vibrational energy states when they were exposed to infrared radiation. The resulting fundamental molecular vibration mechanism³⁷ exhibited specific transitions for each respective chemical bond in the non-linear molecules. These transitions can be readily recorded by a FTIR spectrometer and allowed therefore clear assignments of chemical functionalities to specific frequencies. Table 1 summarizes the most abundant FTIR absorbance bands for lignin-related bond vibrations.

Table 1. Abbreviated summary for FTIR absorbance bands of lignin-related bonds adapted from the literature.^{38,39} Note: FTIR bands of non-detected functional groups in the respective lignin were defined as n.d.

wavenumber [cm ⁻¹] (hardwood ; softwood)	functional group
1033 ; 1031	C-H in-plane deformation (aromatic; G > S)
n.d. ; 1081	C-O deformation (secondary alcohols and aliphatic ethers)
1116 ; n.d.	C-H deformation (aromatic; S-ring)
1151 ; 1150	C-H in-plane deformation (aromatic; G-ring)
1215 ; 1214	C-C and C-O stretching
1269 ; 1269	C-O deformation (G-ring)
1327 ; n.d.	C-O deformation (S-ring)
1425 ; 1427	C-H in-plane deformation and aromatic ring stretching
1462 ; 1463	C-H deformation (methylene and methyl)
1514 ; 1513	aromatic ring vibration
1603 ; 1594	aromatic ring vibration and C=O stretching
1682 ; 1704	C=O stretching (unconjugated)
2840 ; 2840	C-H stretching
2937 ; 2934	C-H stretching
3421 ; 3349	O-H stretching

Therefore, FTIR spectroscopy was often used for simple structure analysis of the used lignin polymers^{9,40,41}, monitoring successful chemical modifications or degradations^{34,42–49}, or evaluating a specific extraction process⁵⁰. The non-destructive measurement of the sample was at this point a major advantage of FTIR spectroscopy compared to other analytical techniques. However, the structural information received by FTIR spectroscopy only exhibited the presence of certain chemical functionalities and didn't give a detailed hint for chemical environments of the respective functional groups, so that additional analytical techniques were used to compensate this drawback. A more detailed analysis can therefore be readily achieved by e.g. NMR spectroscopy^{34,41,45,50} or MS^{9,34,43–48}. Nevertheless, FTIR spectroscopy can be seen as

IV. Introduction

a basic analytical technique for roughly elucidating structure elements of the considered, randomly ordered lignin sample. Therefore, the development of a comprehensive analytical method including rough structural analysis can replace the use of FTIR spectroscopy and reduce the instrumental effort.

4.2.2 Nuclear magnetic resonance spectroscopy

NMR spectroscopy was mainly used for detailed structure elucidation of degraded lignin components or the intact lignin polymer. The basic requirement for a successful NMR analysis is a detectable nuclear magnetic resonance of the sample, located in a strong permanent magnetic field induced by electromagnetic radiation.⁵¹⁻⁵⁴ The most common NMR applications were performed on the ^1H -, ^{13}C - and ^{31}P -nuclei.^{31,41} The magnetic resonance of the respective nuclei exhibited clear deviations for each respective interunit bonding pattern in the considered sample, similar to the specific transitions in FTIR spectroscopy. However, the improved spectral resolution of NMR spectroscopy allowed more detailed structural assignments and therefore exhibited a more detailed view on the chemical structure of lignin or its structural changes after degradation. The primary objective for ^{31}P -NMR spectroscopy was the quantitative analysis of present hydroxyl functions in the lignin polymer or its degraded version.^{4,45,55,56} Here, clear assignments of phenolic/aliphatic alcohols, carboxylic acids or even condensed phenolic units were possible. As a result, chemical bond cleavages on the respective hydroxyl functions were able to be quantitatively determined and provided information about present degradation mechanisms.^{4,45} However, ^{31}P -NMR spectroscopy requires a prior derivatization of the sample with 2-chloro-1,3,2-dioxaphospholane⁵⁶ or 2-chloro-4,4,5,5-tetramethyl-1,3,2-dioxaphospholane^{4,45,55} (Figure 4.1).

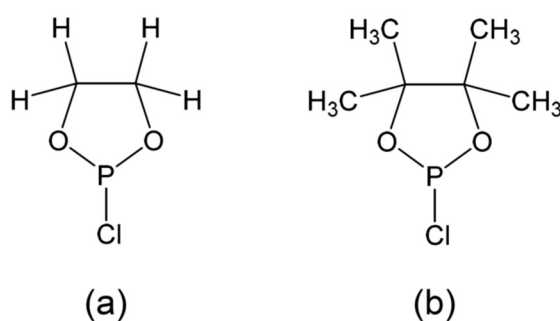


Figure 4.1. Chemical structures of (a) 2-chloro-1,3,2-dioxaphospholane and (b) 2-chloro-4,4,5,5-tetramethyl-1,3,2-dioxaphospholane.

This additional derivatization step extended the duration of the analysis and of course introduced an additional compound to the analytical method. ^1H - and ^{13}C -NMR experiments of (degraded) lignin are readily possible without a derivatization step. Successful lignin depolymerization was determined by simple ^1H -NMR spectroscopy, where signal intensity increases and decreases⁴⁴ as well as signal sharpening of distinct lignin polymer signals⁵⁷ were defined as degradation indicators. Detailed

structural information was achieved by ^{13}C -NMR spectroscopy.⁴⁴ A special application is the solid state ^{13}C cross polarization-magic angle spinning (^{13}C CP/MAS) NMR spectroscopy.^{34,47,58} Here, the ground lignin sample was packed in a zirconia rotor and spun at high rotational speed. The axis of rotation is tilted by the magic angle (θ_m) with respect to the direction of the magnetic field (B_0) (Figure 4.2).

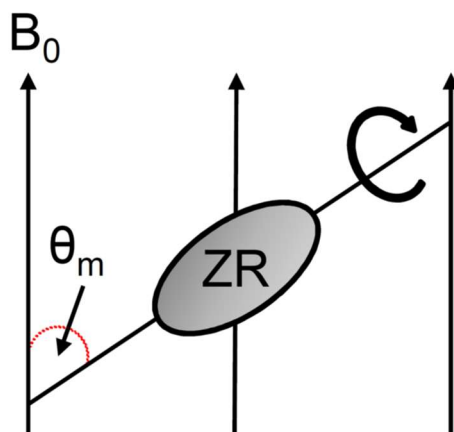


Figure 4.2. Schematic representation of the zirconia rotor (ZR) in the magnetic field B_0 tilted by the angle θ_m for ^{13}C CP/MAS NMR spectroscopy.

The excitation of ^1H nuclei indicated by a pulse sequence followed by a cross polarization of the neighboring ^{13}C -atom resulted in the detection of the characteristic ^{13}C spectra. These spectra exhibited the presence of residual carbohydrates in corn stover or rice straw lignin³⁴, or structural changes of the lignin polymer after treatment⁵⁸. Another NMR application providing a quantitative and structurally detailed analysis was realized by heteronuclear single quantum coherence (HSQC) NMR spectroscopy of ^1H and ^{13}C . This two dimensional application was therefore commonly used for lignin analysis.^{45,55,59–63} The two dimensional NMR spectra exhibited a more detailed view on the structural components and provided therefore deeper insights into degradation mechanisms⁶¹ and lignin's structural design^{59,60,63}. Most of these interunit linkages were summarized in a NMR database.⁶⁴ Therefore, the interpretation of resulting HSQC NMR spectra were simplified. In addition, unexpected interunit linkages resulting from e.g. degradation processes can be identified. However, high spectral resolution for detailed HSQC NMR analysis requires an extensive duration of the analysis. The development of a high-resolution analytical method could therefore be an advantage over high-resolution NMR spectroscopy.

4.2.3 Chromatographic separation

In the field of lignin analysis, chromatographic separation techniques were most frequently coupled to mass spectrometers.^{4,9,12,18,42–48,57,61,65–83} Recent studies on applications using liquid chromatography (LC) or gas chromatography (GC) - mass spectrometry (MS) hyphenation were therefore described in more detail in chapter 4.2.4 Mass spectrometry. Nevertheless, the sole use of chromatographic separation provided important information of the (degraded) lignin sample. The most common chromatographic separation technique is the gel permeation chromatography (GPC). Here, the components of the analyzed sample are separated according to their average molecular weight or hydrodynamic volume.⁸⁴ In contrary to common chromatographic separation, analytes do not chemically or physically interact with the porous stationary phase material. Depending on their hydrodynamic volume, analytes diffuse more or less easily into the pores of the stationary phase. Larger analytes therefore elute quickly while smaller analytes, spending more time in the pores of the stationary phase, elute at longer retention times. GPC was therefore used to determine lignin's average molecular weight^{45,65} or to verify lignin degradation processes^{57,65,67,85}. The sole usage of classic chromatographic separation, where analytes are physically or chemically interacting with the stationary phase, was primary used for the determination of specific analytes. GC was mainly used for qualitative and quantitative analysis of volatile lignin degradation products,^{3,17,86} while LC was primary used for more polar and non-volatile degradation products.^{8,12,87} However, the qualitative analysis of specific degradation products using sole chromatographic separation always require the verification of respective analytes with commercially available standards. This significant disadvantage is related to the lack of structural information given by the used detection technique (UV^{8,12,87}, FID^{3,17,86}). The use of a detection technique providing structural information such as MS can therefore be more beneficial for the analysis of complex lignin degradation samples.

4.2.4 Mass spectrometry

Mass spectrometry (MS) was commonly used in the field of lignin analysis. The basic requirement for a successful analysis is the generation of detectable ions.^{88–90} The most common application for ion generation is the electron ionization.^{4,9,18,43–48,57,61,65–71,73,76,78–80,83} The analytes are exposed under vacuum to an electron beam, which is generated by a heated filament. A close crossing of high-energy electrons and the uncharged analyte induces large fluctuations in the local electric field resulting in a removal of an electron from the uncharged molecule.⁹¹ Furthermore, the formed radical cation can undergo further fragmentation or rearrangement reactions resulting in characteristic mass spectra for certain substance classes.⁹² However, the presence of multiple components in the sample requires an additional chromatographic separation step; often realized by gas chromatography, to deconvolute the complex sample. The vaporized analytes are chromatographically separated *via* partitioning between the liquid stationary phase and the gaseous mobile phase prior to MS detection. The

analysis of the volatile, low-molecular weight fraction of (degraded) lignin is therefore readily feasible. Determined concentrations as well as the variety of phenolic monomers were, *inter alia*, used to characterize the efficiency of a degradation process^{4,9,12,18,57,71,76} or the determination of a necessary intermediate¹². However, the characterization of degraded lignin usually requires a purification step of the raw mixture solution prior to GC/MS analysis, since suspended particles or low-volatile degradation products can impede the analysis or even damage the instrument. Pyrolysis-GC/MS (Py-GC/MS) is a special application for (degraded) lignin characterization. Here, the sample is placed in a quartz tube and heated to temperatures in the range between 600 and 1000 °C in a short time (several milliseconds to seconds). The emerging volatile molecules are directly transferred to a GC/MS instrument and detected *via* MS, so that a purification of the raw material is not necessary. In the case of lignin analysis, the resulting mass spectra provided significant information on the structure elements of the lignin raw material^{70,71} or the influence of a degradation process on the lignin structure modification^{47,48,79}. However, the tremendous complexity of degraded lignin^{47,70,71} allowed the presumption that a single chromatographic separation step is insufficient to detect all volatile components in the respective sample. The introduction of a second orthogonal chromatographic separation step revealed the presence of multiple volatile analytes, that were not distinguishable by single chromatographic separation.^{12,45,78,79} Two-dimensional chromatographic separation extended the amount of gained information and therefore significantly enhanced the characterization of the respective lignin sample. However, GC/MS applications are restricted to volatile and thermal stable compounds, so that the characterization of the sample is limited. Ionization techniques such as electrospray ionization (ESI) or atmospheric pressure chemical ionization (APCI), where ions are generated by simple acid-base-reactions in solution⁹³ or in the gas phase respectively⁹⁴, enhance the detection of common GC/MS applications by e.g. low-volatile compounds. In addition, the resulting soft ionization of the analytes prevents subsequent fragmentation or rearrangement reactions, which is common for electron ionization. Protonated $[M+H]^+$ or deprotonated $[M-H]^-$ molecular species are therefore primary detected, depending on the mode of ionization used (positive ionization mode $\equiv [M+H]^+$; negative ionization mode $\equiv [M-H]^-$). As a result, the amount of detectable lignin degradation products significantly increased, since the phenolic character of the degradation products is predestined for performing these simple acid-base-reactions.³³ A special application, the so-called matrix-assisted laser desorption/ionization (MALDI), utilizes the addition of a matrix. The analytes are embedded in the crystallized matrix. Laser irradiation of this analyte-matrix-crystallites transfers analyte- and matrix molecules into the gas phase, where the ionization takes place.^{95,96} The MALDI technique was commonly used in clinical microbiology^{97,98}, proteomics^{97,99} or glycomics¹⁰⁰. Furthermore, MALDI experiments also provided significant information about (degraded) lignin samples.^{44,68,101} The simplest instrumental setup for performing ESI, APCI or atmospheric pressure photoionization (APPI) experiments utilizes a syringe with a constant flow rate. The sample solution is

IV. Introduction

directly infused into the source chamber, where the ionization takes place. This instrumental setup, also known as direct infusion (DI), provides significant structural and compositional information of the analyzed sample. Consequent analytical strategies enabled a more comprehensive view on interpretation of lignin mass spectra.^{65,75,81,82,95} Polymer sequencing analysis was primarily used in the field of peptide/protein^{103,104} or oligosaccharide analysis^{105,106}. Moreel *et al.* applied a modified sequencing strategy on lignin oligomers.⁸¹ The resulting fragmentation patterns of measured m/z features using collision induced dissociation (CID) allowed clear assignments of specific interunit linkages between lignin monomers and therefore precise characterization of the most common lignin oligomers. This strategy therefore enabled a rapid MS-based characterization of lignin oligomers in plants and could be transferred to degradation processes. However, the degraded lignin sample resulting from degradation processes most probably contains degradation products with uncommon interunit linkages, so that a comprehensive analytical strategy including the characterization of these uncommon products is necessary. Another lignin analysis strategy is based on the utilization of the mass defect, which is characteristic for each respective elemental composition. However, the determination of elemental compositions by MS requires an (ultra-)high mass resolution. The two most common state-of-the-art applications providing such ultra-high mass resolution are the Fourier-transform ion cyclotron resonance (FTICR) mass spectrometer^{107,108} and the Orbitrap mass spectrometer¹⁰⁹. Both applications are able to easily achieve resolving powers higher than 100,000. As a result, analyses using FTICR and Orbitrap mass spectrometers provided comprehensive compositional information of complex samples such as crude oil^{108,110–114} or natural organic matter^{115–123}. Resulting mass spectra exhibited, however, a vast number of m/z features, so that the interpretation of these mass spectra, or rather the analyzed sample became even more complicated. The development of data simplification strategies significantly assisted in the interpretation of complex mass spectra. The most common and well-established data simplification strategies were developed by van Krevelen¹²⁴ and Kendrick¹²⁵. Van Krevelen graphically illustrated the hydrogen to carbon ratio (H/C) vs. the oxygen to carbon ratio (O/C) of each measured elemental composition. This graphical illustration allowed rapid classification of compound classes and revealed the presence of specific chemical transformations¹²⁴. It was therefore applied to interpret, *inter alia*, resulting mass spectra of previously mentioned research fields^{117,123,126–129}. In addition, the so-called van Krevelen plot was also applied to lignin samples.^{76,78,82,130} The visualization of former unknown molecular compositions exhibited the degradation processes' potential to chemically transform the lignin polymer into valuable chemicals beside the production of low-cost chemicals. Furthermore, the van Krevelen plot supported the interpretation of occurring reaction mechanisms.¹³⁰ The lack of information about molecular mass for each respective data point is a major disadvantage of the van Krevelen plot. This disadvantage reduces the scope of information for degraded lignin, especially after an electrochemical degradation. This information is, however, essential, since lignin degradation processes are aimed for the production of low-

molecular weight products. On the other hand, the Kendrick mass defect (KMD) plot provides this essential information. The basic principle of the KMD plot is the transformation of the IUPAC mass scale with carbon as its reference mass point at 12.00000 u to a new reference mass point, which is in that case the CH₂-unit at 14.00000 u, the so called Kendrick mass (KM).¹²⁵ Masses and mass defects of measured *m/z* features are therefore recalculated as follows:

$$KM [CH_2] = m/z (IUPAC) \times \frac{14}{14.01565} \quad (1)$$

$$KMD [CH_2] = \text{nominal measured mass} - KM [CH_2] \quad (2)$$

The graphical illustration of measured *m/z* features using this mass scale redefinition allowed rapid identification of homologous series such as naphthalenes, paraffins or alkyl derivatives. Data points that were arranged in straight lines along the x-axis belonging to the same homologous series and only differ in the number of CH₂ repeating units (see Figure 4.3).

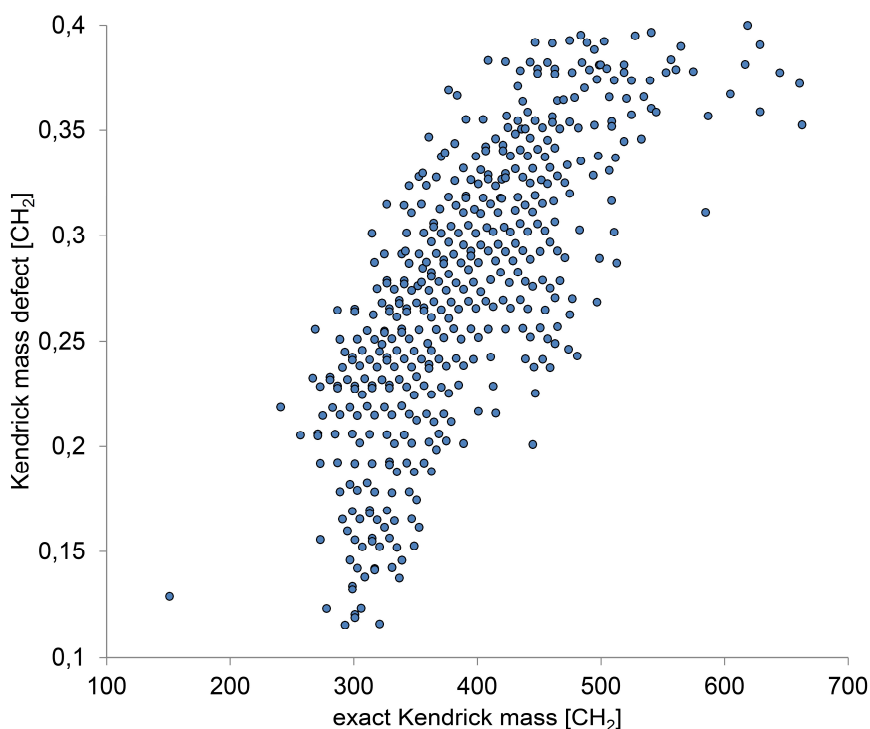


Figure 4.3. Exemplary illustration of the Kendrick mass defect plot. Straight lines along the x-axis represent homologous series. The data points originate from an electrochemically degraded lignin sample using DI-APCI in negative ionization mode.

Kendrick plots were usually applied to crude oil^{108,123,127,131,132}, natural organic matter^{119,126,133,134} or other samples^{134–137}. The benefits in terms of compositional analysis given by the KMD plot were, of course, also suitable for complex lignin samples.^{82,102} KMD plots assisted in the interpretation of the chemical composition of the tremendously complex lignin samples. The correlation between measured *m/z* signals and the KMD revealed the presence of further repeating units and indicated a

IV. Introduction

rather ordered than randomized structure for lignin.¹⁰² Nevertheless, KMD plots are only able to visualize connections between elemental compositions. Chemical structures of the respective m/z features are still unknown and need an additional orthogonal analytical method. The hyphenation of a mass spectrometer and a HPLC system can add this necessary orthogonal dimension. Chemical interactions of degradation products with the stationary phase and subsequent mass spectrometric analysis deconvoluted the complex lignin sample and therefore significantly enhanced the interpretation of the degradation products.^{42,44,72,74,77} In conclusion, mass spectrometry is a versatile, easily modifiable platform for lignin analysis. However, the high complexity of degraded lignin samples makes data and instrumental setup modifications necessary to provide a comprehensive analytical method.

4.3 Aim of the thesis

Lignin degradation in ionic liquids is attracting increasing attention.¹³⁸ However, an electrochemical application is rather unexplored, but appears promising due to the formation of uncommon degradation products. The development of a comprehensive analytical technique can therefore significantly support the interpretation of the resulting degradation mixture. Possible reaction mechanisms during the degradation process can consequently be determined to provide a better understanding of the electrochemical approach. As a result, parameters influencing the effectiveness of the electrochemical lignin degradation can be investigated by using the developed analytical technique. Therefore, the analytical technique has to meet several requirements, e.g. the detection of a wide range of degradation products in order to provide the desired information. In this context, MS provides the versatility and modifiability that is needed for meeting these requirements, so that the objectives for the thesis can be defined as follows:

1. Cover as many degradation products as possible by using the most suitable ionization technique.
2. Develop a data visualization strategy to simplify the complex data sets.
3. Classify the complex mixture into distinct compound classes to gather information about the mixture's chemical composition.
4. Find and characterize degradation products that are unique for an electrochemical degradation to enable the possibility to propose electrochemical reaction mechanisms.
5. Develop a chromatographic separation method to deconvolute the present isobaric content and to enable a fractionation of the complex mixture.

V. List of Publications

The results of the dissertation have been published in the following peer-reviewed journals:

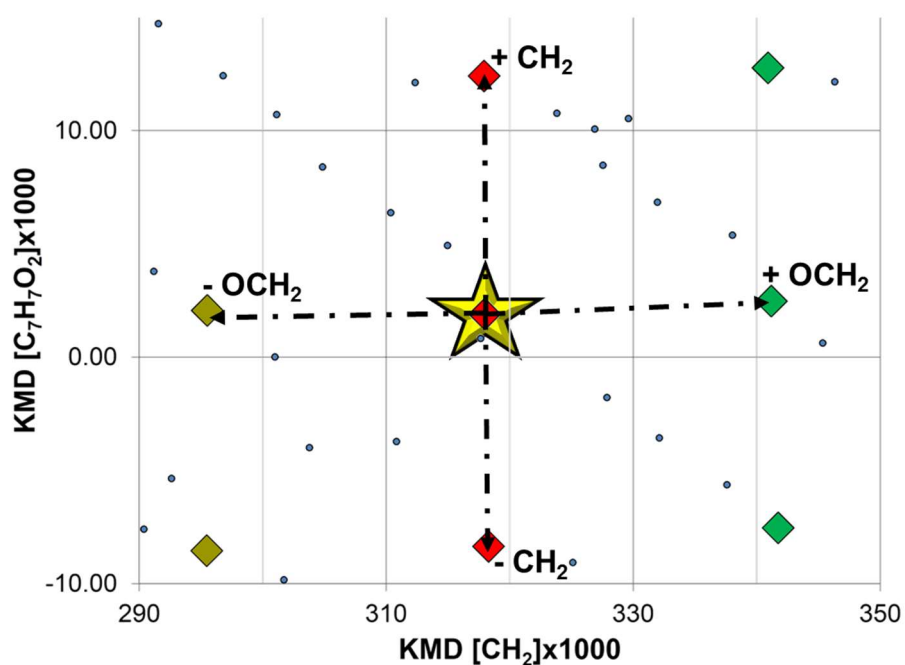
1. T.K.F. Dier, K. Egele, V. Fossog, R. Hempelmann, D.A. Volmer, Enhanced Mass Defect Filtering to Simplify and Classify Complex Mixtures of Lignin Degradation Products, *Anal. Chem.*, **2016**, 88, 1328-1335.
2. T.K.F. Dier, R. Rauber, J. Jauch, R. Hempelmann, D.A. Volmer, Novel Mixed-Mode Stationary Phases for Chromatographic Separation of Complex Mixtures of Decomposed Lignin, *ChemistrySelect*, **2017**, 2, 779-786
3. T.K.F. Dier, M. Fleckenstein, H. Miltz, D.A. Volmer, Exploring the Potential of High Resolution Mass Spectrometry for the Investigation of Lignin-Derived Phenol Substitutes in Phenolic Resin Syntheses, *Anal. Bioanal. Chem.*, **2017**, DOI: 10.1007/s00216-017-0282-1

Publication 1

Enhanced Mass Defect Filtering To Simplify and Classify Complex Mixtures of Lignin Degradation Products

T.K.F. Dier, K. Egele, V. Fossog, R. Hempelmann, D.A. Volmer

Anal. Chem., **2016**, 88, 1328-1335



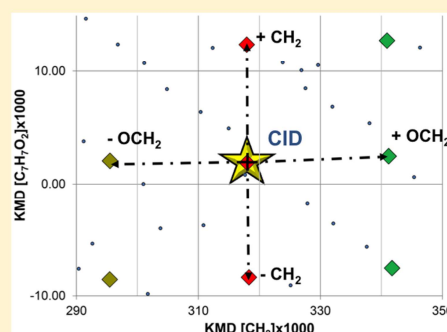
Reprinted with permission from T.K.F. Dier *et al.*, *Anal. Chem.*, **2016**, 88, 1328-1335. Copyright (2016) American Chemical Society.

Enhanced Mass Defect Filtering To Simplify and Classify Complex Mixtures of Lignin Degradation Products

Tobias K. F. Dier,[†] Kerstin Egele,[†] Verlaïne Fossog,[‡] Rolf Hempelmann,[‡] and Dietrich A. Volmer^{*,†}[†]Institute of Bioanalytical Chemistry, Saarland University, 66123 Saarbrücken, Germany[‡]Institute of Physical Chemistry, Saarland University, 66123 Saarbrücken, Germany

Supporting Information

ABSTRACT: High resolution mass spectrometry was utilized to study the highly complex product mixtures resulting from electrochemical breakdown of lignin. As most of the chemical structures of the degradation products were unknown, enhanced mass defect filtering techniques were implemented to simplify the characterization of the mixtures. It was shown that the implemented ionization techniques had a major impact on the range of detectable breakdown products, with atmospheric pressure photoionization in negative ionization mode providing the widest coverage in our experiments. Different modified Kendrick mass plots were used as a basis for mass defect filtering, where Kendrick mass defect and the mass defect of the lignin-specific guaiacol ($C_7H_7O_2$) monomeric unit were utilized, readily allowing class assignments independent of the oligomeric state of the product. The enhanced mass defect filtering strategy therefore provided rapid characterization of the sample composition. In addition, the structural similarities between the compounds within a degradation sequence were determined by comparison to a tentatively identified product of this compound series. In general, our analyses revealed that primarily breakdown products with low oxygen content were formed under electrochemical conditions using protic ionic liquids as solvent for lignin.



Lignin is one of the most abundant natural polymers, which is produced primarily as a waste product from the wood pulp and sugar cane milling industries. Lignin has a complex structure, the aromatic part of which is composed of *p*-hydroxybenzene, guaiacyl (4-alkyl-2-methoxyphenol), and syringyl (4-alkyl-2,5-dimethoxyphenol) units (Figure 1). While existing markets for lignin products focus on simple products, for example, dispersing or binding agents, its potential for conversion to biofuels^{1–4} and for recovery of renewable chemicals such as valuable low molecular weight aromatic

chemicals^{4,5} has attracted significant interest. Attempts at characterization of the aromatic content of lignin began almost 100 years ago.^{6–9} Adler showed that distinct phenolic components form the basis of the lignin polymer (Figure 1).¹⁰ The guaiacyl and syringyl units allow the classification of lignin into two categories, soft and hardwood lignins.¹¹ Guaiacyl lignin (softwood lignin) mainly consists of guaiacyl-type units (>95%). The remainder of the structure is dominated by *p*-coumaryl-alcohol units and traces of syringyl units. Guaiacyl-syringyl lignin (hardwood lignin) on the other hand comprises varying amounts of both guaiacyl and syringyl units.

Today, research on lignin mostly focuses on the technical degradation of the polymer. Decomposition of lignin can principally be achieved by hydrolysis reactions, catalytic reductions, or catalytic oxidation reactions. Hydrolyses and reductions disrupt the structure and remove chemical functionalities from lignin to produce simpler phenols, whereas oxidation reactions tend to form complex aromatic compounds. Pulping,^{12–15} bleaching,^{16–18} or photocatalyzed processes^{19,20} have been applied for decomposition, with cinnamaldehyde structures of the respective lignin-specific units readily formed, due to predominant bond cleavages at the β -O-4 sites.^{14,15}

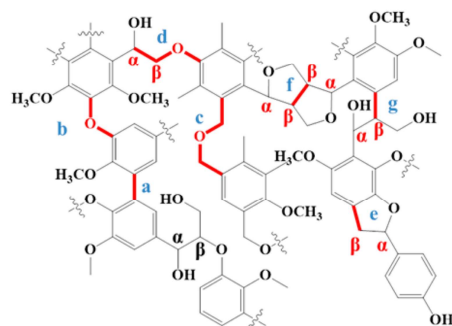


Figure 1. Schematic representation of the lignin polymer.²² The common linkages are highlighted: (a) biphenyl, (b) diphenyl ether, (c) dibenzyl ether, (d) β -O-4, (e) β -5, (f) β - β , and (g) β -1.

Received: October 8, 2015

Accepted: December 11, 2015

Published: December 11, 2015

Optimization of the degradation processes to direct cleavages to other linkage sites has extended the product spectrum and have enabled the formation of potentially useful chemical precursors and/or fossil fuel alternatives.²¹

Electrochemical decomposition of lignin has been established as a new promising and environmental friendly degradation technique.^{22–24} Electrochemical decomposition permits single electron transfer (SET) oxidation processes, resulting primarily in C_α-C_β bond cleavages. Electrolyses in aqueous solutions are restricted, however, by formation of oxygen at the anode and H₂ reduction at the cathode (=1.23 V). Ionic liquids (IL) have extended the applicable potential to values up to 1.7 V, depending on the ionic liquid used.²² The increased electric potentials combined with the IL's stability at higher temperatures and during oxidative processes²⁵ have enabled additional oxidative and reductive cleavages. Condensation reactions during the electrochemical process, however, made interpretation of the generated product spectrum more complicated. For example, ILs were able to catalyze aldol and Mannich reactions²⁶ as well as Michael-additions.²⁷ The increased complexity required high resolution analytical methodologies to characterize product mixtures, including 2-dimensional nuclear magnetic resonance spectroscopy (2D-NMR).²⁸ In these NMR experiments, most of the relevant information was seen in the region between 50 and 90 ppm in ¹³C spectra and between 2.8 and 5.5 ppm in ¹H spectra.²⁸ High-resolution mass spectrometry (HRMS) has also been applied to characterization of complex lignin mixtures, after data simplification and visualization for reliable compound assignments.^{29–31} The implemented visualization methods are not a recent invention, but date back to the 1950s, when van Krevelen developed the first complex filtering methods.³² In his experiments, van Krevelen cross-plotted the O/C ratio of compounds against their corresponding H/C ratios, which enabled fast classification of reaction types commonly seen during coal treatment.³² Chemical transformations such as decarboxylation, demethanation, or dehydration are represented by straight lines in these plots, due to the incremental loss of linked C, O, or H content. Kendrick developed a second important simplification method in 1963.³³ Kendrick reduced the complexity of data sets by implementing a mass scale based upon CH₂ rather than ¹²C. In this transformed scale, CH₂ is defined as exactly 14.00000 u as opposed to the 14.01565 u in the IUPAC ¹²C scale. The Kendrick mass of a molecule is calculated as follows:

$$\text{Kendrick mass} = m/z(^{12}\text{C}) \times 14/14.01565 \quad (1)$$

Kendrick readily demonstrated identification of homologous series such as naphthalenes, paraffins, or alkyl derivatives using this mass scale.³³ All connected *m/z* signals, differing in CH₂ content, share the same mass defect in these plots. Today, Kendrick and van Krevelen plots are frequently used in HRMS data interpretation routines, often modified to fit specific compound classes or sample types.³⁴ For example, research in natural organic matter (NOM)^{34–36} polymeric decomposition products³⁷ and lignin utilizes van Krevelen plots and similar mass defect filtering (MDF) techniques.^{29–31,38–40}

In this study, we have performed a detailed investigation of the oxidative and reductive pathways of lignin. We systematically applied MDF techniques including modified Kendrick and van Krevelen plots, to simplify Fourier-transform ion cyclotron resonance (FTICR) HRMS data of complex product mixtures generated by electrochemical decomposition of lignin dissolved in ionic liquids. The study demonstrated that the ability to

resolve and determine accurate *m/z* ratios and elemental formulas of multiple components significantly accelerated the structural elucidation process for complex lignin samples. The electrochemical lignin degradation resulted in removal and transformation of -CH₂, -OH, phenyl, and other groups and subsequent formation of -CHO, -COOH, etc., therefore generating molecules belonging to different consecutive series. Their existence was illustrated by interrogation of the HRMS raw data via mass defect filtering: if lignin degradation occurred, the *m/z* values detected using FTICR-MS were identifiable and predictable based on their mass defects, which were then correlated to the chemical reactions causing the degradation process. The resulting MDF plots showed linked *m/z* series and pointed to similarities and genealogical connectivities between species and therefore served as a tool for fast classification of products into general classes as well as identification of specific lignin monomeric units.

EXPERIMENTAL SECTION

Reagents and Chemicals. Methanol (HPLC grade) and acetic acid (technical) were purchased from VWR (Darmstadt, Germany); toluene (anhydrous, 99.8%) and alkali lignin were from Sigma-Aldrich (Steinheim, Germany). Ammonium hydroxide (25%) and diethyl ether (>99%) were from an in-house university supply. Ultrapure water was generated using an Elga (Celle, Germany) Purelab Ultra purification system. Triethylammonium methanesulfonate was synthesized as described previously.²²

Instrumentation. Electrospray ionization (ESI), atmospheric pressure photoionization (APPI), and atmospheric pressure chemical ionization (APCI) were performed in negative ionization mode on a Bruker (Bremen, Germany) solariX 7 T FTICR instrument equipped with an Infinity cell. For direct infusion experiments, 16 transients with estimated resolving power of 280 000 at *m/z* 400 were collected and coadded. For the individual ionization techniques, the specific source parameters were optimized and described in Table S1. For MS/MS, sample solutions at 100 ng/μL were directly infused and collision induced dissociation (CID) performed in the collision quadrupole prior to the FTICR cell with N₂ as collision gas. The isolation window for precursor ion selection was 1 u wide, and the collision energy was raised from 0 to 27 V in 3 V steps. Mass spectra were externally calibrated using the Agilent (Waldbronn, Germany) ESI and APCI/APPI tuning mix. In these experiments, the measured transients with estimated resolving power of 280 000 at *m/z* 400 were collected and 32 transients coadded. Restrictions for chemical compositions of measured *m/z* values with relative abundances >0.1% (corresponding to S/N > 4) in the *m/z* ranging from 100 to 1000 were set based on data from others⁴¹ and CHNO analyses (data not shown): composition was restricted to C, H, and O with double bond equivalents (DBE) between 4 and 25 and H/C ratios from 0.5 to 2.5 for both odd and even electron ions. The chemical formulas were determined using Bruker's DataAnalysis 4.2 software with a mass tolerance window of ±5 ppm. The *m/z* signals were exported to Excel spreadsheets and measured *m/z* ratios converted from the IUPAC ¹²C scale to the Kendrick mass scale³³ (see eq 1) as well as a new mass scale representing the guaiacol repeating units (C₇H₇O₂):

$$m/z(\text{C}_7\text{H}_7\text{O}_2) = m/z(^{12}\text{C}) \times 123/123.044605 \quad (2)$$

where 123 u is the nominal mass of guaiacol ($C_7H_7O_2$) and 123.044605 u represents the calculated exact mass of this repeating unit

Kendrick mass defects (KMD) were calculated as follows:

$$\text{KMD} = (\text{measured nominal mass} - \text{Kendrick mass}) \times 1000 \quad (3)$$

An analogous KMD equation was used for the $C_7H_7O_2$ scale. Average values and standard deviations of related mass defect tolerance windows for elemental differences were calculated using Matlab (MathWorks, Natick, MA, USA).

Degradation and Analysis of Soluble Lignin. The electrochemical degradation process was performed in a glass cell with a cylindrical Ti-wire mesh coated with transition metal oxides based catalyst as working electrode, a cylindrical Pt-wire mesh counter electrode, and an Ag-quasi-reference electrode.²² Alkali lignin (15% w/w) was dissolved in triethylammonium methanesulfonate and electrochemically converted for 4 h at 80 °C using a potential of 1.7 V. Subsequently, three mass equivalents of water (with reference to ionic liquid) followed by 0.5 weight equivalents of diethyl ether were added. This led to a three-phase system after centrifugation: organic phase with the degraded products, undecomposed lignin cake, and aqueous phase containing dissolved IL constituents. The residual lignin polymer was washed with water and extracted with diethyl ether. The IL was recovered from the aqueous phase by evaporation under reduced pressure. The organic phase was washed with distilled water and dried over $MgSO_4$. After evaporation under reduced pressure, a yellow powder (yield, 20% w/w, based on mass of lignin precursor) was obtained. Of this powder, 100 μg was dissolved in 1 mL of methanol (+1% acetic acid) for ESI and APCI measurements. For APPI, a 100 ng/ μL solution in methanol/toluene (90:10 v/v) was used. For basic pH experiments, 100 μg was dissolved in 1 mL of methanol (+1% ammonium hydroxide).

RESULTS AND DISCUSSION

In this study, we performed degradation of lignin in an oxygen-free environment (N_2 atmosphere and anhydrous IL),²² resulting in products originating entirely from the lignin polymer. We expected syringol, guaiacol, *p*-hydroxyphenol, and other derivatives of monomeric units as well as abundant oligomers as degradation products, as previously seen in other lignin studies,^{23,38,42–45} with product series originating from the same lignin-specific compound class, but varying degrees of saturation and/or oxygen content. The wide variety of degradation reactions (oxidations, reductions, thermal repolymerizations, and combinations of the three) made the characterization of the wide spectrum of degradation products very challenging and required simplification strategies. Mass defect filtering (MDF) is often utilized for complex product mixtures,^{36,37,46–49} because each elemental composition exhibits a characteristic mass defect. Expanding MDF techniques to more complex strategies^{49,50} enables even faster and more reliable assignments of measured m/z and chemical class or compound identity by illustrating genealogical links of products with chemically connected degradation mechanisms. In these advanced plots, the Kendrick mass defect (KMD) is often chosen for the first dimension, while the second dimension sorts the degradation products according to the lignin-specific monomeric units. In addition, these plots provide information on double bond equivalents (DBE), oxygen content, and clustering of products in specific regions.

In our experiments, MS analyses of extracts of the electrochemical process exhibited highly complex mixtures as a result of small compositional differences of functional groups and molecular masses. Figure 2 illustrates a typical mass

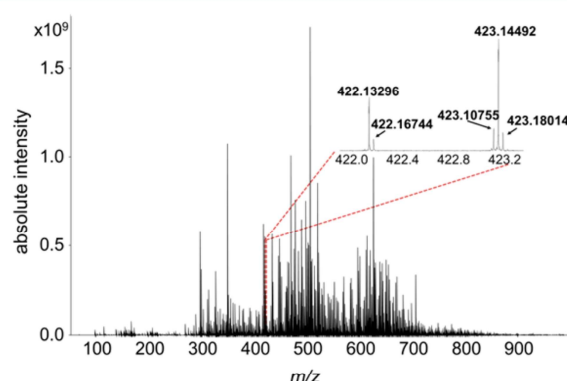


Figure 2. APPI mass spectrum of electrochemically degraded lignin.

spectrum of a degradation mixture, exhibiting thousands of mass spectral features between m/z 100 and 1000, from dimers, trimers, tetramers etc. of lignin repeat units. Several volatile products such as guaiacol, syringol, and other products with low oxygen content (e.g., 3-methylfuran) were also seen, which have been previously identified by GC/MS.²² Unfortunately, the majority of products was nonvolatile, and repolymerization reactions also occurred, thus precluding the use of GC/MS for comprehensive characterization of the mixtures. Therefore, to obtain wider coverage, ultra high resolution mass spectrometry (HRMS) using FTICR was implemented, which has previously been applied to lignin analyses.^{30,31,43,51}

Compound Coverage. Lignin decomposition results in product mixtures with a wide range of molecular weights and physicochemical properties. To obtain the widest coverage, different ionization techniques, namely, ESI, APCI, and APPI, were investigated over a m/z range of 100–1000 (Figure S1 illustrates spectra for the different ionization methods). The number of detected features, i.e., unique elemental formulas of products, varied significantly between the techniques (Figure S2). The applied ionization technique strongly influenced the number of accessible molecules, as molecular changes during degradation changed the number of ionizable functional groups (Table 1). ESI ionized more compounds at lower or higher pH as compared to neutral pH, which can be related to ion formation in solution. APCI generally provided a similar number of features as compared to ESI, but also included cycloalkanes and higher saturated products. APPI, however, permitted the detection of by far the largest number of products, in particular for the important range of low molecular weight compounds between 200 and 500 Da (Table 1).

The degradation reactions were visualized in the van Krevelen diagram shown in Figure 3, exhibiting separation according to H/C ratio, to illustrate degree of saturation, and separation according to O/C ratio for oxygen content. In comparison to the lignin precursor,^{31,41,52,53} electrochemical degradation shifted product distributions to molecules with lower oxygen content, which is readily seen in the van Krevelen plot (Figure 3), where O/C ratios of the chemical formulas (using elemental restrictions as given in the Experimental Section) were plotted against their corresponding H/C ratios.

Table 1. (a) Total Number of Features in m/z Segments of 100 u Width. (b) Number of Common and Unique m/z Features Observed under the Different Ionization Techniques Used

(a) segment	ESI pH 3	ESI pH 7	ESI pH 10	APCI	APPI
100–200	0	1	1	1	1
200–300	11	11	23	0	37
300–400	26	83	109	107	218
400–500	86	73	80	62	166
500–600	56	49	40	25	64
600–700	65	14	35	28	58
700–800	40	4	27	45	55
800–900	15	2	13	30	40
900–1000	8	0	3	12	15
Σ	307	237	331	310	654

(b) ionization	ESI pH 3	ESI pH 7	ESI pH 10	APCI	APPI	unique feat.
ESI pH 3		13	20	14	14	261
ESI pH 7	13		111	41	119	74
ESI pH 10	20	111		39	125	155
APCI	14	41	39		71	216
APPI	14	119	125	71		417

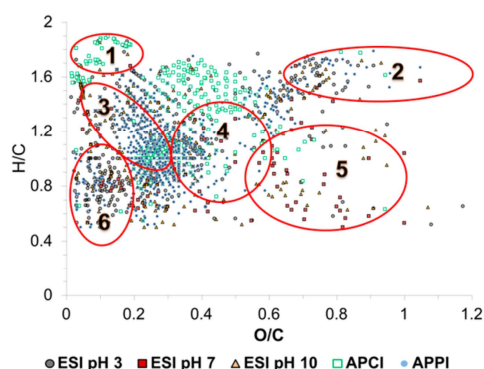


Figure 3. Van Krevelen plot of electrochemically degraded lignin. The circular borders were drawn based on previous studies^{41,52–54} and regions were assigned as follows: 1, cyclic alkanes; 2, polysaccharides; 3, alkylphenols; 4, lignins; 5, tannins; 6, polycyclic hydrocarbons.

While many of the components were readily assigned to previously reported compound classes, numerous other m/z features, mostly exhibiting lower oxygen content and higher or lower degrees of saturation, could not be readily assigned to specific class regions. We assumed that many of these unknown compounds originated from reductive degradation processes. Most of them were only visible in the APPI spectra and remained undetected in the ESI and APCI analyses. On the basis of the results of these experiments, we decided to conduct all subsequent experiments by APPI.

Visualization of Linked Series of Degradation Products. Several major connected m/z series were readily detected from the complex lignin data sets using Kendrick diagrams; that is, by plotting Kendrick mass defects as a function of measured accurate Kendrick masses.^{31,33,47} Linked m/z series with identical KMD appear as horizontal lines in these diagrams, normalized to 14.0000 u of the CH_2 units. The differences of mass defect along a vertical line provide information on the oxygen content of the product; that is, higher KMD values show higher oxygen contents (Figure 4). APPI experiments exhibited most degradation products in the m/z range of m/z 200 to 500 (Figure 4), indicating formation of monomeric to trimeric lignin units. Several distinct m/z series were readily visible. Consistent with degradation mechanisms discussed above, the measured KMD values and elemental formulas showed that the majority of degradation products exhibited low oxygen content. Longer alkylation series of related substance classes within a narrow KMD band illustrate controlled breakdown reactions to common substance classes,⁴³ e.g., oxidized resinols (O_7 , DBE 11), oxidized β -O-4 linked products (O_6 , DBE 10), or 5–5 linked compounds (O_6 , DBE 9; O_6 , DBE 11). In addition, these systematically arranged compound classes reflect the highly complex lignin structure: oxidized β -O-4 linked products, namely, $\text{C}_{20}\text{H}_{22}\text{O}_6$ (KMD: 0.26), exhibited 12 m/z features in the spectra, which was the longest alkylation series in our analyses. The unknown compound classes in Figure 3 presumably resulted from reduction reactions and were thus unique to the electrochemical decomposition process. Of course, assignment of m/z signals to elemental formulas does not provide conclusive information on the specific functional groups and molecular structures of the breakdown products. Improved structural information can be

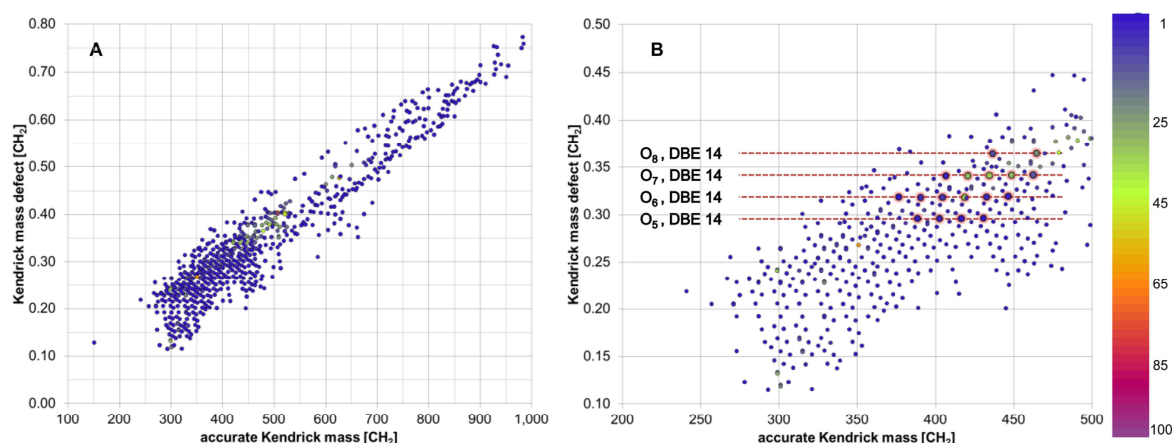


Figure 4. KMD plots of a degraded lignin sample for (left) all measured m/z features; (right) restricted to monomeric/dimeric/trimeric content. (Compound classes presumably resulting from reductive reactions were highlighted.) Color scale represents relative intensity.

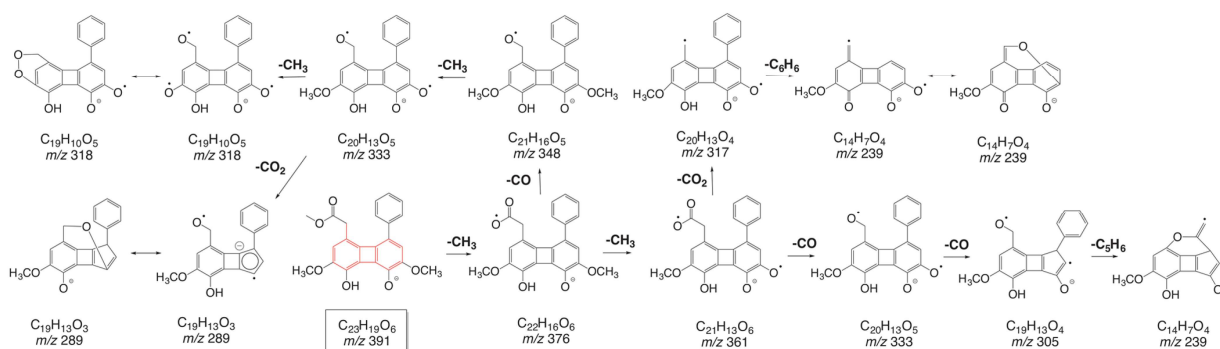


Figure 5. Proposed fragmentation scheme for m/z 391 [$C_{23}H_{20}O_6$] (structure highlighted). The molecular region containing the additional CH_2 units giving the consecutive product series at m/z 405, 419, and 433 is highlighted in red.

obtained through collision induced dissociation (CID) experiments of the product species. As an example, we describe the m/z series 391.11795, 405.13441, 419.15054, and 433.16617 (O_6 , DBE 14) in more detail. For m/z 391.11795, an elemental formula of $C_{23}H_{20}O_6$ was determined using the atom restrictions described in the **Experimental Section**. Three additional CH_2 units give the m/z ratios at the nominal m/z 405, 419, and 433. Considering the oxygen content, with O/C ratios between 0.23 and 0.26 and H/C ratios between 0.83 and 0.96, these m/z ratios fell directly into regions of the unknown classes mentioned above. CID of m/z 391.11795 showed successive CH_3^\bullet eliminations as most abundant product ions (**Figure 5**). Justesen described similar dissociation reactions for methoxylated flavonoids,⁵⁵ and previous studies have also shown that C–O–ether bonds primarily dissociate to the corresponding radicals.^{56,57} The additional neutral losses of 27.9949 Da (CO) and 43.9898 Da (CO_2), which are common for esters⁴³ and *o*-methoxyphenols,⁵⁸ support the proposed structure of m/z 391.11795 shown in **Figure 5**. The structure contains three methoxy groups, with at least one of the methoxy groups located in *ortho* position of a hydroxyl group or two methoxy and one methyl ester group. Minor dissociations included losses of cyclic aromatic structures (C_6H_6 , 78.0470 u; C_5H_6 , 66.0470 u) following CH_3^\bullet elimination from a methoxy group,⁵⁹ suggesting an aromatic ring system and at least one aromatic hydroxyl group, which is characteristic for degraded lignin.^{6,8,10,15,43,60} The proposed structure for $C_{23}H_{20}O_6$ (**Figure 5**) requires further confirmation by nuclear magnetic resonance (NMR) using a synthetic standard which is currently commercially unavailable and therefore would require synthetic preparation. The CID spectra of the other species of the ion series exhibited only minor differences of fragmentation pattern (**Table S2**). Importantly, the added CH_2 units in the product series did not give additional CH_3^\bullet cleavages in the CID spectra, allowing the conclusion that no additional methoxy functionalities or ester groups were present. The additional CH_2 units were rather located on the cyclic carbon skeleton, which was also confirmed by the presence of the same neutral losses for the heavier analogs (**Figure 5**). Highly unsaturated compounds, specifically biphenylene-type molecules, have previously been suggested as dimeric lignin degradation products.⁴³ The proposed dissociation schemes are given in **Figures S3 and S4**. (A complete list of observed product ions is summarized in **Table S2**.) Methoxy groups linked to the aromatic skeleton are a characteristic structural element of lignins. The number of CH_3^\bullet cleavages

observed in the CID spectra therefore can be used as a marker for a specific lignin monomeric unit.⁴³ For example, the number of observed CH_3^\bullet eliminations for 4-hydroxybenzaldehyde, coniferaldehyde, and syringaldehyde increased from 0 to 2.⁴³

Enhanced Mass Defect Filtering. Using characteristic structure elements of lignin (monomer units) as a complementary m/z scaling factor gives us further possibilities for simplifying the complex mass spectra. For example, rescaling the mass spectra using the guaiacol core unit ($=C_7H_7O_2$) as basis for the m/z scale will show a linked m/z series of breakdown products as horizontal lines that only differ in the number of lignin-specific monomeric units if the corresponding “guaiacol mass defect” (KMD [$C_7H_7O_2$]) was used as y axis, analogous to a regular Kendrick diagram. Here, we have chosen instead to plot both regular KMD [CH_2] and KMD [$C_7H_7O_2$] in one diagram (**Figure 6**), including both CH_2 and OCH_2

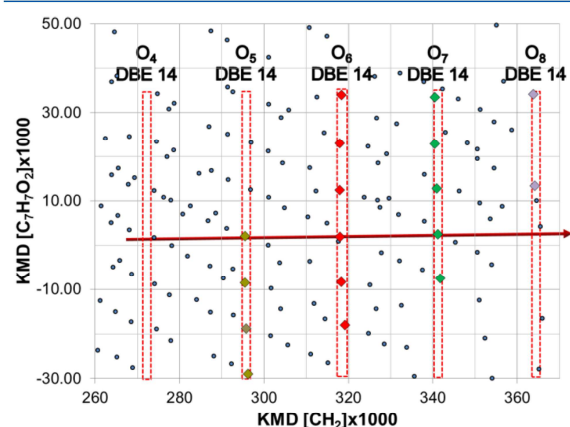


Figure 6. Visualization of the advanced mass defect filter: horizontal lines along the x -axis represent differences in lignin-specific monomeric units (see arrow); vertical lines along the y -axis represent CH_2 groups. Tolerance bands are only shown for OCH_2 differences.

repeat units. Normalized mass defects across compound classes differed within 1 to 3 decimal places after the decimal point. For visualization purposes, all calculated KMD values were multiplied by a factor of 1000. The benefits of the mass defect filter are illustrated by following the near horizontal line along the x -axis in **Figure 6** from lower to higher KMD [CH_2] values. Here, additional methoxy groups for the respective m/z features were assigned, which is seen for the m/z series O_6 ,

DBE 14 to O_7 , DBE 14. Utilizing the proposed structure in Figure 5 (O_6 , DBE 14 \rightarrow O_7 , DBE 14) allowed us to place the additional methoxy group at the phenyl ring or the phenyl acetate moiety. Aromatic methoxy groups were exclusively assigned in *o*-position to the hydroxyl function. Therefore, CID experiments of the " O_7 , DBE 14" series should show one additional CH_3^\bullet elimination, if it is connected to the " O_6 , DBE 14" series. In addition to the described neutral losses for the " O_6 , DBE 14" series (CH_3^\bullet radicals [3 \times], CO and CO_2 , and complete cyclic structures), a low abundant fourth CH_3^\bullet cleavage was observed for m/z 421.12940 and 449.16052. Additional neutral losses of CO, CO_2 , and C_3H_5 were also present. Fragmentation patterns for compounds differing in one methoxy group were investigated by Kang et al.⁵⁹ The authors determined product ions of daidzein and glycitein. These two compounds, differing only in one methoxy group, showed similar fragmentation patterns, including the additional CH_3^\bullet elimination for glycitein. Measured product ions of m/z 421.12940 and 449.16052 allowed us to place the methoxy group at the phenyl ring in *m*-position to the second ring of biphenylene. Nonfunctionalized phenyls have never been reported in studies focusing on lignin decomposition. The electrochemical degradation process appeared to be able to reduce aromatic methoxy and/or hydroxyl groups to compounds with fewer oxygen atoms. Electrochemical reductions of phenol-like substances have only been shown for quinones^{61,62} or phosphates.⁶³ We propose that the extended voltage used here (1.7 V) leads to additional reduction reactions of phenolic derivatives. An example for the proposed reduction mechanism is shown in Figure S5. This hypothesized reductive pathway was also applied to the compound classes mentioned above, namely, oxidized resinols, oxidized β -O-4 linked products, and 5-5 linked compounds, resulting in demethoxylated products with well-defined KMD values. Using the corresponding KMD values ($KMD [CH_2]$ and $KMD [C_7H_7O_2]$) for these demethoxylated products for the mass defect filter suggested the capability for electrochemical reduction during electrolysis of lignin. The alkali lignin used here mainly consists of varying amounts of guaiacyl and syringyl units.^{22,64} Therefore, existing degradation products, which formally contain one or multiple *p*-coumaryl-alcohol units, can be assigned to reduced degradation products.

Using a complex mass defect filtering strategy, of course, requires well-defined tolerance bands to assign potential m/z signals to a specific compound class or to a linked m/z series, to avoid misclassification. In our experimental samples, we observed that linked product series with functional differences corresponding to 4-hydroxylaldehyde versus coniferaldehyde ($=OCH_2$) exhibited mass defects of the following ranges:

$$\Delta KMD[CH_2] = 23.0917 \pm 0.1622 \quad (n = 116) \quad (3a)$$

$$\Delta KMD[C_7H_7O_2] = 0.48 \pm 0.15 \quad (n = 116) \quad (3b)$$

For CH_2 , ranges were as follows:

$$\Delta KMD[CH_2] = 0.2951 \pm 0.1595 \quad (n = 212) \quad (4a)$$

$$\Delta KMD[C_7H_7O_2] = 10.29 \pm 0.20 \quad (n = 212) \quad (4b)$$

General Classification of Degradation Products. The extended mass defect filtering technique described in the previous section allowed us to classify the breakdown products (Figure 7), similar to the van Krevelen plot (Figure 3), based on parameters derived from the elemental compositions, such

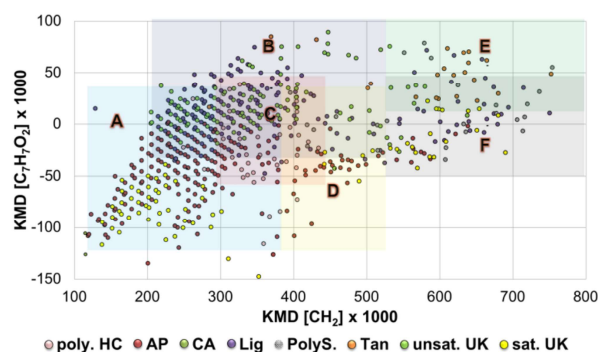


Figure 7. Regional differentiation of electrochemically degraded lignin using mass defect filtering: (A) alkylphenols (AP) and saturated unknowns (sat. UK); (B) lignins (Lig) and unsaturated unknowns (unsat. UK); (C) polycyclic hydrocarbons (poly. HC); (D) alkylphenols and polycyclic hydrocarbons; (E) tannins (Tan) and lignins; (F) mainly polysaccharides (PolyS.).

as DBE, oxygen content, and carbon number. In general, the carbon number increased with $KMD[CH_2]$ as well as DBE and oxygen content (see Figure S6 for more details), allowing a rapid survey of the lignin sample. This systematic trend was linear up to a $KMD[CH_2] \times 1000$ value of ~ 450 , representing the trimers. The nonlinearity for higher values suggested that products of higher molecular weight and therefore higher degree of oligomerization primarily result from repolymerization reactions after initial degradation. The demethoxylated products mentioned before were allocated to the regions of alkylphenols or unsaturated unknowns, while the oxidized forms of compound classes were assigned to the region of lignins without exception. The connection, therefore, between different regions, namely, lignins and alkylphenols/unsaturated unknowns, is linked to demethoxylation of lignins, which was previously confirmed as a reductive pathway.

It is clear that other possible reductive pathways such as hydrogenation are also occurring during the electrochemical decomposition. The mass defect plot suggested two successive hydrogenation reactions (tolerance bands for hydrogenation; see Table 2) for the oxidized β -O-4 linked product series. The KMD values related to the first hydrogenation are probably not resulting from electrochemical reduction, but rather originate from unmodified β -O-4 linked products. Similar to the demethoxylation described above, hydrogenation proceeds via single electron transfer (SET) and the protons are provided by the protic ionic liquid. These hydrogenations were also observed for the other series in our study. The mass defect filter plot is not restricted to the investigation of oxidative or reductive pathways. It can be readily used for elemental formula assignments from raw data, similar to the well-established fractional mass defect filtering,^{65,66} which is common in drug discovery and metabolite identification. Biotransformations and resulting differences of functional groups of metabolites affect the mass defect in a similar manner as the reductive pathways discussed here. Table 2 summarizes calculated tolerance bands for anticipated functional and atomic differences of lignin degradation products.

CONCLUSIONS

The electrochemical degradation performed in our study generated a wide range of products. While several of these products have previously been reported, many additional

Table 2. Calculated KMD Tolerance Bands for Assignments of Anticipated Functional Differences of Lignin Degradation Products

functional difference	$\Delta\text{KMD}[\text{CH}_2]$ (# matching values)	$\Delta\text{KMD}[\text{C}_x\text{H}_y\text{O}_z]$ (# matching values)
CO ₂	59.3625 ± 0.2257 (152)	26.18 ± 0.22 (152)
H ₂	13.3441 ± 0.1945 (244)	14.86 ± 0.20 (244)
CO	36.3686 ± 0.2707 (272)	15.26 ± 0.27 (272)
O _x → O _{x+1}	22.8811 ± 0.2803 (418)	10.79 ± 0.30 (418)
C _x → C _{x+1}	9.7680 ± 0.2591 (200)	6.76 ± 0.26 (200)
C _x → C _{x+2}	4.0456 ± 0.2815 (196)	1.98 ± 0.28 (196)
C _x → C _{x+3}	7.7026 ± 0.2716 (64)	6.19 ± 0.28 (64)
+1 DBE, +1 C	13.1999 ± 0.2980 (288)	4.15 ± 0.30 (288)

compounds with lower oxygen content were discovered, which are believed to be formed as a result of the extended potential available in the described electrochemical setup and the additional mechanistic possibilities. The shown enhanced mass defect filtering strategy greatly aided the interpretation and elucidation of these reductive pathways, namely, hydrogenation and demethoxylation, and provided a rapid overview of connected lignin-specific compound series. Structural classification of all members of the linked compound series was based on the identification of a single product of the series. Numerical calculations allowed proper assignments of elemental compositions for CHO-related content. The information content gained from the mass defect filtering plots was comparable to the data obtained from the combined use of established simplification strategies for data visualization such as van Krevelen and Kendrick mass defect plots. The mass defect filtering plots are useful for obtaining a quick overview of major compound classes or general sample compositions or gaining detailed insight into unknown degradation mechanisms. Future studies will focus on expanding the mass defect strategy to CHNO and CHOS-related compounds. Furthermore, a more detailed interrogation of the CHO content of the degradation mixtures will be obtained by using an additional chromatographic separation step. Ion suppression effects and isobaric interferences have undoubtedly limited the number of detected species reported here. The differences of functional groups across the generated product spectrum will likely permit separation by liquid chromatography, thus further increasing the number of detected electrolytic degradation products.

■ ASSOCIATED CONTENT

● Supporting Information

The Supporting Information is available free of charge on the ACS Publications website at DOI: 10.1021/acs.analchem.5b03790.

Instrumental parameters for ESI, APCI, and APPI; observed product ions for selected *m/z* ratios after CID; mass spectra of lignin degradation products in negative ion mode; Kendrick mass defect plot; linked fragmentation reactions; proposed lignin degradation

reactions; comparison of mass defect filtering and DBE, C number, and O content (PDF)

■ AUTHOR INFORMATION

Corresponding Author

*Tel: +49 681 302 3433. Fax: +49 681 302 2963. E-mail: dietrich.volmer@mx.uni-saarland.de.

Author Contributions

The manuscript was written through contributions of all authors. All authors have given approval to the final version of the manuscript.

Notes

The authors declare no competing financial interest.

■ ACKNOWLEDGMENTS

This work was supported by the German Research Foundation (DFG VO 1355/4-1) and the FTICR-MS Facility (DFG INST 256/356-1). We acknowledge technical support by Reiner Wintringer (Institute of Bioanalytical Chemistry). D.A.V. acknowledges support by the Alfred Krupp von Bohlen und Halbach-Stiftung.

■ REFERENCES

- (1) De la Torre, M. J.; Moral, A.; Hernández, M. D.; Cabeza, E.; Tijero, A. *Ind. Crops Prod.* **2013**, *45*, 58–63.
- (2) Linger, J. G.; Vardon, D. R.; Guarneri, M. T.; Karp, E. M.; Hunsinger, G. B.; Franden, M. A.; Johnson, C. W.; Chupka, G.; Strathmann, T. J.; Pienkos, P. T.; Beckham, G. T. *Proc. Natl. Acad. Sci. U. S. A.* **2014**, *111* (33), 12013–12018.
- (3) Wang, H.; Xue, Y.; Chen, Y.; Li, R.; Wei, J. *Ind. Crops Prod.* **2012**, *37* (1), 170–177.
- (4) Beauchet, R.; Monteil-Rivera, F.; Lavoie, J. M. *Bioresour. Technol.* **2012**, *121*, 328–334.
- (5) Gosselink, R. J. A.; Teunissen, W.; van Dam, J. E. G.; de Jong, E.; Gellerstedt, G.; Scott, E. L.; Sanders, J. P. M. *Bioresour. Technol.* **2012**, *106*, 173–177.
- (6) Freudenberg, K.; Engler, K.; Flickinger, E.; Sobek, A.; Klink, F. *Ber. Dtsch. Chem. Ges. B* **1938**, *71* (9), 1810–1820.
- (7) Klason, P. *Ber. Dtsch. Chem. Ges. B* **1920**, *53* (5), 706–711.
- (8) Freudenberg, K.; Hess, H. *Justus Liebigs Ann. Chem.* **1926**, *448* (1), 121–133.
- (9) Jonas-Breslau, K. G. *Angew. Chem.* **1921**, *34* (51), 289–291.
- (10) Adler, E. *Wood Sci. Technol.* **1977**, *11*, 169–218.
- (11) Pandey, K. K. *J. Appl. Polym. Sci.* **1999**, *71* (May), 1969–1975.
- (12) Gellerstedt, G.; Gierer, J.; Pettersson, E.-L.; Szabo-Lin, I. *Liebigs Ann. Chem.* **1976**, *1976*, 2021–2036.
- (13) Gellerstedt, G.; Gierer, J.; Pettersson, E.-L.; El-Feraly, F. S.; Nørskov, L.; Schroll, G. *Acta Chem. Scand.* **1977**, *31b*, 735–741.
- (14) Gierer, J. *Wood Sci. Technol.* **1980**, *14* (4), 241–266.
- (15) Froass, P. M.; Ragauskas, A. J.; Jiang, J. J. *Wood Chem. Technol.* **1996**, *16* (4), 347–365.
- (16) Gellerstedt, G.; Agnemo, R.; Mannervik, B.; von Bahr, C.; Glaumann, H. *Acta Chem. Scand.* **1980**, *34b*, 461–462.
- (17) Johansson, E.; Ljunggren, S. *J. Wood Chem. Technol.* **1994**, *14* (4), 507–525.
- (18) Nagarathnamma, R.; Bajpai, P.; Bajpai, P. K. *Process Biochem.* **1999**, *34* (9), 939–948.
- (19) Kobayakawa, K.; Sato, Y.; Nakamura, S.; Fujishima, A. *Bull. Chem. Soc. Jpn.* **1989**, *62*, 3433–3436.
- (20) Ohnishi, H.; Matsumura, M.; Tsubomura, H.; Iwasaki, M. *Ind. Eng. Chem. Res.* **1989**, *28* (6), 719–724.
- (21) Zakzeski, J.; Bruijninx, P. C. a; Jongerius, A. L.; Weckhuysen, B. M. *Chem. Rev.* **2010**, *110* (6), 3552–3599.
- (22) Reichert, E.; Wintringer, R.; Volmer, D. A.; Hempelmann, R. *Phys. Chem. Chem. Phys.* **2012**, *14* (15), 5214–5221.

- (23) Shao, D.; Liang, J.; Cui, X.; Xu, H.; Yan, W. *Chem. Eng. J.* **2014**, *244*, 288–295.
- (24) Zhu, H.; Wang, L.; Chen, Y.; Li, G.; Li, H.; Tang, Y.; Wan, P. *RSC Adv.* **2014**, *4* (56), 29917–29924.
- (25) Kulkarni, P. S.; Branco, L. C.; Crespo, J. G.; Nunes, M. C.; Raymundo, A.; Afonso, C. A. M. *Chem. - Eur. J.* **2007**, *13* (30), 8478–8488.
- (26) Yang, X. F.; Wang, M.; Varma, R. S.; Li, C. J. *Org. Lett.* **2003**, *5* (5), 657–660.
- (27) Ranu, B. C.; Banerjee, S. *Org. Lett.* **2005**, *7* (14), 3049–3052.
- (28) Ede, R. M.; Kilpeläinen, I. *Res. Chem. Intermed.* **1995**, *21* (3–5), 313–328.
- (29) Bai, X.; Kim, K. H.; Brown, R. C.; Dalluge, E.; Hutchinson, C.; Lee, Y. J.; Dalluge, D. *Fuel* **2014**, *128*, 170–179.
- (30) Smith, E. A.; Park, S.; Klein, A. T.; Lee, Y. J. *Energy Fuels* **2012**, *26*, 3796–3802.
- (31) Waggoner, D. C.; Chen, H.; Willoughby, A. S.; Hatcher, P. G. *Org. Geochem.* **2015**, *82*, 69–76.
- (32) Van Krevelen, D. W. *Fuel* **1950**, *29* (11), 269–285.
- (33) Kendrick, E. *Anal. Chem.* **1963**, *35* (13), 2146–2154.
- (34) Ohno, T.; Parr, T. B.; Gruselle, M.-C. I.; Fernandez, I. J.; Sleighter, R. L.; Hatcher, P. G. *Environ. Sci. Technol.* **2014**, *48*, 7229–7236.
- (35) Mann, B. F.; Chen, H.; Herndon, E. M.; Chu, R. K.; Tolic, N.; Portier, E. F.; Roy Chowdhury, T.; Robinson, E. W.; Callister, S. J.; Wullschleger, S. D.; Graham, D. E.; Liang, L.; Gu, B. *PLoS One* **2015**, *10* (6), e0130557.
- (36) Zhang, F.; Harir, M.; Moritz, F.; Zhang, J.; Witting, M.; Wu, Y.; Schmitt-Kopplin, P.; Fekete, A.; Gaspar, A.; Hertkorn, N. *Water Res.* **2014**, *57*, 280–294.
- (37) Myers, A. L.; Jobst, K. J.; Mabury, S. A.; Reiner, E. J. *J. Mass Spectrom.* **2014**, *49* (4), 291–296.
- (38) Kim, J.-Y.; Park, J.; Hwang, H.; Kim, J. K.; Song, I. K.; Choi, J. W. *J. Anal. Appl. Pyrolysis* **2015**, *113*, 99–106.
- (39) Kloekhorst, A.; Shen, Y.; Yie, Y.; Fang, M.; Heeres, H. J. *Biomass Bioenergy* **2015**, *80* (0), 147–161.
- (40) Xu, W.; Miller, S. J.; Agrawal, P. K.; Jones, C. W. *ChemSusChem* **2012**, *5* (4), 667–675.
- (41) Kim, S.; Kramer, R. W.; Hatcher, P. G. *Anal. Chem.* **2003**, *75* (20), 5336–5344.
- (42) Clifford, D. J.; Carson, D. M.; McKinney, D. E.; Bortiatynski, J. M.; Hatcher, P. G. *Org. Geochem.* **1995**, *23* (2), 169–175.
- (43) Jarrell, T. M.; Marcum, C. L.; Sheng, H.; Owen, B. C.; O'Lenick, C. J.; Maraun, H.; Bozell, J. J.; Kenttämä, H. I. *Green Chem.* **2014**, *16* (5), 2713–2727.
- (44) Fox, S. C.; McDonald, A. G. *BioResources* **2010**, *5*, 990–1009.
- (45) Van den Bosch, S.; Schutyser, W.; Vanholme, R.; Driessen, T.; Koelewijn, S.-F.; Renders, T.; De Meester, B.; Huijgen, W. J. J.; Dehaen, W.; Courtin, C.; Lagrain, B.; Boerjan, W.; Sels, B. F. *Energy Environ. Sci.* **2015**, *8*, 1748–1763.
- (46) Mead, R. N.; Mullaugh, K. M.; Brooks Avery, G.; Kieber, R. J.; Willey, J. D.; Podgorski, D. C. *Atmos. Chem. Phys.* **2013**, *13* (9), 4829–4838.
- (47) Hughey, C. A.; Hendrickson, C. L.; Rodgers, R. P.; Marshall, A. G.; Qian, K. *Anal. Chem.* **2001**, *73* (19), 4676–4681.
- (48) Stevens, D.; Shi, Q.; Hsu, C. S. *Energy Fuels* **2013**, *27* (1), 167–171.
- (49) Kilgour, D. P. A.; Mackay, C. L.; Langridge-Smith, P. R. R.; O'Connor, P. B. *Anal. Chem.* **2012**, *84*, 7436–7439.
- (50) Roach, P. J.; Laskin, J.; Laskin, A. *Anal. Chem.* **2011**, *83*, 4924–4929.
- (51) Kekäläinen, T.; Venäläinen, T.; Jänis, J. *Energy Fuels* **2014**, *28*, 4596.
- (52) Visser, S. A. *Environ. Sci. Technol.* **1983**, *17* (7), 412–417.
- (53) De Wild, P.; Van der Laan, R.; Kloekhorst, A.; Heeres, E. *Environ. Prog. Sustainable Energy* **2009**, *28* (3), 461–469.
- (54) Stubbins, A.; Spencer, R. G. M.; Chen, H.; Hatcher, P. G.; Mopper, K.; Hernes, P. J.; Mwamba, V. L.; Mangangu, A. M.; Wabakanghanzi, J. N.; Six, J. *Limnol. Oceanogr.* **2010**, *55* (4), 1467–1477.
- (55) Justesen, U. *J. Mass Spectrom.* **2001**, *36* (2), 169–178.
- (56) Van Scheppingen, W.; Dorrestijn, E.; Arends, I.; Mulder, P.; Korth, H.-G. *J. Phys. Chem. A* **1997**, *101* (97), 5404–5411.
- (57) Colussi, A. J.; Zabel, F.; Benson, S. W. *Int. J. Chem. Kinet.* **1977**, *9*, 161–178.
- (58) Attygalle, A. B.; Ruzicka, J.; Varughese, D.; Bialecki, J. B.; Jafri, S. *J. Mass Spectrom.* **2007**, *42*, 1207–1217.
- (59) Kang, J.; Hick, L. A.; Price, W. E. *Rapid Commun. Mass Spectrom.* **2007**, *21*, 857–868.
- (60) Bai, X.; Kim, K. H.; Brown, R. C.; Dalluge, E.; Hutchinson, C.; Lee, Y. J.; Dalluge, D. *Fuel* **2014**, *128*, 170–179.
- (61) Katsumi, J.; Nakayama, T.; Esaka, Y.; Uno, B. *Anal. Sci.* **2012**, *28* (3), 257.
- (62) Senne, J. K.; Marple, L. W. *Anal. Chem.* **1970**, *42* (11), 1147–1150.
- (63) Shono, T.; Matsumura, Y.; Tsubata, K.; Sugihara, Y. *J. Org. Chem.* **1979**, *44* (25), 4508–4511.
- (64) Piñkowska, H.; Wolak, P.; Złocińska, A. *Chem. Eng. J.* **2012**, *187*, 410–414.
- (65) Mortishire-Smith, R. J.; O'Connor, D.; Castro-Perez, J. M.; Kirby, J. *Rapid Commun. Mass Spectrom.* **2005**, *19* (18), 2659–2670.
- (66) Zhang, H.; Zhang, D.; Ray, K.; Zhu, M. *J. Mass Spectrom.* **2009**, *44* (7), 999–1016.

Supporting Information

Enhanced mass defect filtering to simplify and classify
complex mixtures of lignin degradation productsTobias K.F. Dier,[†] Kerstin Egele,[†] Verlainé Fossog,[‡] Rolf Hempelmann,[‡]
Dietrich A. Volmer^{†,*}[†]*Institute of Bioanalytical Chemistry, Saarland University, 66123 Saarbrücken, Germany*[‡]*Institute of Physical Chemistry, Saarland University, 66123 Saarbrücken, Germany**Corresponding author:Prof. Dr. Dietrich A. Volmer
Saarland University
Institute of Bioanalytical Chemistry
D-66123 Saarbrücken, Germany
Tel +49 681 302 3433; Fax +49 681 302 2963
Email: Dietrich.Volmer@mx.uni-saarland.deTable of content:

Table S1. Instrumental parameters for ESI, APCI and APPI.....	2
Table S2. Observed product ions for selected m/z ratios after CID (O_6 ; DBE 14)	3
Table S3. Observed product ions for selected m/z ratios after CID (O_7 ; DBE 14)	4
Figure S1. Mass spectra of depolymerized lignin in negative ion mode	6
Figure S2. Kendrick mass defect plot	7
Figure S3. Linked fragmentation reactions for m/z 391, 405, 419, 433	8
Figure S4. Linked fragmentation reactions for m/z 421, 435, 440, 469	9
Figure S5. Proposed lignin degradation reactions.....	10
Figure S6. Comparison between mass defect filtering and DBE, C number, O content.	11

Table S1. Instrumental parameters for ESI, APCI and APPI

	ESI	APCI	APPI
Flow rate [μ L/min]	2.0	5.83	150.0
Dry gas temperature [$^{\circ}$ C]	200	350	350
Vaporizer temperature [$^{\circ}$ C]	-	350	350
Nebulizer gas pressure [bar]	1.0	2.5	2.5
Dry gas flow rate [L/min]	4.0	4.0	6.0
Capillary voltage [kV]	4.5	2.0	2.0
Corona needle current [nA]	-	40,000	-

Table S2. Observed product ions for selected m/z ratios after collision-induced dissociation (compound class O_6 ; DBE 14)

Elemental composition	MS ² product ion (m/z)	Calculated exact mass	Measured accurate mass	Error [ppm]	Elemental composition	MS ² product ion (m/z)	Calculated exact mass	Measured accurate mass	Error [ppm]
m/z 391					m/z 419				
C ₂₃ H ₁₉ O ₆		391.118165	391.11795	-0.55	C ₂₅ H ₂₃ O ₆		419.149465	419.15054	2.56
C ₂₂ H ₁₆ O ₆	391-CH ₃ (376)	376.09469	376.09523	1.44	C ₂₄ H ₂₀ O ₆	419-CH ₃ (404)	404.12599	404.12637	0.94
C ₂₁ H ₁₃ O ₆	376-CH ₃ (361)	361.071215	361.0716	1.07	C ₂₃ H ₁₇ O ₆	404-CH ₃ (389)	389.102515	389.10297	1.17
C ₂₁ H ₁₆ O ₅	376-CO (348)	348.099775	348.10008	0.88	C ₂₃ H ₂₀ O ₅	404-CO (376)	376.131075	376.13061	-1.24
C ₂₀ H ₁₃ O ₅	361-CO (333)	333.0763	333.07683	1.59	C ₂₂ H ₁₇ O ₅	389-CO (361)	361.1076	361.10832	1.99
	348-CH ₃ (333)	333.0763	333.07683	1.59		376-CH ₃ (361)	361.1076	361.10832	1.99
C ₁₉ H ₁₀ O ₅	333-CH ₃ (318)	318.052825	318.05382	3.13	C ₂₁ H ₁₄ O ₅	361-CH ₃ (346)	346.084125	346.08468	1.6
C ₂₀ H ₁₃ O ₄	361-CO ₂ (317)	317.081385	317.08178	1.25	C ₂₂ H ₁₇ O ₄	389-CO ₂ (345)	345.112685	345.11229	-1.14
C ₁₉ H ₁₃ O ₄	333-CO (305)	305.081385	305.08195	1.85	C ₂₁ H ₁₇ O ₄	361-CO (333)	333.112685	333.11207	-1.85
C ₁₉ H ₁₃ O ₃	333-CO ₂ (289)	289.08647	289.08700	1.83	C ₁₆ H ₁₁ O ₄	345-C ₆ H ₆ (267)	267.065735	267.06637	2.38
C ₁₄ H ₇ O ₄	317-C ₆ H ₆ (239)	239.034435	239.03494	2.11		333-C ₆ H ₆ (267)	267.065735	267.06637	2.38
	305-C ₆ H ₆ (239)	239.034435	239.03494	2.11	m/z 433				
m/z 405					C ₂₅ H ₂₂ O ₆	433-CH ₃ (418)	418.14164	418.14118	-1.1
C ₂₄ H ₂₁ O ₆		405.133815	405.13441	1.47	C ₂₄ H ₁₉ O ₆	418-CH ₃ (403)	403.118165	403.11693	-3.06
C ₂₃ H ₁₈ O ₆	405-CH ₃ (390)	390.11034	390.11087	1.36	C ₂₃ H ₁₆ O ₆	403-CH ₃ (388)	388.09469	388.09477	0.21
C ₂₂ H ₁₅ O ₆	390-CH ₃ (375)	375.086865	375.08735	1.29	C ₂₃ H ₁₉ O ₅	403-CO (375)	375.12325	375.12448	3.28
C ₂₂ H ₁₈ O ₅	390-CO (362)	362.115425	362.11599	1.56	C ₂₂ H ₁₆ O ₅	388-CO (360)	360.099775	360.09946	-0.87
C ₂₁ H ₁₂ O ₆	375-CH ₃ (360)	360.06339	360.06404	1.81	C ₂₃ H ₁₉ O ₄	403-CO ₂ (359)	359.128335	359.12821	-0.35
C ₂₁ H ₁₅ O ₅	362-CO (347)	347.09195	347.09241	1.33	C ₂₂ H ₁₉ O ₄	375-CO (347)	347.128335	347.12918	2.43
	375-CO (347)	347.09195	347.09241	1.33	C ₁₈ H ₁₃ O ₄	359-C ₅ H ₆ (293)	293.081385	293.08183	1.52
C ₂₀ H ₁₂ O ₅	360-CO (332)	332.068475	332.06914	2	C ₁₇ H ₁₃ O ₄	347-C ₅ H ₆ (281)	281.081385	281.08205	2.37
C ₂₁ H ₁₅ O ₄	375-CO ₂ (331)	331.097035	331.09736	0.98	C ₁₆ H ₁₀ O ₄	360-C ₆ H ₆ O (266)	266.05791	266.05862	2.67
C ₂₀ H ₁₅ O ₄	347-CO (319)	319.097035	319.09764	1.9		281-CH ₃ (266)	266.05791	266.05862	2.67
C ₂₀ H ₁₅ O ₃	347-CO ₂ (303)	303.10212	303.10263	1.68	C ₁₇ H ₁₃ O ₃	293-CO (265)	265.08647	265.08669	0.83
C ₁₅ H ₉ O ₄	331-C ₆ H ₆ (253)	253.050085	253.05073	2.55					
	319-C ₅ H ₆ (253)	253.050085	253.05073	2.55					
C ₁₄ H ₉ O ₃	303-C ₆ H ₆ (225)	225.05517	225.05578	2.71					
	253-CO (225)	225.05517	225.05578	2.71					

S-3

Table S3. Observed product ions for selected m/z ratios after collision-induced dissociation (compound class O₇; DBE 14)

Elemental composition	MS ² product ion (m/z)	Calculated exact mass	Measured accurate mass	Error [ppm]	Elemental composition	MS ² product ion (m/z)	Calculated exact mass	Measured accurate mass	Error [ppm]
m/z 421					m/z 449				
C ₂₄ H ₂₁ O ₇		421.128730	421.12940	1.59	C ₂₆ H ₂₃ O ₇		449.160030	449.16052	1.09
C ₂₃ H ₁₈ O ₇	421-CH ₃ (406)	406.105255	406.10588	1.54	C ₂₅ H ₂₂ O ₇	449-CH ₃ (434)	434.136555	434.1371	1.26
C ₂₂ H ₁₅ O ₇	406-CH ₃ (391)	391.081780	391.08237	1.51	C ₂₄ H ₁₉ O ₇	434-CH ₃ (419)	419.113080	419.11366	1.38
C ₂₁ H ₁₂ O ₇	391-CH ₃ (376)	376.058305	376.0589	1.58	C ₂₃ H ₁₆ O ₇	419-CH ₃ (404)	404.089605	404.0901	1.22
C ₂₁ H ₁₅ O ₆	391-CO (363)	363.086865	363.08748	1.69	C ₂₃ H ₁₉ O ₆	419-CO (391)	391.118165	391.11876	1.52
C ₂₂ H ₁₈ O ₅	406-CO ₂ (362)	362.115425	362.11598	1.53	C ₂₄ H ₂₂ O ₅	434-CO ₂ (390)	390.146725	390.14733	1.55
C ₂₀ H ₉ O ₇	376-CH ₃ (361)	361.034830	361.03557	2.05	C ₂₂ H ₁₃ O ₇	404-CH ₃ (389)	389.066130	389.06689	1.95
C ₂₀ H ₁₂ O ₆	376-CO (348)	348.063390	348.06400	1.75	C ₂₂ H ₁₆ O ₆	404-CO (376)	376.094690	376.09521	1.38
	363-CH ₃ (348)	348.063390	348.06400	1.75	C ₂₃ H ₁₉ O ₅	419-CO ₂ (375)	375.123250	375.12384	1.57
C ₂₁ H ₁₅ O ₅	362-CH ₃ (347)	347.091950	347.09257	1.79	C ₂₂ H ₁₆ O ₅	404-CO ₂ (360)	360.099775	360.10031	1.49
C ₂₀ H ₁₂ O ₅	376-CO ₂ (332)	332.068475	332.06905	1.73		375-CH ₃ (360)	360.099775	360.10031	1.49
C ₂₀ H ₁₅ O ₄	347-CO (319)	319.097035	319.09762	1.83	C ₂₁ H ₁₆ O ₅	376-CO (348)	348.099775	348.10037	1.71
C ₁₉ H ₁₂ O ₄	348-CO ₂ (304)	304.073560	304.07414	1.91	C ₂₁ H ₁₆ O ₄	376-CO ₂ (332)	332.104860	332.10505	0.57
C ₁₅ H ₇ O ₅	332-C ₃ H ₅ (267)	267.029350	267.02992	2.13		360-CO (332)	332.104860	332.10505	0.57
C ₁₅ H ₉ O ₄	319-C ₃ H ₆ (253)	253.050085	253.05073	2.55	C ₂₀ H ₁₆ O ₄	348-CO (320)	320.104860	320.10549	1.97
C ₁₄ H ₇ O ₄	332-C ₆ H ₉ O (239)	239.034435	239.03498	2.28	C ₁₆ H ₁₁ O ₅	348-C ₃ H ₅ (283)	283.060650	283.06123	2.05
	304-C ₃ H ₅ (239)	239.034435	239.03498	2.28	C ₁₆ H ₁₁ O ₄	332-C ₃ H ₅ (267)	267.065735	267.06629	2.08
	267-CO (239)	239.034435	239.03498	2.28	C ₁₅ H ₁₁ O ₃	332-C ₆ H ₉ O (239)	239.070820	239.0714	2.43
						267-CO (239)	239.070820	239.0714	2.43
m/z 435					m/z 463				
C ₂₅ H ₂₃ O ₇		435.144380	435.14492	1.24	C ₂₇ H ₂₇ O ₇		463.17568	463.17638	1.51
C ₂₄ H ₂₀ O ₇	435-CH ₃ (420)	420.120905	420.12147	1.34	C ₂₆ H ₂₄ O ₇	463-CH ₃ (448)	448.152205	448.15287	1.48
C ₂₃ H ₁₇ O ₇	420-CH ₃ (405)	405.097430	405.09804	1.51	C ₂₅ H ₂₁ O ₇	448-CH ₃ (433)	433.128730	433.12931	1.34
C ₂₂ H ₁₄ O ₇	405-CH ₃ (390)	390.073955	390.07460	1.65	C ₂₄ H ₂₁ O ₆	433-CO (405)	405.133815	405.13437	1.37
C ₂₃ H ₂₀ O ₅	420-CO ₂ (376)	376.131075	376.13161	1.42	C ₂₅ H ₂₄ O ₅	448-CO ₂ (404)	404.162375	404.16296	1.45
C ₂₁ H ₁₄ O ₆	390-CO (362)	362.079040	362.07954	1.38	C ₂₄ H ₂₁ O ₅	404-CH ₃ (389)	389.138900	389.13949	1.52
C ₂₂ H ₁₇ O ₅	376-CH ₃ (361)	361.107600	361.10813	1.47	C ₂₃ H ₁₈ O ₅	389-CH ₃ (374)	374.115425	374.11599	1.51
C ₂₁ H ₁₄ O ₅	390-CO ₂ (346)	346.084125	346.08476	1.83	C ₂₂ H ₁₅ O ₅	374-CH ₃ (359)	359.091950	359.09254	1.64

$C_{20}H_{14}O_5$	362-CO (334)	334.084125	334.08465	1.57	$C_{18}H_{15}O_5$	389-C ₆ H ₆ (311)	311.091950	311.09248	1.7
$C_{18}H_{13}O_5$	376-C ₅ H ₅ (311)	311.091950	311.09243	1.54	$C_{17}H_{13}O_5$	374-C ₆ H ₅ (297)	297.076300	297.07688	1.95
$C_{17}H_{12}O_5$	311-CH ₃ (296)	296.068475	296.06908	2.04	$C_{16}H_{13}O_4$	297-CO (269)	269.081385	269.08194	2.06
$C_{16}H_{11}O_5$	361-C ₆ H ₆ (283)	283.060650	283.06120	1.94	$C_{15}H_{13}O_2$	269-CO ₂ (225)	225.091555	225.09211	2.47
$C_{15}H_8O_5$	334-C ₅ H ₆ (268)	268.037175	268.03771	2	$C_{14}H_{10}O_2$	225-CH ₃ (210)	210.06808	210.06866	2.76
$C_{14}H_5O_4$	334-C ₆ H ₅ O (241)	241.050085	241.05064	2.3					

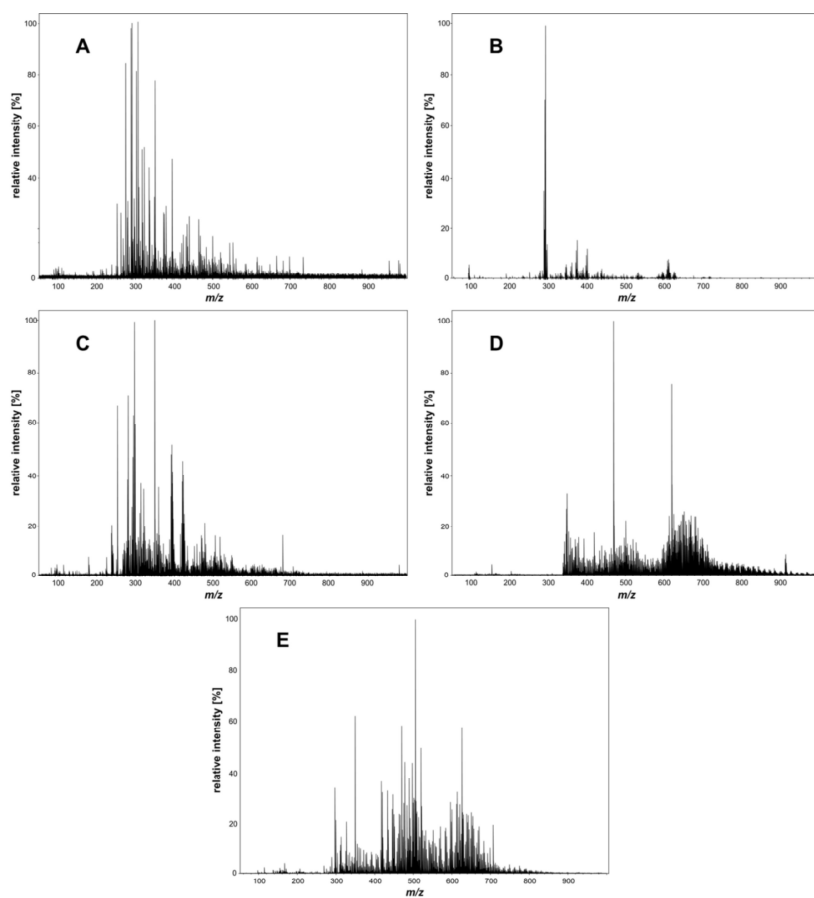


Figure S1. Mass spectra of lignin degradation products in negative ion-mode using (A) ESI at pH 3; (B) ESI at pH 7; (C) ESI at pH 10; (D) APCI; (E) dopant-assisted APPI

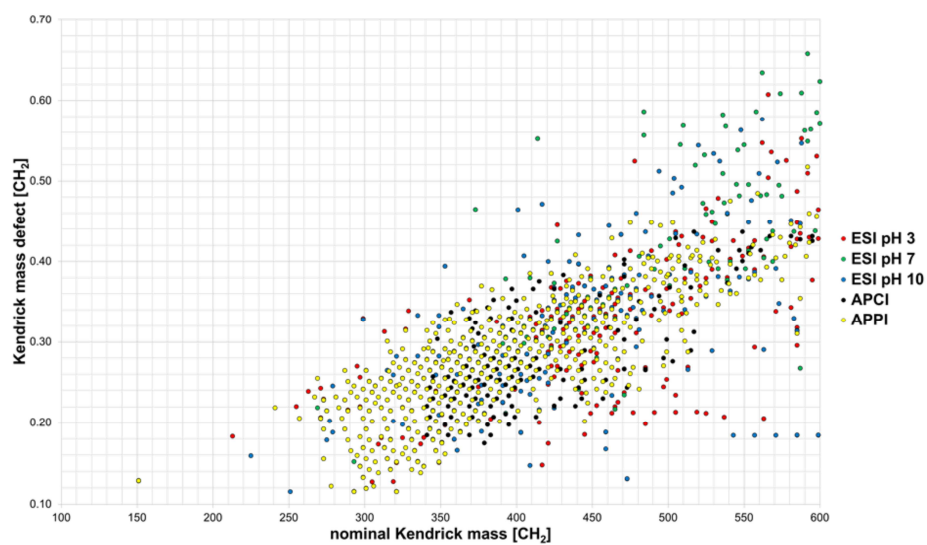


Figure S2. Enlarged areas of Kendrick mass defect plot.

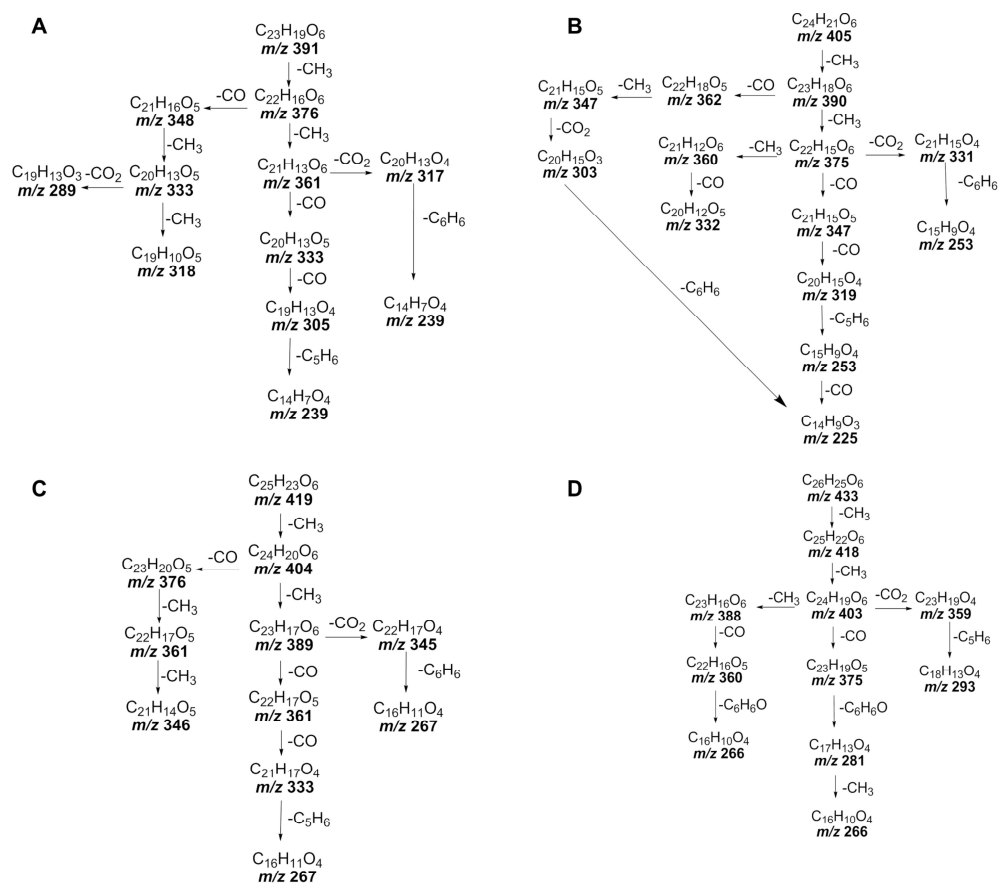


Figure S3. Linked fragmentation reactions for **A** m/z 391.11795, **B** m/z 405.13441, **C** m/z 419.15054, (D) m/z 433.16617.

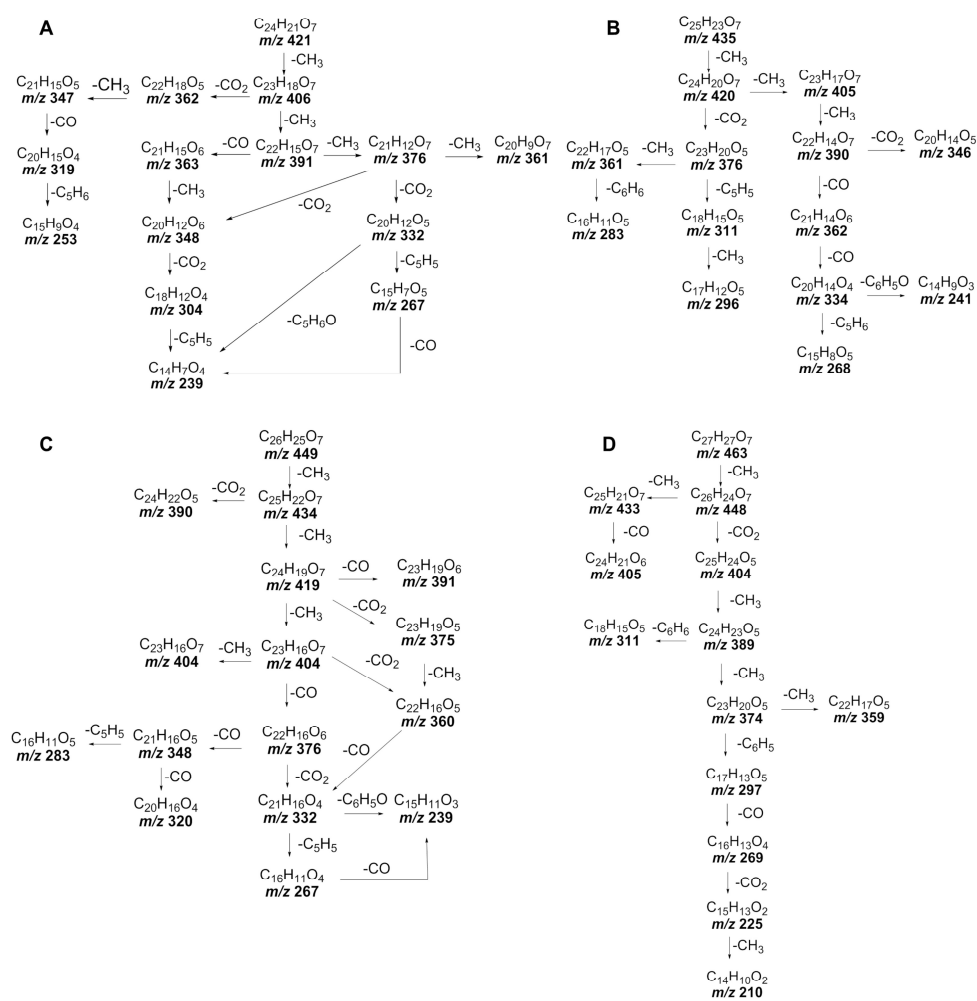


Figure S4. Linked fragmentation reactions for **A** m/z 421.12940, **B** m/z 435.14492, **C** m/z 449.16052, **D** m/z 463.17638

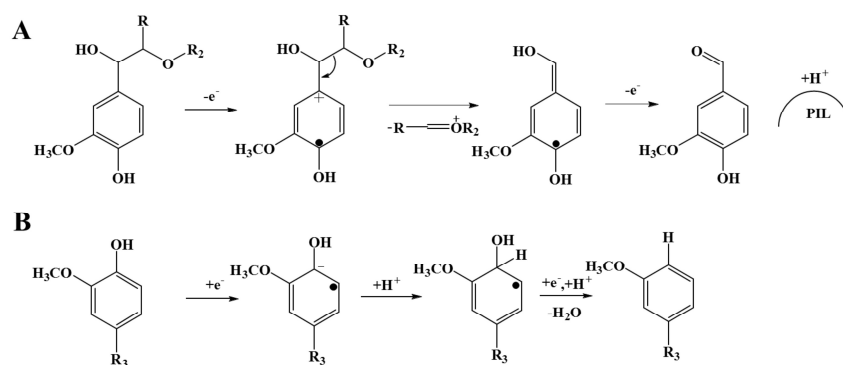


Figure S5. Proposed lignin degradation reactions by **A** electrochemical oxidation (adapted from Reichert, E.; Wintringer, R.; Volmer, D. A.; Hempelmann, R. *Phys. Chem. Chem. Phys.* **2012**, *14* (15), 5214-5221; reprinted with permission) and **B** electrochemical reduction.

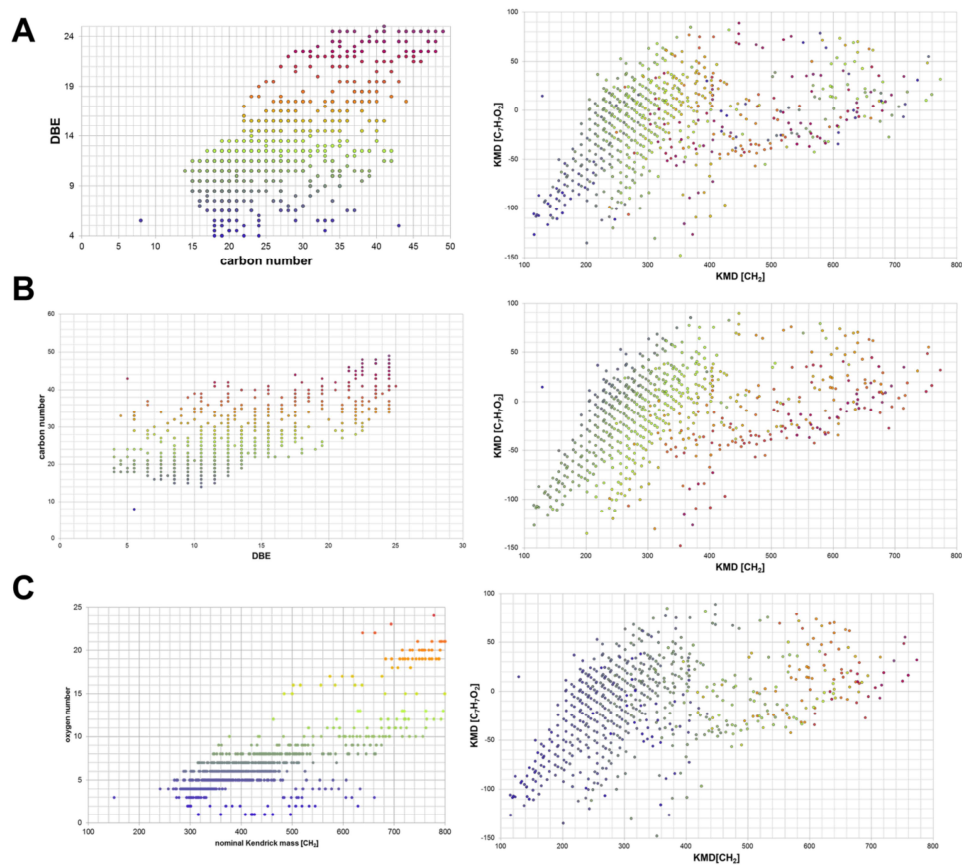
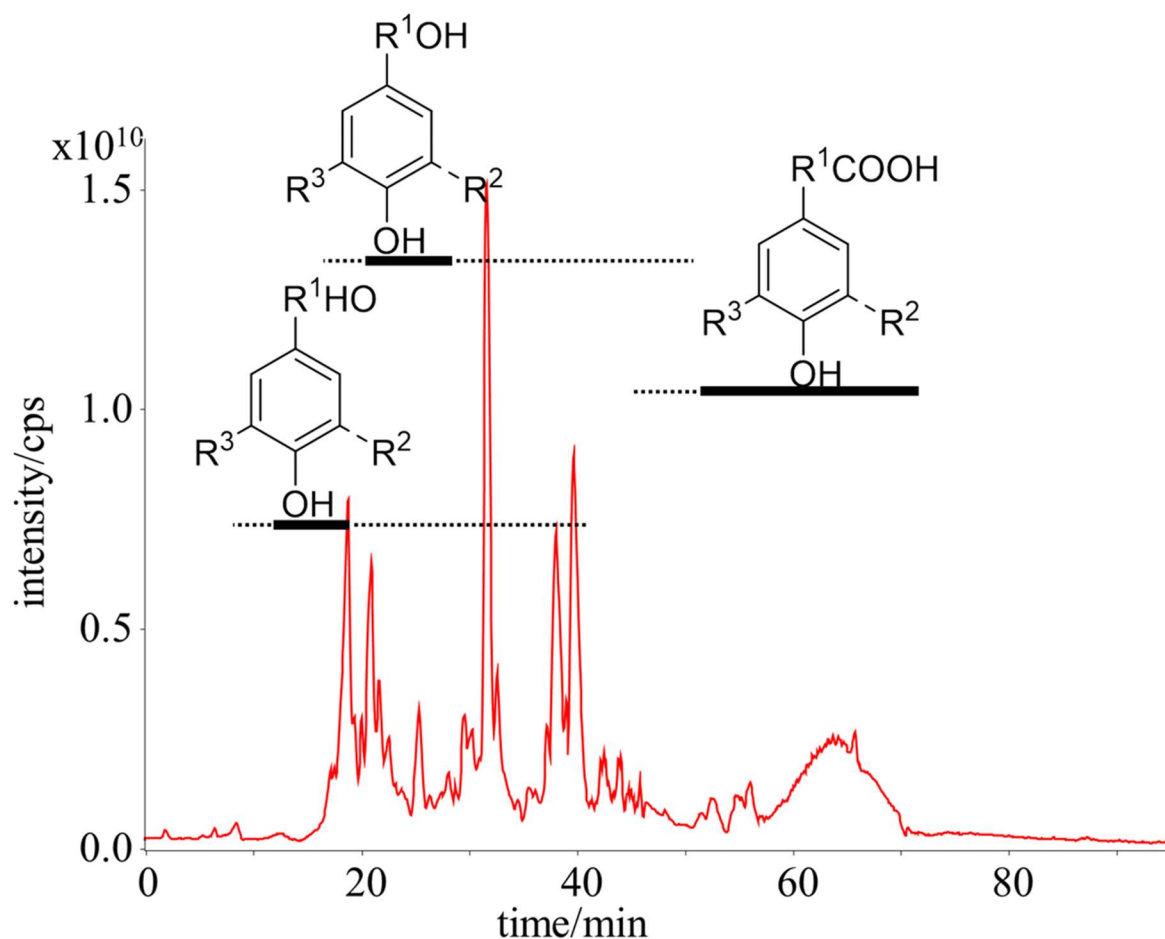


Figure S6. Comparison of enhanced mass defect filtering and **A** DBE, **B** carbon number, and **C** oxygen-content.

Publication 2

Novel Mixed-Mode Stationary Phases for Chromatographic Separation of Complex Mixtures of Decomposed Lignin

T.K.F. Dier, D. Rauber, J. Jauch, R. Hempelmann, D.A. Volmer
ChemistrySelect, **2017**, 2, 779-786



Reprinted with permission from T.K.F. Dier *et al.*, *ChemistrySelect*, **2017**, 2, 779-786. Copyright (2017) John Wiley & Sons, Inc.

Analytical Chemistry

Novel Mixed-Mode Stationary Phases for Chromatographic Separation of Complex Mixtures of Decomposed Lignin

Tobias K. F. Dier,^[a] Daniel Rauber,^[b] Johann Jauch,^[c] Rolf Hempelmann,^[b] and Dietrich A. Volmer^{*[a]}

Electrochemical degradation of lignin results in a large number of unknown products, formed by both oxidative and reductive decomposition pathways, which have previously been studied by direct mass spectrometry experiments without prior liquid chromatography separation, revealing the presence of many isobaric molecules. In this study, novel phosphonium-based ionic liquid stationary phases were synthesized and applied in conjunction with high resolution mass spectrometry, to further increase the resolving power of the analytical methodology.

The new stationary phases exhibited a wide range of interaction mechanisms in comparison to reversed-phase materials, and the preliminary results of this proof-of-concept study illustrated class-specific isolation and separation of the major chemical classes of the lignin breakdown products members into very specific retention time windows. For the investigated electrochemically decomposed lignin, the separations revealed predominantly aldehydes and alcohols, and also confirmed the presence of a significant number of isobars.

Introduction

Lignin is one of the most abundant natural polymers and a potential renewable source for aromatic compounds. Its unsystematic, polymeric structure mainly results from biocatalyzed coupling reactions of three monomeric units: *p*-coumaryl alcohol (H), coniferyl alcohol (G), syringyl alcohol (S) (Figure 1),^[1] Banoub *et al.* suggested that lignin polymers exhibit ordered rather than random structures,^[2] which enable sequencing techniques similar to those used for proteins or nucleic acids to characterize the complement of oligomers.^[3] Oxidative radical formation of the phenols followed by combinatorial radical couplings^[4,5] further increase the number of lignin oligomers. The relative proportion of individual monomeric units in the plant polymer depends both on the individual plant species and the nature of the regulating enzymes. For example, regulation of ferulate 5-hydroxylase (F5H) expression levels controls S-unit content,^[6] while *p*-coumarate 3-hydroxylase (C3H) modulates the number of H-

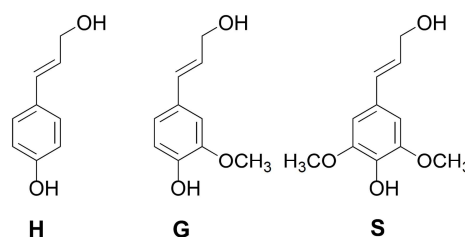


Figure 1. Chemical structure of lignin monomers: *p*-coumaryl alcohol (H), coniferyl alcohol (G), syringyl alcohol (S).

units.^[7] This highly flexible bio-catalyzed pathway provides various lignin polymers in different plants with different function.

Softwood lignin mainly consists of G-type units^[8] and is often found in gymnosperms^[9–14]. It is therefore a potential source for G-type monomers. On the other hand, hardwood lignin (e.g. from angiosperms) is a possible source for S-type monomers, due to its higher syringyl content.^[8,15–17] Lignin degradation processes for recovering valuable chemicals are a growing area of research; they are often applied for production of biofuels^[18–20], low molecular weight aromatic chemicals,^[18,21–24] fatty acids,^[25] polycyclic hydrocarbons^[26] and pyruvate/lactate.^[27] Electrochemical lignin degradation was established as a potential sustainable alternative to common degradation processes. The major benefit of electrochemical degradation is the availability of single electron transfer reactions that induce oxidative and reductive bond cleavages of the lignin polymer.^[28–32] Electrochemical decomposition yields both simple low molecular weight products as previously observed^[28,29,31] as well as complex distributions of combinatorial products.^[32] The latter mixtures have been classified using enhanced mass

[a] T. K. F. Dier, Prof. Dr. D. A. Volmer
Institute of Bioanalytical Chemistry
Saarland University
66123 Saarbrücken, Germany
Tel +49 681 302 3433
Fax +49 681 302 2963
E-mail: Dietrich.Volmer@mx.uni-saarland.de

[b] D. Rauber, Prof. Dr. R. Hempelmann
Institute of Physical Chemistry
Saarland University
66123 Saarbrücken, Germany

[c] Prof. Dr. J. Jauch
Institute of Organic Chemistry
Saarland University
66123 Saarbrücken, Germany

Supporting information for this article is available on the WWW under <http://dx.doi.org/10.1002/slct.201601673>

defect filtering techniques and high resolution mass spectrometry (HRMS),^[32] revealing significant hidden complexity from isobaric components.

Gas chromatography (GC) and high-performance liquid chromatography (HPLC) are often used for separation of lignin degradation products^[33–39] or identification and quantification of specific products or compound classes.^[21,22,24,27,40] GC is restricted to volatile monomers and thermally stable compounds and therefore only provides partial characterization of the lignin decomposition process, as shown for electrochemical degradation of lignin using protic ionic liquids.^[31] Nevertheless, new developments in GC, in particular pyrolysis GC-MS, have extended the application range to structural analyses of lignin^[41–43] and to investigation of lignin degradation processes.^[44–46] Despite these advances, liquid chromatography (LC) is generally more suitable to lignin breakdown product analysis than GC, considering the preferential formation of oligomers during electrochemical degradation.^[32] In addition, appropriate stationary phase selectivity is crucial for successful analysis of mixtures containing both diverse chemical functionalities as well as significant numbers of isomeric/isobaric molecules. Commercial reversed phase (RP), e.g. C₁₈^[34,35,47–50] and phenyl-based columns,^[33,35] have mainly been used for the separation of small lignin oligomers (< 1000 Da) based on hydrophobic interactions. However, the significant complexity of degraded lignin makes full baseline separations of many products difficult or even impossible, due to overlapping elution windows of single oligomeric states.^[33,35] Therefore, the ability to separate compound classes within small, characteristic elution windows is a desirable feature. Ionic liquids (IL), with their particular ability to dissolve large quantities of lignin^[51,52] as compared to common solvents,^[53–55] are promising stationary phase materials for separation of decomposed lignin. Armstrong *et al.* developed the first IL-based stationary phases for GC.^[56] The IL's dual interaction properties allowed separation of non-acidic/non-basic non-polar compounds in similar fashion to commercial stationary phases, and strong retention of more polar compounds, namely phenols or amines.^[56] Further developments of IL^[57–61] and their ability to function as solvent^[62] extended the application ranges in analytical applications and confirmed the unique separation behavior of IL. Sun *et al.* developed the first ionic liquid-based stationary phase for HPLC.^[63] The authors showed that imidazolium-based stationary phases were useful for separation of *n*-alkylbenzenes and halogenated benzenes, comparable to established RP chromatography. Phosphonium-based stationary phases revealed excellent separation of polar analytes^[64] and selective separation of non-polar analytes.^[65]

The aim of the present study was the development and application of IL-based stationary phases for analysis of complex lignin degradation products. Phosphonium-based IL were chosen here, because of the larger hydrophobicity of phosphonium *versus* imidazolium material, to also utilize the hydrophobic character of the decomposed lignin samples for separation.^[32] We focused on the evaluation of trioctylphosphonium-based stationary phases, which have not been applied to lignin analysis before. The synthesized stationary phases were comparable to commercial C₈ columns with respect to hydro-

phobicity and surface coverage. Importantly, however, the phosphonium-based stationary phases exhibited different selectivity as compared to RP phases. The columns permitted retention of both hydrophobic as well as polar analytes, readily providing separation of lignin-related aromatics depending on the functional groups attached to the core structures. Preliminary data for the highly complex, electrochemically decomposed lignin readily demonstrated product separations into distinct retention windows for aromatic aldehydes, alcohols and acids, thus highlighting that the phosphonium-based stationary phases exhibit significant potential for separation of these complex mixtures.

Results and Discussion

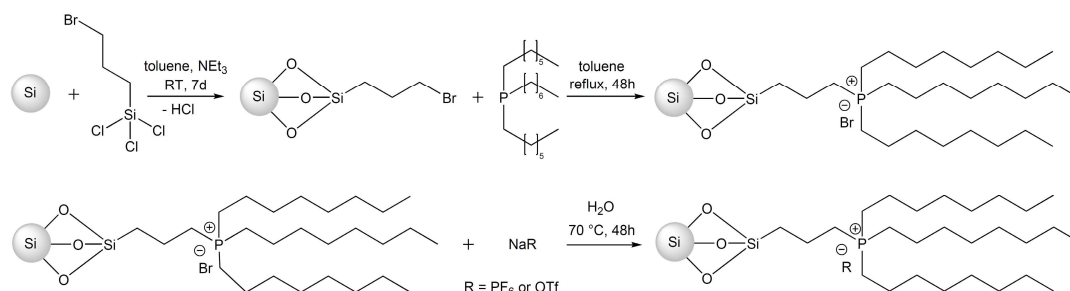
Preliminary characterization of phosphonium-based stationary phases

The reaction of trichloroalkylsilanes with porous SiO₂ particles is a common synthesis scheme for surface modifications.^[66,67] Si₃N₂ addition of bromoalkyl compounds to phosphines,^[68] which is also used for preparation of phosphonium-based ionic liquids,^[69,70] enables fast endcapping of trioctylphosphine. This procedure uses the linking agent (3-bromopropyl)trichlorosilane and therefore gives the resulting ionic liquid-based stationary phase cationic character. Scheme 1 illustrates the synthesis scheme.

Changing the anionic counterpart of the ionic liquid results in large differences of solvent interaction behavior of ionic liquids.^[71] Therefore, we expected equally significant differences of retention behavior on columns using this IL in the Jungheim/Engelhardt test as well as for the lignin compound classes (see below). The step-wise reaction was monitored by CHN analyses, where differences in carbon content for each intermediate and/or final product were indicative of a successful reaction. Preparation of the phosphonium-based stationary phases resulted in a carbon loading of 14.02% for SiPrPhoBr, 12.74% for SiPrPhoPF₆, and 13.35% for SiPrPhoOTf. The slight differences between these loadings (showing differences of surface coverages between the three counterions) resulted from partial anion exchange and/or incomplete washing of SiPrPhoBr. However, to demonstrate the proof-of-principle of applying phosphonium-based stationary phases to lignin analyses, we considered these small differences acceptable. The surface coverage *N* (in units of μmol m⁻²) was calculated according to Berendsen and de Galan:^[66]

$$N = C^{\%} / (1200 \cdot n_c - C^{\%} \cdot (M-1)) \cdot 10^6 / S \quad (1)$$

where *C*[%] is the carbon loading in percent, *n_c* the number of carbon atoms, *M* the molecular weight of the bonded silane molecule, and *S* the specific surface area of the silica material. Surface coverages of 1.85 μmol m⁻² (SiPrPhoBr), 1.55 μmol m⁻² (SiPrPhoPF₆), and 1.58 μmol m⁻² (SiPrPhoOTf) were achieved, which were comparable to previously reported numbers for ionic liquid-based stationary phases.^[72] To characterize RP phases, several standardized column tests are available^[73–77] and



Scheme 1. Schematic representation of the synthesis pathways for phosphonium-based stationary phases.

for this work, we chose the established Jungheim/Engelhardt test,^[66] the detailed results of which are summarized in the Supporting Information. Briefly, this characterization readily demonstrated that phosphonium stationary phases were comparable to C_8 phases with respect to hydrophobicity, but exhibited significant interactions with more polar components, namely phenol and *p*-ethylaniline. In addition, significant differences of interaction mechanisms of phosphonium materials were seen for different counter-anions.

Separation of lignin mixture

Initially, we chose a mixture of several lignin-related model monomers and dimers, to simulate a breakdown mixture of lignin, for the evaluation of the new stationary phases. LC-UV traces and LC-MS extracted ion current chromatograms (EICC) for the model mixture are shown in Figure 2 (additional data

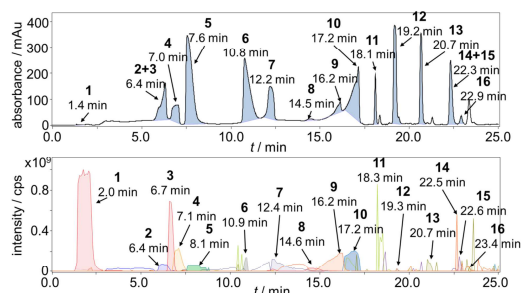


Figure 2. LC-UV chromatogram (top) and EICC (bottom) traces of lignin model mixture on a C_{18} column (regular gradient elution program (see Experimental, Supporting Information), flow rate 0.25 mL min^{-1} , UV detection at 254 nm, EIC mass tolerance $\pm 0.0005 \text{ u}$). Compounds: 1, DL-HPA; 2, vanillic acid; 3, HVA; 4, syringic acid; 5, 4-HB; 6, vanillin; 7, *p*-coumaric acid; 8, SA; 9, *trans* ferulic acid; 10, sinapic acid; 11, G- β -O-4-G; 12, SPA; 13, G- β -5-G; 14, S- β - β -S; 15, G- β - β -S; 16, G- β -G.

are illustrated in the Supporting Information, Figure S2). The separations were consistent with calculated Engelhardt param-

eters and separations reported in other studies.^[33,48] Importantly, the reversed phase C_{18} column did not provide separation according to the chemical functionalities but rather an unspecific hydrophobic separation, as expected, with resulting overlapping regions of aromatic acids, aromatic aldehydes and lignin dimers.

On the other hand, a clear chemical class-specific separation was achieved on the phosphonium-based stationary phases (Table 1). Such class separations are clearly helpful for separation of very complex samples. For aromatic aldehydes, retention was comparable to C_{18} and Sphinx. The primary difference to RP phases was seen in the retention behavior for aromatic acids. Long retention times for aromatic acids demonstrated the capability for strong hydrophilic interaction, as phosphonium-based IL have shown high H-bond basicity values;^[65] on the other hand, the capacity for significant hydrophobic interactions can be explained by increasing hydrophobic mass of the aromatic acids. As a result, all investigated phosphonium-based stationary phases were able to separate the aromatic acids from other chemical functionalities. Variable specificity was seen for the retention of the monomeric aldehydes, dimeric alcohols (G- β -O-4-G, G- β -5-G) and resinols (G- β - β -G, G- β - β -S, S- β - β -S), as a function of the nature of the anionic species. Overall, SiIPrPhoPF₆ exhibited chemical class separations without any overlapping regions of classes, demonstrating the potential of SiIPrPhoPF₆ for application to separation of the important low molecular weight products resulting from the lignin decomposition. This intricate separation behavior is common for ionic liquid-based stationary phases due to the large variety of available interactions,^[63,64,78,79] which can be readily modified.^[64,80] As expected for immobilized ionic liquids,^[79] however, the presence of additional ion exchange mechanisms^[81,82] reduces the concentration of counter-anions, which are responsible for part of the unique separation behavior of IL columns (see Supporting Information, Figure S3). Such reductions lead to minor retention time changes, as seen from the higher RSD values for the phosphonium-based stationary phases. Therefore, counter-anion regeneration should be considered in routine applications of these columns for consistent performance.

Table 1. Composition of lignin model mixture and retention times (t_r) for each standard on the various investigated stationary phases using regular gradient elution program (exceptions are indicated; retention times were determined from EICC traces).							
		Elemental formula	C_{18}^a	Sphinx ^b	SiIPrPhoBr ^b	SiIPrPhoPF ₆ ^b	SiIPrPhoOTf ^b
			t_r (\pm RSD) [min]				
Aromatic aldehydes	4-HB	$C_8H_6O_2$	8.1 (\pm 0.08)	7.7 (\pm 0.02)	6.9 (\pm 0.08)	12.4 (\pm 0.03)	15.7 (\pm 0.17)
	vanillin	$C_8H_8O_3$	10.9 (\pm 0.05)	10.8 (\pm 0.02)	8.2 (\pm 0.02)	13.8 (\pm 0.03)	14.8 (\pm 0.30)
	SA	$C_9H_{10}O_4$	14.6 (\pm 0.04)	14.2 (\pm 0.04)	9.5 (\pm 0.07)	14.2 (\pm 0.02)	14.0 (\pm 0.19)
	SPA	$C_{11}H_{12}O_4$	19.3 (\pm 0.03)	19.1 (\pm 0.00)	17.0 (\pm 0.12)	17.8 (\pm 0.15)	18.4 (\pm 0.12)
	vanillic acid	$C_8H_8O_4$	6.4 (\pm 0.08)	5.6 (\pm 0.07)	25.1 (\pm 0.08)	61.7 ^c (\pm 0.11)	60.1 ^c (\pm 0.25)
	syringic acid	$C_9H_{10}O_5$	7.1 (\pm 0.07)	6.8 (\pm 0.05)	26.4 (\pm 0.27)	60.7 ^c (\pm 0.34)	60.9 ^c (\pm 0.11)
	HVA	$C_9H_{10}O_4$	6.7 (\pm 0.02)	6.3 (\pm 0.03)	36.4 (\pm 0.16)	51.5 ^c (\pm 0.27)	53.9 ^c (\pm 0.30)
	<i>p</i> -coumaric acid	$C_9H_8O_3$	12.4 (\pm 0.06)	10.5 (\pm 0.22)	28.9 (\pm 0.10)	57.3 ^c (\pm 0.22)	55.9 ^c (\pm 0.26)
	<i>trans</i> ferulic acid	$C_{10}H_{10}O_4$	16.2 (\pm 0.02)	13.6 (\pm 0.09)	30.8 (\pm 0.17)	61.0 ^c (\pm 0.00)	59.4 ^c (\pm 0.26)
	sinapic acid	$C_{11}H_{12}O_5$	17.2 (\pm 0.12)	16.1 (\pm 0.07)	31.9 (\pm 0.04)	72.4 ^c (\pm 0.33)	72.8 ^c (\pm 0.24)
Aromatic acids	DL-HPA	$C_9H_{10}O_4$	2.0 (\pm 0.03)	2.2 (\pm 0.03)	40.0 (\pm 0.11)	73.0 ^c (\pm 0.14)	72.7 ^c (\pm 0.13)
	G- β -O4-G	$C_{20}H_{24}O_7$	18.3 (\pm 0.07)	18.1 (\pm 0.08)	14.4 (\pm 0.17)	20.7 (\pm 0.04)	16.2 (\pm 0.06)
	G- β -5-G	$C_{20}H_{22}O_6$	20.7 (\pm 0.04)	20.7 (\pm 0.03)	20.3 (\pm 0.08)	20.8 (\pm 0.06)	20.7 (\pm 0.12)
	G- β -G	$C_{20}H_{22}O_6$	23.4 (\pm 0.18)	23.0 (\pm 0.00)	21.8 (\pm 0.00)	22.7 (\pm 0.22)	22.2 (\pm 0.25)
	G- β -S	$C_{21}H_{24}O_7$	22.6 (\pm 0.03)	22.4 (\pm 0.02)	21.6 (\pm 0.11)	21.6 (\pm 0.00)	21.7 (\pm 0.11)
	S- β -S	$C_{22}H_{26}O_8$	22.5 (\pm 0.03)	22.2 (\pm 0.02)	21.2 (\pm 0.06)	21.2 (\pm 0.09)	21.0 (\pm 0.14)
Chromatographic parameters	<i>N</i>		3745	4491	417	1067	1069
	<i>G</i>		1.4	1.4	1.4	1.4	1.4
	$k_{0,1}$		19.7	16.8	24.0	44.9	42.6
	P_c		582	660	70	212	209

^a $n = 5$, ^b $n = 3$, ^c Single injection of corresponding analyte using modified gradient elution program ($n = 2$).

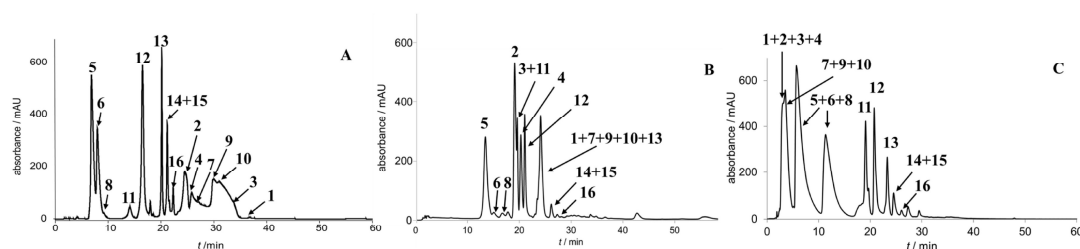


Figure 3. HPLC-UV chromatograms of a lignin model mixture on SiIPrPhoBr (regular gradient elution program (see Experimental [Supporting Information]); flow rate, 0.25 mL min⁻¹; UV detection at 254 nm): A, elution with untreated solvents; B, elution with acidified solvents (+1% acetic acid); C elution with buffered solvents (6.0 μ mol L⁻¹ sodium acetate). Compounds: 1, DL-HPA; 2, vanillic acid; 3, HVA; 4, syringic acid; 5, 4-HB; 6, vanillin; 7, *p*-coumaric acid; 8, SA; 9, *trans* ferulic acid; 10, sinapic acid; 11, G- β -O4-G; 12, SPA; 13, G- β -5-G; 14, S- β -S; 15, G- β -S; 16, G- β -G.

Another important aspect for separation of complex mixtures is the peak capacity of the stationary phase. This was critical here, as electrochemical lignin degradation yields convoluted mixtures of hundreds of independent m/z features.^[32] For gradient elution, the peak capacity P_c depends on the number of theoretical plates N , the gradient slope G and the retention factor of the last-eluting compound at the beginning of the gradient $k_{0,1}$, as shown by Neue:^[83]

$$P_c = 1 + N^{1/2}/4 \cdot \ln(k_{0,1})/(G + 1). \quad (2)$$

As expected, the calculated peak capacities for the investigated prototype stationary phases with immobilized IL were lower than the corresponding numbers obtained for the investigated commercial columns, because the custom-made columns exhibited significantly lower numbers of theoretical plates. Consequently, the large number of electrochemical

degradation products exceeded the peak capacity of the new stationary phases, making full baseline resolution of every component in the lignin mixtures impossible. Nevertheless, the unique chemical class selectivity described above demonstrated the phosphonium stationary phases' potential as separation medium for complex mixtures such as those studied here.

Figure 3 illustrates the major changes of retention and selectivity for simple aromatic aldehydes and acids for the SiIPrPhoBr phase upon changing mobile phase pH or eluent buffering system. Obviously, the ionization state of the organic acids shifted to protonated species after adjusting pH to acidic levels. Consequently, the interaction of the aromatic acids with the cationic phosphonium weakened, due to elimination of ion-ion interactions. However, the more hydrophobic, monomeric *trans*-3,5-dimethoxy-4-hydroxycinnamaldehyde and lignin-related dimers exhibited no significant change of retention.

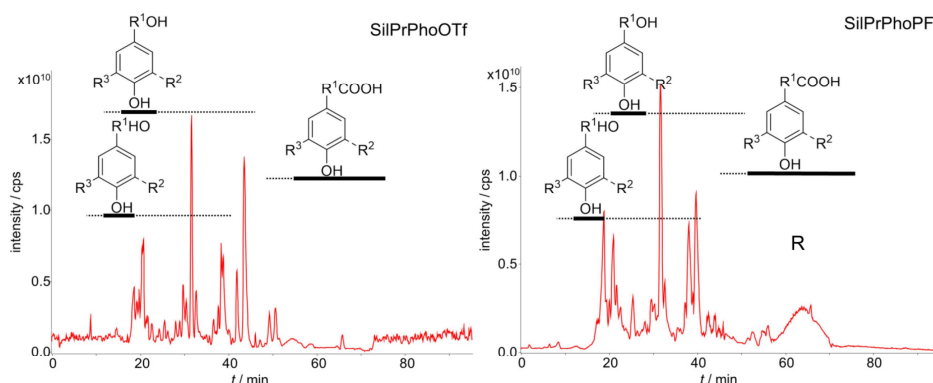


Figure 4. Base peak chromatograms for electrochemically degraded lignin using LC-HRMS (modified gradient elution program; see Experimental [Supporting Information]): (left) SilPrPhoOTf; (right) SilPrPhoPF₆. Solid line, region adopted from standards; dashed line, suggested extended range including expected dimer/trimer/oligomer contributors (range not verified with standards). R¹ = modified aromatic core (H,G,S) or modified aliphatic side chain; R² = hydrogen (H^{*}), OCH₃, or 5–5 bond to another modified aromatic core (H,G,S); R³ = hydrogen (H^{*}), OCH₃, or 5–5 bond to another modified aromatic core (H,G,S). (Note: the broad band between 58 and 70 min in the base peak chromatogram of SilPrPhoPF₆ was caused by an unknown contaminant at *m/z* 507.17906, not belonging to the lignin degradation process).

It can therefore be postulated that hydrophobic interactions dominate for more hydrophobic and/or larger aromatic molecules. Acetate buffer was used at concentration levels much lower than usually employed,^[64,84] which almost completely eliminated the interactions between aromatic acids and stationary phase, as seen for the acids' retention times (Figure 3c). The buffer also affected the retention of the smallest lignin aldehyde monomers. Importantly, however, the carboxylic acid modifier occupied the cationic interaction sites, so that only C₈ chains remained as sole interacting groups. Of course, the latter assumption requires experimental verification, but is in agreement with Alpert,^[85] who observed similar retention time reductions for acidic peptides after changing buffer concentration. Therefore, the results suggest strong interactions of aromatic acids and simple aromatic aldehydes with the ionic groups of the stationary phase. At the same time, the phosphonium stationary phases were very sensitive to changes in mobile phase compositions and pH.

Most one-dimensional chromatography separations are aimed at full separation of as many as possible of the relevant components.^[47,64,86] Obtaining distinct class-specific bands in narrow retention regions can be advantageous for the separation of very complex samples, however, to obtain information on composition and quantities of certain functionalities from mixtures that are largely uncharacterized. Therefore, the separations achieved by using phosphonium-based stationary phases with gradient elution were promising for application to analysis of complex mixtures containing organic components; *inter alia*, decomposed lignin, which has been shown to contain several thousand components.^[32] Furthermore, the new chromatography materials are potentially equally promising in preparative applications, for recovering valuable low molecular weight aromatic molecules from lignin

wastes after decomposition^[18–24,27] in technical waste valorization projects.

Separation of electrochemically decomposed lignin

We have previously shown that electrochemically decomposed lignin contains multiple compound classes, which were preliminarily categorized into several main classes after direct infusion HRMS experiments.^[32] In this study, the MS analysis was supported by HPLC experiments using the new phases SilPrPhoPF₆ and SilPrPhoOTf. The results demonstrated that the quality of the analysis of electrochemically decomposed lignin samples was significantly improved by this additional dimension of separation prior to MS. Importantly, the separation of aromatic aldehydes/alcohols and aromatic acids was considerably better for these two columns than for SilPrPhoBr, allowing improved classifications. Most of the degradation products were observed at retention times between 18 to 44 min for SilPrPhoOTf and 18 to 40 min for SilPrPhoPF₆ (Figure 4).

Compounds could therefore be readily classified into aromatic aldehydes or aromatic alcohols, by comparison with the retention time windows of the respective compound class from the lignin model mixture. The long retention times seen for some additional molecules in these analyses matched the results of our previous study,^[32] where the main fraction of decomposed lignin products were seen between *m/z* 200 and 600. Restricting the *m/z* window to low molecular weight products ($\leq 450 \text{ g mol}^{-1}$), thus specifically targeting lignin monomers or small molecules as is performed in most previous studies,^[18,21,23,26,27] provided a more detailed analysis of electrochemically decomposed lignin and improved the assignments to the previously verified class regions.

For a preliminary assessment of the yields of the products to support process analysis, the relative content of each

compound classes within the lignin sample was estimated by using normalized peak areas for each detected m/z feature (class assignments were based on van Krevelen plots and enhanced mass defect filtering as previously reported;^[32] the peak area versus retention time diagrams are summarized in the Supporting Information, Figure S4). Degradation products eluting between the simple aromatic aldehyde/alcohol region ($t_r=10$ -35 min) and acid region ($t_r=70$ -95 min) were classified as polyhydric aromatic alcohols; the predominantly hydrophobic content of the mixtures such as polycyclic hydrocarbons also eluted in this time window ($t_r=35$ -70 min). Importantly, the combination of LC-HRMS, novel immobilized ionic liquids and mass defect filtering revealed further product classes within the samples; e.g., resin acids (t_r [poly HC] ≥ 65 min), which were not previously visible in our direct infusion experiments^[32] (resin acids have been shown to be formed by Kraft pulping^[87] or fungal treatment of wood chips^[88]). In summary, the relative quantities in the electrochemically degraded lignin were approximately 9% aromatic aldehydes & alcohols (≤ 450 g mol⁻¹), 14% polyhydric, aromatic alcohols & hydrophobic content (≤ 450 g mol⁻¹), 7% aromatic acids (≤ 450 g mol⁻¹) and 70% oligomeric degradation products (>450 g mol⁻¹) in the investigated degradation mixture.

LC-HRMS experiments also clearly illustrated abundant isobaric components for several compound classes and showed that the homologous series differing in the number of $-\text{CH}_2$ units did not originate from a single but rather multiple series of compounds. The previously observed oxidized β -O-4 class, which exhibited a total of 12 m/z features,^[32] was in fact made up of three individual compound classes, as seen from the class-selective separation on the phosphonium-based columns; two of them belonging to aromatic aldehydes (retention times for SiPrPhoOTf: 18.1-18.7 min and 19.2-24.3 min), and one to aromatic acids (retention times for SiPrPhoOTf: 63.7-66.3 min). Isomers were not considered in our study, as differentiation of stereoisomers requires an additional dimension of separation, for example ion mobility spectrometry. In addition, the retention time differences for m/z features that varied only in the degree of saturation were small in comparison to standard RP conditions.^[89,90] The separation power of phosphonium-based stationary phases for molecules with small "2H" saturation differences was therefore poor, but still beneficial for the target aim of narrow retention time windows for group functionalities (a complete list of the oxidized β -O-4 class is shown in the Supporting Information, Table S1). In this study, dilution effects of the sample and the small number of transients in the FTICR analysis (to allow LC-HRMS with a sufficient number of data points across the chromatographic peaks) significantly reduced the number of detected m/z features. For example, for the oxidized β -O-4 class only 5 of the previous 12 m/z features were seen.^[32] A full comparison of LC-HRMS and direct injection HRMS analysis of electrochemically decomposed lignin was therefore not possible.

Conclusions

Phosphonium-based stationary phases were successfully synthesized in this study for separation of highly complex samples from lignin decomposition reactions, as demonstrated by successful separation of the abundant isobaric components of lignin products as well as by sorting chemical classes into distinct retention time regions. While the number of detected products using phosphonium-based LC-HRMS was comparable to previous direct infusion HRMS analyses, the additional separation dimension of unique selectivity allowed for a more precise compositional analysis of complex samples. Subsequent, more detailed classification of the regions revealed members of lignins, unsaturated unknowns and alkylphenolics belonging, in structural terms, to aromatic aldehydes, alcohols, polyhydric alcohols/hydrophobics or acids. Importantly, these materials provided an entirely different selectivity as compared to traditional reversed phase materials, with multiple available separation mechanisms, which benefited the deconvolution of highly complex samples containing multiple chemical functionalities. Our preliminary results illustrate the potential of these columns for purification, fractionation and preparative chromatography. In analytical applications, the phosphonium columns are potentially very useful for deconvoluting complex mixtures from "shotgun" ballistic degradation processes such as those encountered in electrochemical lignin degradation. Future studies will focus on the precise interaction mechanisms and the exact role of eluent additives, to improve performance and increase robustness of phosphonium-based stationary phases further. We will also work on up-scaled versions for preparative chromatography, to allow selective extraction of certain compound classes, which are useful in different sectors such as energy storage/production, bio-fuels or basic chemicals for further processing.

Supporting Information Summary

The Supporting Information contains the results of the Engelhardt test, results for lignin model compound analyses (chromatograms and percent distributions of low molecular weight chromatographic fractions) as well as a complete list of measured members of the β -O-4 class of the same sample. In addition, the experimental procedures used in this study and the synthesis routes for the dimeric standards are summarized in the Supporting Information.

Acknowledgements

This work was supported by the German Research Foundation (DFG VO 1355/4-1 and FTICR-MS Facility, DFG INST 256/356-1). We acknowledge technical support by Reiner Wintringer (Institute of Bioanalytical Chemistry), Christopher Scherrer and Ammar Tatlisu (Institute of Organic Chemistry). DAV acknowledges general research support by the Alfried Krupp von Bohlen und Halbach-Stiftung.

Conflict of Interest

The authors declare no conflict of interest.

Keywords: ionic liquids · lignin · liquid chromatography · mass spectrometry · sustainable chemistry

- [1] R. Vanholme, B. Demedts, K. Morreel, J. Ralph, W. Boerjan, *Plant Physiol.* **2010**, *153*, 895–905.
- [2] J. H. Banoub, M. Delmas, *J. Mass Spectrom.* **2003**, *38*, 900–903.
- [3] K. Morreel, O. Dima, H. Kim, F. Lu, C. Niculaes, R. Vanholme, R. Dauwe, G. Goeminne, D. Inze, E. Messens, et al., *Plant Physiol.* **2010**, *153*, 1464–1478.
- [4] J. Ralph, K. Lundquist, G. Brunow, F. Lu, H. Kim, P. F. Schatz, J. M. Marita, R. D. Hatfield, S. A. Ralph, J. H. Christensen, et al., *Phytochem. Rev.* **2004**, *3*, 29–60.
- [5] R. Hatfield, J. Ralph, J. H. Grabber, *Planta* **2008**, *228*, 919–928.
- [6] R. Franke, C. M. McMichael, K. Meyer, A. M. Shirley, J. C. Cusumano, C. Chappie, *Plant J.* **2000**, *22*, 223–234.
- [7] R. Franke, M. R. Hemm, J. W. Denault, M. O. Ruegger, J. M. Humphreys, C. Chappie, *Plant J.* **2002**, *30*, 47–59.
- [8] K. K. Pandey, *J. Appl. Polym. Sci.* **1999**, *71*, 1969–1975.
- [9] J. M. Bortiatynski, P. G. Hatcher, *Org. Geochem.* **1995**, *23*, 169–175.
- [10] D. Crawford, M. Barder, A. Pometto, R. Crawford, *Arch. Microbiol.* **1982**, *131*, 140–145.
- [11] J. Ke, D. Singh, X. W. Yang, S. L. Chen, *Biomass Bioenergy* **2011**, *35*, 3617–3626.
- [12] J. Peng, F. Lu, J. Ralph, *J. Agric. Food Chem.* **1998**, *46*, 553–560.
- [13] C. Saiz-Jimenez, J. W. de Leeuw, *Org. Geochem.* **1984**, *6*, 417–422.
- [14] C. H. Vane, *Int. Biodeterior. Biodegrad.* **2003**, *51*, 67–75.
- [15] C. Lapiere, B. Pollet, C. Rolando, *Res. Chem. Intermed.* **1995**, *21*, 397–412.
- [16] F. Lu, J. Ralph, *J. Agric. Food Chem.* **1998**, *46*, 547–552.
- [17] A. T. Martinez, G. Almendros, F. J. González-Vila, R. Fründ, *Solid State Nucl. Magn. Reson.* **1999**, *15*, 41–48.
- [18] R. Beauchet, F. Monteil-Rivera, J. M. Lavoie, *Bioresour. Technol.* **2012**, *121*, 328–334.
- [19] M. J. de la Torre, A. Moral, M. D. Hernández, E. Cabeza, A. Tijero, *Ind. Crops Prod.* **2013**, *45*, 58–63.
- [20] B. S. Dien, D. J. Miller, R. E. Hector, R. A. Dixon, F. Chen, M. McCaslin, P. Reisen, G. Sarath, M. A. Cotta, *Bioresour. Technol.* **2011**, *102*, 6479–6486.
- [21] Y. Chen, Y. Zheng, M. Li, X. Zhu, *Fuel Process. Technol.* **2015**, *134*, 46–51.
- [22] R. J. A. Gosselink, W. Teunissen, J. E. G. van Dam, E. de Jong, G. Gellerstedt, E. L. Scott, J. P. M. Sanders, *Bioresour. Technol.* **2012**, *106*, 173–177.
- [23] K. A. Jung, S. H. Woo, S.-R. Lim, J. M. Park, *Chem. Eng. J.* **2015**, *259*, 107–116.
- [24] D. Shen, J. Zhao, R. Xiao, S. Gu, *J. Anal. Appl. Pyrolysis* **2015**, *111*, 47–54.
- [25] E. Baltierra-Trejo, J. M. Sánchez-Yáñez, O. Buenrostro-Delgado, L. Márquez-Benavides, *Bioresour. Technol.* **2015**, *196*, 418–425.
- [26] J. Kong, M. He, J. A. Lercher, C. Zhao, *Chem. Commun.* **2015**, 3–6.
- [27] C. W. Johnson, G. T. Beckham, *Metab. Eng.* **2015**, *28*, 240–7.
- [28] H. Zhu, L. Wang, Y. Chen, G. Li, H. Li, Y. Tang, P. Wan, *RSC Adv.* **2014**, *4*, 29917–29924.
- [29] D. Shao, J. Liang, X. Cui, H. Xu, W. Yan, *Chem. Eng. J.* **2014**, *244*, 288–295.
- [30] D. Schmitt, C. Regenbrecht, M. Hartmer, F. Stecker, S. R. Waldvogel, *Beilstein J. Org. Chem.* **2015**, *11*, 473–480.
- [31] E. Reichert, R. Wintringer, D. A. Volmer, R. Hempelmann, *Phys. Chem. Chem. Phys.* **2012**, *14*, 5214–5221.
- [32] T. K. F. Dier, K. Egele, V. Fossog, R. Hempelmann, D. A. Volmer, *Anal. Chem.* **2016**, *88*, 1328–1335.
- [33] T. M. Jarrell, C. L. Marcum, H. Sheng, B. C. Owen, C. J. O'Lenick, H. Maraua, J. J. Bozell, H. I. Kenttämaa, *Green Chem.* **2014**, *16*, 2713–2727.
- [34] L. Sun, R. G. M. Spencer, P. J. Hernes, R. Y. Dyda, K. Mopper, *Limnol. Ocean. Methods* **2015**, *13*, 1–8.
- [35] B. C. Owen, L. J. Hauptert, T. M. Jarrell, C. L. Marcum, T. H. Parsell, M. M. Abu-Omar, J. J. Bozell, S. K. Black, H. I. Kenttämaa, *Anal. Chem.* **2012**, *84*, 6000–6007.
- [36] E. Lazzari, T. Schena, C. T. Primaz, G. P. da Silva Maciel, M. E. Machado, C. A. L. Cardoso, R. A. Jacques, E. B. Caramão, *Ind. Crops Prod.* **2016**, *83*, 529–536.
- [37] D. Tamburini, J. J. Lucejko, E. Ribechini, M. P. Colombini, *J. Mass Spectrom.* **2015**, *50*, 1103–1113.
- [38] Z. Ma, Q. Sun, J. Ye, Y. Qiufang, C. Zhao, *J. Anal. Appl. Pyrolysis* **2015**, *117*, 116–124.
- [39] M. Mukhopadhyay, R. Banerjee, *Agric. Res.* **2015**, *4*, 309–318.
- [40] D. R. Vardon, M. A. Franden, C. W. Johnson, E. M. Karp, M. T. Guarnieri, J. G. Linger, M. J. Salm, T. J. Strathmann, G. T. Beckham, *Energy Environ. Sci.* **2015**, *8*, 617–628.
- [41] T. Ohra-Aho, F. J. B. Gomes, J. L. Colodette, T. Tamminen, *J. Anal. Appl. Pyrolysis* **2013**, *101*, 166–171.
- [42] J. S. Lupoi, S. Singh, R. Parthasarathi, B. A. Simmons, R. J. Henry, *Renew. Sustain. Energy Rev.* **2015**, *49*, 871–906.
- [43] S. Constant, H. L. J. Wienk, A. E. Frissen, P. de Peinder, R. Boelens, D. S. van Es, R. J. H. Grisel, B. M. Weckhuysen, W. J. J. Huijgen, R. J. A. Gosselink, et al., *Green Chem.* **2016**, *18*, 2651–2665.
- [44] W. Mu, H. Ben, A. Ragauskas, Y. Deng, *Bioenergy Res.* **2013**, *6*, 1183–1204.
- [45] L. El Fels, L. Lemee, A. Ambles, M. Hafidi, *Int. Biodeterior. Biodegrad.* **2014**, *92*, 26–35.
- [46] M. Brebu, T. Tamminen, I. Spiridon, *J. Anal. Appl. Pyrolysis* **2013**, *104*, 531–539.
- [47] S. C. Gouveia, P. C. Castilho, *Food Res. Int.* **2012**, *45*, 362–368.
- [48] E. Kiyota, P. Mazzafera, A. C. H. F. Sawaya, *Anal. Chem.* **2012**, *84*, 7015–20.
- [49] I. Nicoletti, D. Martini, A. De Rossi, F. Taddei, M. G. D'Egidio, D. Corradini, *J. Agric. Food Chem.* **2013**, *61*, 11800–11807.
- [50] J. Pan, J. Fu, S. Deng, X. Lu, *Energy Fuels* **2014**, *28*, 1380–1386.
- [51] Y. Pu, N. Jiang, A. Ragauskas, *J. Wood Chem. Technol.* **2007**, *27*, 23–33.
- [52] D. Glas, C. Van Doorslaer, D. Depuydt, F. Liebner, T. Rosenau, K. Binnemans, D. E. De Vos, *J. Chem. Technol. Biotechnol.* **2015**, *90*, 1821–1826.
- [53] Y. Ni, Q. Hu, *J. Appl. Polym. Sci.* **1995**, *57*, 1441–1446.
- [54] Q. Wang, K. Chen, J. Li, G. Yang, S. Liu, J. Xu, *BioResources* **2011**, *6*, 3034–3043.
- [55] C. Schuerch, *J. Am. Chem. Soc.* **1952**, *74*, 5061–5067.
- [56] D. W. Armstrong, L. He, Y. S. Liu, *Anal. Chem.* **1999**, *71*, 3873–3876.
- [57] M. Qi, D. W. Armstrong, *Anal. Bioanal. Chem.* **2007**, *388*, 889–899.
- [58] J. L. Anderson, D. W. Armstrong, *Anal. Chem.* **2005**, *77*, 6453–6462.
- [59] C. F. Poole, S. K. Poole, *J. Sep. Sci.* **2011**, *34*, 888–900.
- [60] C. Ragonese, P. Q. Tranchida, D. Sciarone, L. Mondello, *J. Chromatogr. A* **2009**, *1216*, 8992–8997.
- [61] J. L. Anderson, D. W. Armstrong, *Anal. Chem.* **2003**, *75*, 4851–4858.
- [62] A. Berthod, L. He, D. W. Armstrong, *Chromatographia* **2001**, *53*, 63–68.
- [63] Y. Sun, B. Cabovska, C. E. Evans, T. H. Ridgway, A. M. Stalcup, *Anal. Bioanal. Chem.* **2005**, *382*, 728–734.
- [64] H. Qiu, E. Wanigasekara, Y. Zhang, T. Tran, D. W. Armstrong, *J. Chromatogr. A* **2011**, *1218*, 8075–8082.
- [65] D. W. Armstrong, Z. S. Breitbach, *Anal. Bioanal. Chem.* **2008**, *390*, 1605–1617.
- [66] G. E. Berendsen, L. de Galan, *J. Liq. Chromatogr.* **1978**, *1*, 561–586.
- [67] L. C. Sander, S. A. Wise, C. H. Lochmüller, *CRC Cr. Rev. Anal. Chem.* **1987**, *18*, 299–415.
- [68] A. W. Hofmann, *Phil. Trans. R. Soc. Lond.* **1860**, *150*, 449–496.
- [69] C. J. Bradaric, A. Downard, C. Kennedy, A. J. Robertson, Y. Zhou, *Green Chem.* **2003**, *5*, 143–152.
- [70] F. Atefi, M. T. Garcia, D. Singer, P. J. Scammells, *Green Chem.* **2009**, *11*, 1595–1604.
- [71] L. Crowhurst, P. R. Mawdsley, J. M. Perez-Arlandis, P. A. Salter, T. Welton, *Phys. Chem. Chem. Phys.* **2003**, *5*, 2790–2794.
- [72] M. Zhang, X. Liang, S. Jiang, H. Qiu, *TrAC - Trends Anal. Chem.* **2014**, *53*, 60–72.
- [73] H. Engelhardt, M. Arangio, T. Lobert, *LC GC* **1997**, *15*, 856–866.
- [74] H. Engelhardt, M. Jungheim, *Chromatographia* **1990**, *29*, 59–68.
- [75] A. P. Goldberg, *Anal. Chem.* **1982**, *345*, 342–345.
- [76] U. D. Neue, B. A. Alden, T. H. Walter, *J. Chromatogr. A* **1999**, *849*, 87–100.
- [77] N. Tanaka, K. Kimata, K. Iwaguchi, S. Onishi, K. Jinno, R. Eksteen, K. Hosoya, M. Araki, *J. Chromatogr. Sci.* **1989**, *27*, 721–728.
- [78] H. Qiu, A. K. Mallik, M. Takafuji, X. Liu, S. Jiang, H. Ihara, *Anal. Chim. Acta* **2012**, *738*, 95–101.



- [79] H. Qiu, A. K. Mallik, M. Takafuji, S. Jiang, H. Ihara, *Analyst* **2012**, *137*, 2553–2555.
- [80] Q. Wang, G. A. Baker, S. N. Baker, L. A. Colón, *Analyst* **2006**, *131*, 1000–1005.
- [81] H. Qiu, S. Jiang, X. Liu, *J. Chromatogr. A* **2006**, *1103*, 265–270.
- [82] A. Berthod, M. J. Ruiz-Ángel, S. Carda-Broch, *J. Chromatogr. A* **2008**, *1184*, 6–18.
- [83] U. D. Neue, *J. Chromatogr. A* **2008**, *1184*, 107–130.
- [84] H. Qiu, Q. Jiang, Z. Wei, X. Wang, X. Liu, S. Jiang, *J. Chromatogr. A* **2007**, *1163*, 63–69.
- [85] A. J. Alpert, *Anal. Chem.* **2008**, *80*, 62–76.
- [86] H. Qiu, Q. Jiang, X. Liu, S. Jiang, *Chromatographia* **2008**, *68*, 167–171.
- [87] K. P. Kringstad, K. Lindström, *Environ. Sci. Technol.* **1984**, *18*, 236 A–248 A.
- [88] L. Levin, L. Villalba, V. Da Re, F. Forchiassin, L. Papinutti, *Process Biochem.* **2007**, *42*, 995–1002.
- [89] M. I. Avelano, M. VanRollins, L. A. Horrocks, *J. Lipid Res.* **1983**, *24*, 83–93.
- [90] C. M. Seppanen, A. S. Csallany, *J. Am. Oil Chem. Soc.* **2001**, *78*, 1253–1260.

Submitted: November 3, 2016

Accepted: January 5, 2017



Supporting Information

© Copyright Wiley-VCH Verlag GmbH & Co. KGaA, 69451 Weinheim, 2016

Novel Mixed-Mode Stationary Phases for Chromatographic Separation of Complex Mixtures of Decomposed Lignin

Tobias K. F. Dier, Daniel Rauber, Johann Jauch, Rolf Hempelmann, and Dietrich A. Volmer*

Supporting Information

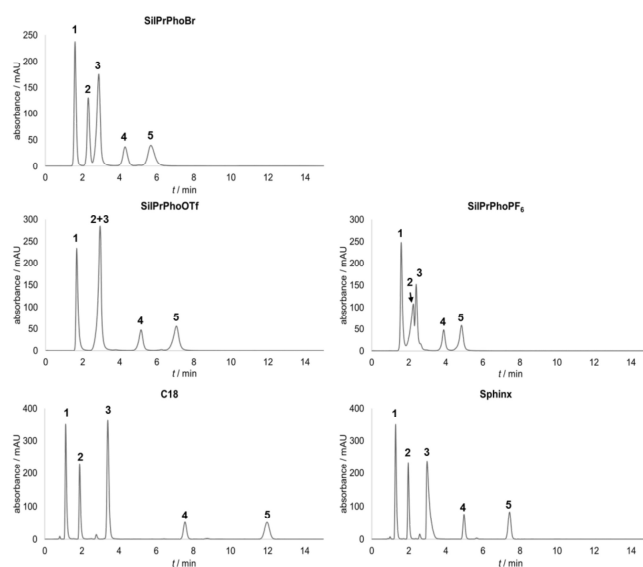
Table of content:

Figure S1. Chromatograms for different stationary phases using the Engelhardt test mixture/conditions: 1, uracil; 2, phenol; 3, <i>p</i> -ethylaniline; 4, toluene; 5, ethylbenzene.	2
Figure S2. HPLC-UV chromatograms (left) and EIC traces (right) for the lignin model mixture using selected columns. Regular gradient elution: acetonitrile/H ₂ O (10:90 v/v); flow rate 0.25 mL/min, UV detection at 254 nm; EIC mass tolerance, \pm 0.0005 u. Compounds: 1, DL-HPA; 2, vanillic acid; 3, HVA; 4, syringic acid; 5, 4-HB; 6, vanillin; 7, <i>p</i> -coumaric acid; 8, SA; 9, <i>trans</i> ferulic acid; 10, sinapic acid; 11, G- β -O-4-G; 12, SPA; 13, G- β -5-G; 14, S- β - β -S; 15, G- β - β -S; 16, G- β - β -G.	3
Figure S3. HPLC-UV chromatograms of lignin standard mixture using SilPrPhoBr (top-left), SilPrPhoOTf (top-right) and SilPrPhoPF ₆ (bottom-left). Upper half showing UV chromatogram at 254nm, lower half showing EIC trace of the appropriate counter-anion.....	4
Figure S4. Percent distributions of low molecular weight fractions along the HPLC-HRMS time scale using the modified gradient elution: lignins (Lig), unsaturated unknowns (unsat. UK), alkylphenolics (AP), saturated unknowns (sat. UK), tannins (Tan), polycyclic hydrocarbons (poly HC), cyclic alkanes (CA), and not classifiable compounds <i>via</i> van-Krevelen plot and enhanced mass defect filtering classification (n.c.).....	4
Figure S5. Chemical structures of commercial and custom-made reference compounds. Compounds: 1, DL-HPA; 2, vanillic acid; 3, HVA; 4, syringic acid; 5, 4-HB; 6, vanillin; 7, <i>p</i> -coumaric acid; 8, SA; 9, <i>trans</i> ferulic acid; 10, sinapic acid; 11, G- β -O-4-G; 12, SPA; 13, G- β -5-G; 14, S- β - β -S; 15, G- β - β -S; 16, G- β - β -G.....	6
Table S1. Jungheim/Engelhardt parameters for each investigated stationary phase (EB=ethylbenzene, T=toluene, P=phenol, EA= <i>p</i> -ethylaniline).....	2
Table S2. Retention times for members of the β -O-4 class on SilPrPhoOTf and SilPrPhoPF ₆ stationary phases using HPLC-HRMS modified gradient elution. EIC mass tolerance \pm 0.0005 u (nd=not detected).....	5
Scheme S1. Synthesis of starting materials coniferyl alcohol 20 and sinapyl alcohol 23.....	7
Scheme S2. Synthesis of dilignols 11, 13, 14, 15 and 16.....	9
Experimental Section	12
References	13

Jungheim/Engelhardt test

Table S1. Jungheim/Engelhardt parameters for the investigated stationary phases (EB=ethylbenzene, T=toluene, P=phenol, EA=*p*-ethylaniline).

	<i>N</i> (EB)	<i>k</i> (EB)	α (P/T)	α (T/EB)	<i>A_s</i> (EA)
SilPrPhoBr	417 ^a	2.55	3.82	1.52	1.0
SilPrPhoOTf	1069 ^a	3.22	2.74	1.55	0.83
SilPrPhoPF ₆	1067 ^a	2.05	3.45	1.41	1.67
C ₁₈	3745 ^a	9.59	8.61	1.69	1.03
Sphinx	4491 ^a	4.77	5.4	1.67	2.4

^anumber of theoretical plates for 150 mm column length.**Figure S1.** Chromatograms for different stationary phases using the Engelhardt test mixture/conditions: 1, uracil; 2, phenol; 3, *p*-ethylaniline; 4, toluene; 5, ethylbenzene.

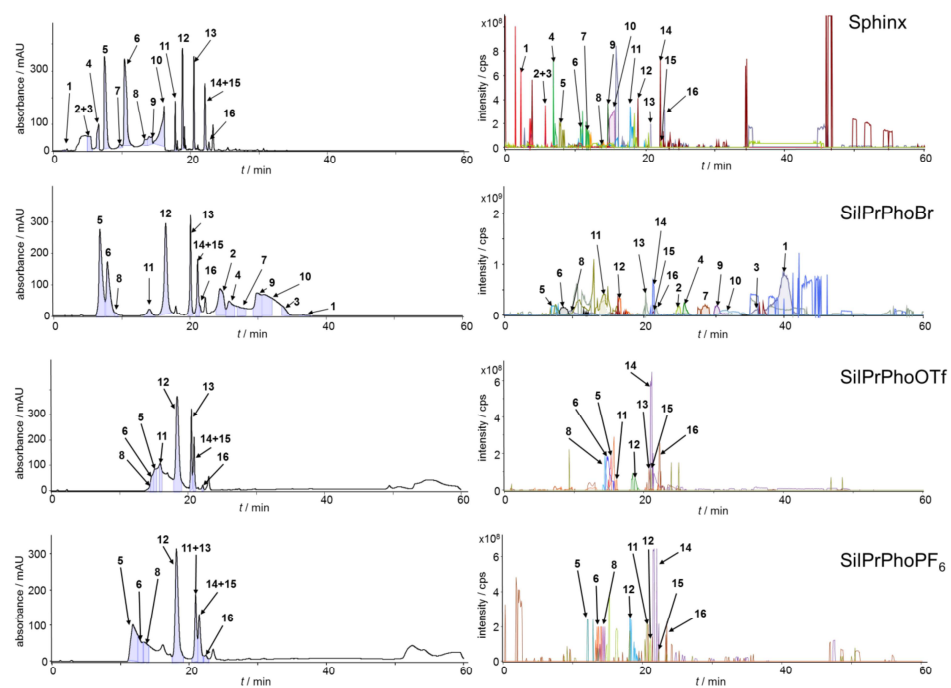


Figure S2. HPLC-UV chromatograms (left) and LC-MS (EIC) traces (right) for the lignin model mixture using selected columns. Regular gradient elution: acetonitrile/H₂O (10:90 v/v); flow rate 0.25 mL/min, UV detection at 254 nm; EIC mass tolerance, ± 0.0005 u. Compounds: **1**, DL-HPA; **2**, vanillic acid; **3**, HVA; **4**, syringic acid; **5**, 4-HB; **6**, vanillin; **7**, *p*-coumaric acid; **8**, SA; **9**, *trans* ferulic acid; **10**, sinapic acid; **11**, G- β -O-4-G; **12**, SPA; **13**, G- β -5-G; **14**, S- β -S; **15**, G- β -S; **16**, G- β -G.

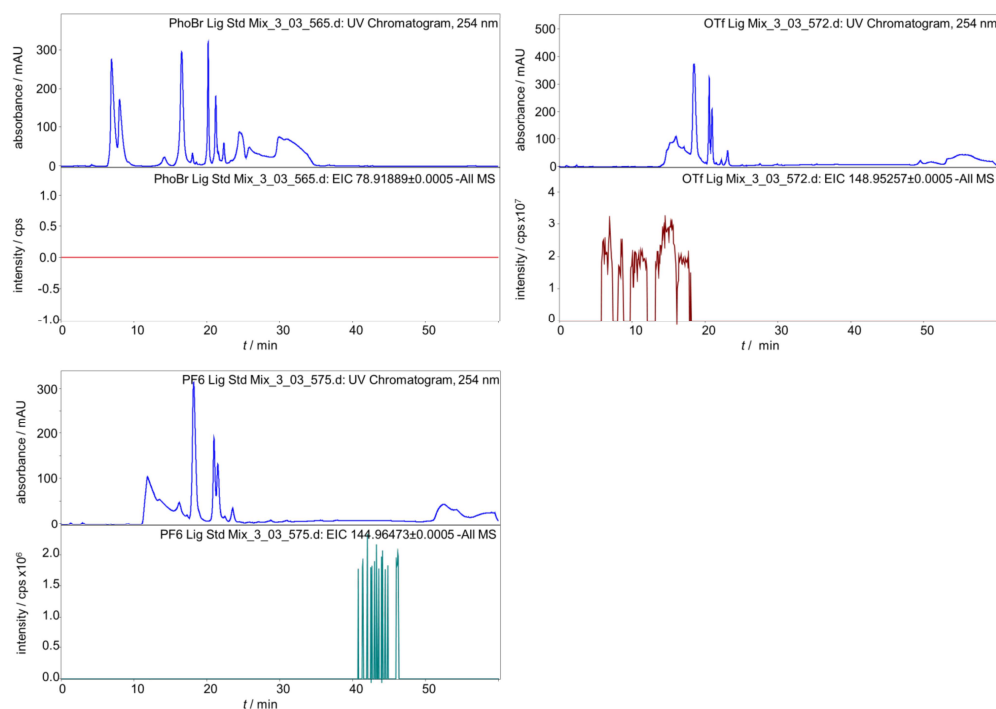


Figure S3. HPLC-UV chromatograms of lignin standard mixture using SilPrPhoBr (top-left), SilPrPhoOTf (top-right) and SilPrPhoPF₆ (bottom-left). Upper half showing UV chromatogram at 254 nm, lower half showing EIC trace of the appropriate counter-anion.

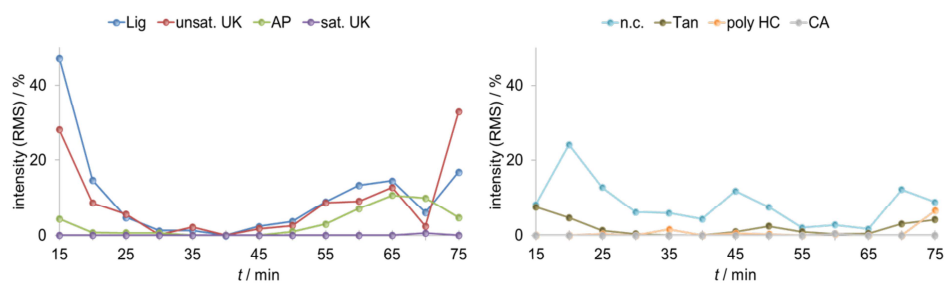


Figure S4. Percent distributions of low molecular weight fractions along the LC-HRMS time scale using the modified gradient elution: lignins (Lig), unsaturated unknowns (unsat. UK), alkylphenolics (AP), saturated unknowns (sat. UK), tannins (Tan), polycyclic hydrocarbons (poly HC), cyclic alkanes (CA), and not classifiable compounds *via* van-Krevelen plot and enhanced mass defect filtering classification (n.c.).

Table S2. Retention times for members of the β -O-4 class on SiPrPhoOTf and SiPrPhoPF₆ stationary phases using LC-HRMS modified gradient elution. EIC m/z tolerance: ± 0.0005 u (nd=not detected).

ion formula	calculated exact mass	SiPrPhoOTf			SiPrPhoPF ₆		
		t_r [min]	measured accurate mass	error [ppm]	t_r [min]	measured accurate mass	error [ppm]
C ₁₅ H ₁₁ O ₆	287.056112	nd			nd.		
C ₁₆ H ₁₃ O ₆	301.071762	nd			nd.		
C ₁₈ H ₁₇ O ₆	329.103062	nd			nd.		
C ₁₉ H ₁₉ O ₆	343.118712	18.7	343.11866	-0.15	19.1	343.11876	0.13
		19.2	343.11863	-0.23	20.1	343.11870	-0.03
		66.3	343.11874	0.09	70.5	343.11866	-0.15
C ₂₀ H ₂₁ O ₆	357.134362	18.5	357.13440	0.11	18.6	357.13437	0.04
		20.5	357.13398	-1.06	20.0	357.13438	0.04
		65.4	357.13436	0.01	65.8	357.13397	-1.10
C ₂₁ H ₂₃ O ₆	371.150012	18.1	371.15001	0.12	18.3	371.14997	-0.10
		24.3	371.15039	1.03	19.9	371.15040	1.06
		63.7	371.14996	-0.14	70.5	371.14977	-0.66
C ₂₂ H ₂₅ O ₆	385.165662	nd			nd		
C ₂₃ H ₂₇ O ₆	399.181312	nd			nd		
C ₂₄ H ₂₉ O ₆	413.196962	65.6	413.19696	0.01	71.1	413.19666	-0.87
C ₂₅ H ₃₁ O ₆	427.212612	nd			n.d		
C ₂₆ H ₃₃ O ₆	441.228262	nd			nd		
C ₂₇ H ₃₅ O ₆	455.243912	62.9	455.24394	0.05	72.5	455.24412	0.45
C ₁₅ H ₁₃ O ₆	289.071762	nd			nd		
C ₁₆ H ₁₅ O ₆	303.087412	nd			nd		
C ₁₈ H ₁₉ O ₆	331.118712	nd			nd		
C ₁₉ H ₂₁ O ₆	345.134362	18.8	345.13433	-0.09	19.3	345.13436	0.01
		19.2	345.13429	-0.21	20.1	345.13436	0.01
C ₂₀ H ₂₃ O ₆	359.150012	nd			nd		
C ₂₁ H ₂₅ O ₆	373.165662	25.2	373.16486	-2.15	18.5	373.16571	0.12
C ₂₃ H ₂₉ O ₆	401.196962	nd			nd		
C ₂₆ H ₃₅ O ₆	443.243912	nd			nd		
C ₂₇ H ₃₇ O ₆	457.259562	nd			nd		
C ₁₅ H ₁₅ O ₆	291.087412	nd			nd		
C ₁₆ H ₁₇ O ₆	305.103062	nd			nd		
C ₁₈ H ₂₁ O ₆	333.134362	nd			nd		
C ₁₉ H ₂₃ O ₆	347.150012	18.8	347.15011	0.27	19.5	347.15008	0.18
		19.9	347.14969	-0.92	19.9	347.15004	0.08
C ₂₀ H ₂₅ O ₆	361.165662	17.7	361.16567	0.02	18.5	361.16568	0.05
		18.4	361.16562	-0.12	19.8	361.16573	0.19
C ₂₁ H ₂₇ O ₆	375.181312	nd			nd		
C ₂₂ H ₂₉ O ₆	389.196962	nd			nd		
C ₂₇ H ₃₉ O ₆	459.275213	nd			nd		

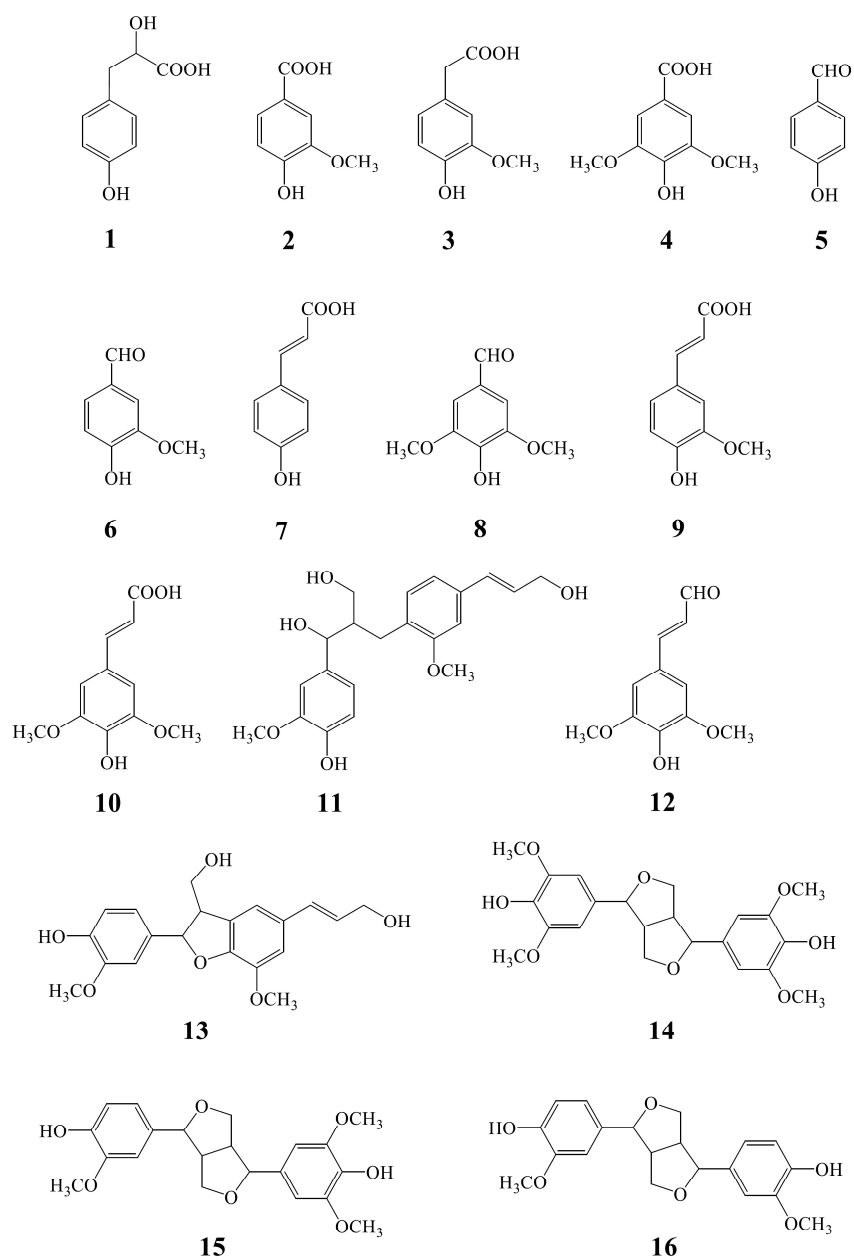
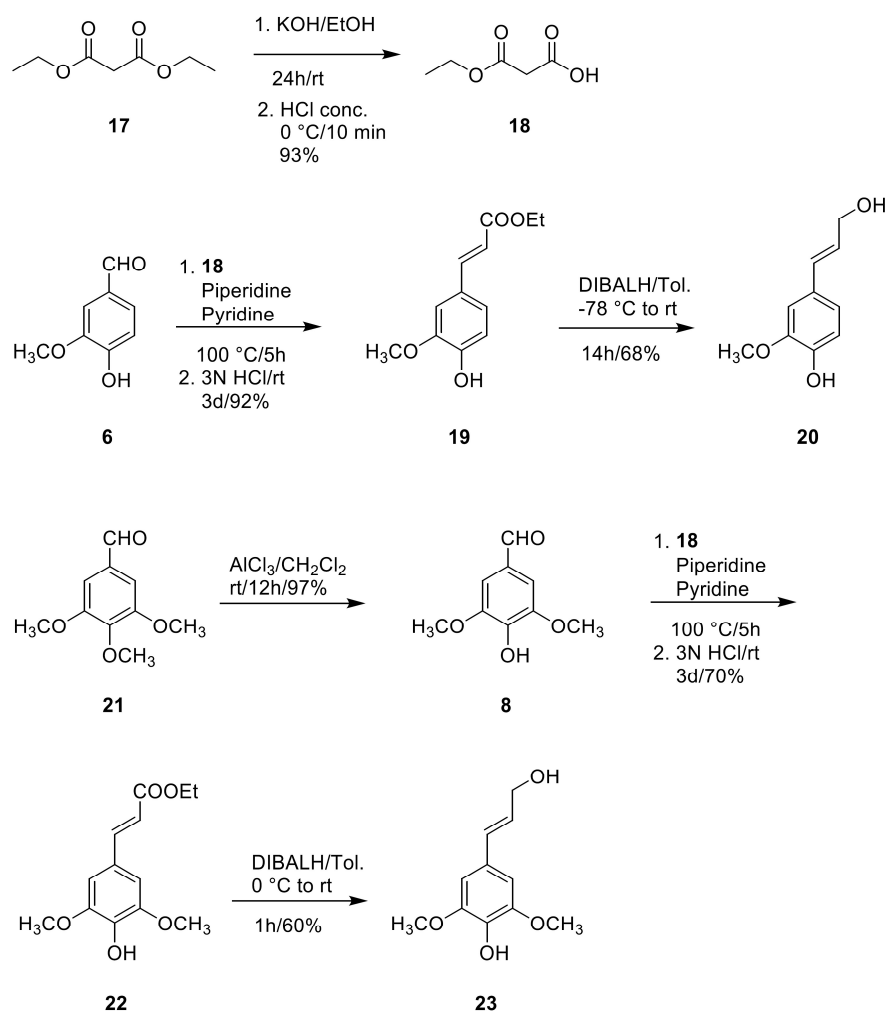


Figure S5. Chemical structures of commercial and custom-made reference compounds. Compounds: **1**, DL-HPA; **2**, vanillic acid; **3**, HVA; **4**, syringic acid; **5**, 4-HB; **6**, vanillin; **7**, *p*-coumaric acid; **8**, SA; **9**, *trans* ferulic acid; **10**, sinapic acid; **11**, G- β -O-4-G; **12**, SPA; **13**, G- β -5-G; **14**, S- β - β -S; **15**, G- β - β -S; **16**, G- β - β -G.



Scheme S1. Synthesis of starting materials coniferyl alcohol **20** and sinapyl alcohol **23** (general information included).

General information. Compounds **6**, **17** and **21** were purchased from Sigma Aldrich (Steinheim, Germany). All reactions were performed under an atmosphere of dry nitrogen. Solvents for chromatography were distilled. Toluene was dried with sodium, ethanol was dried with sodium/diethyl phthalate. Pyridine and piperidine were dried with calcium hydride. Analytical TLC was performed on glass plates Si60 F₂₅₄ (*d*=0.25 mm) from Merck (Darmstadt, Germany). The compounds were visualized under UV, with I₂ and anis aldehyde reagent (0.5 ml anis aldehyde, 5 ml conc. sulfuric acid, 10 ml glacial acetic acid and 85 ml of methanol). Preparative TLC was performed on glass plates Si60 F₂₅₄ (*d*=1.0 mm) from Merck, Darmstadt (Germany). Compounds were visualized with UV.

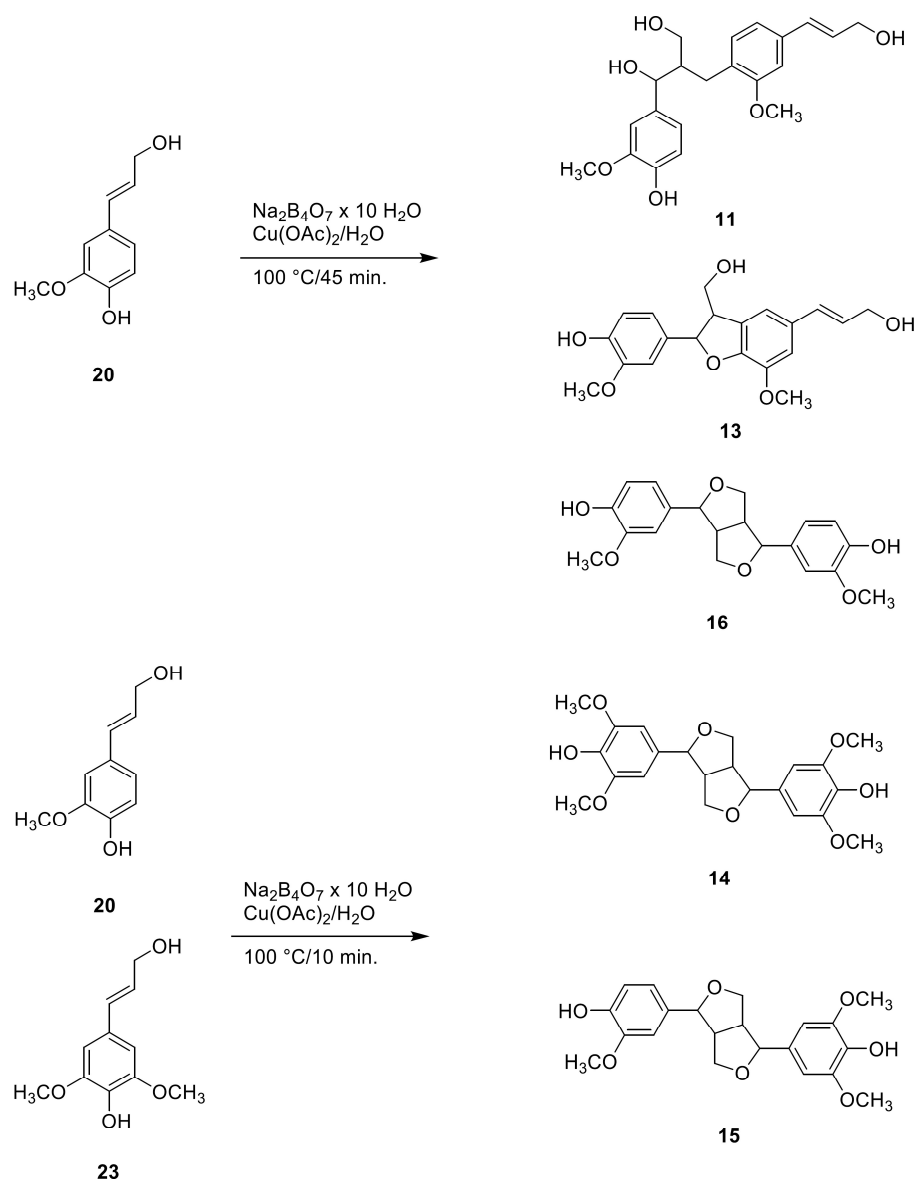
Proton NMR spectra were recorded on a Bruker AV II 400 NMR spectrometer at 400 MHz. Carbon NMR spectra were recorded on the same instrument at 100 MHz.

18 was synthesized according to R. E. Strube, *Org. Synth.* **1957**, *37*, 34-36.

19 and **22** were synthesized according to Y. Xia, X. Dai, H. Liu, C. Chai, *J. Chem. Sci.* **2014**, *126*, 813-820.

8 was synthesized from **21** according to A. Shirali, M. Sriram, J. J. Hall, B. L. Nguyen, R. Guddneppanavar, M. B. Hadimani, J. Freeland Ackley, R. Siles, C. J. Jelinek, P. Artasery, R. C. Brown, V. L. Murrell, A. McMordie, S. Sharma, D. J. Chaplin, Kevin G. Pinney, *J. Nat. Prod.* **2009**, *72*, 414-421.

20 and **23** were synthesized according to S. Quideau and J. Palph, *J. Agric. Food Chem.* **1992**, *40*, 1108-1110.

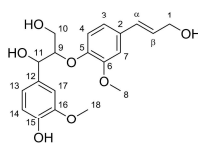


Scheme S2. Synthesis and NMR characterization of dilignols **11**, **13**, **14**, **15** and **16**.

The dilignols **11**, **13**, **14**, **15** and **16** were prepared according to L. L. Landucci, S. Luque, S. Ralph, *J. Wood Chem. Technol.* **1995**, *15*, 493-513.

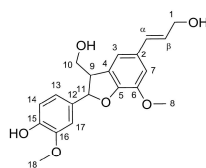
Procedure for 11, 13 and 16. In a 250 ml tree necked round bottom flask with magnetic stirr bar and reflux condenser was placed coniferyl alcohol **20** (360 mg, 2.00 mmol) under an atmosphere of dry N₂. A solution of Na₂B₄O₇ x 10 H₂O (100 ml, 0.05 M) was added and the mixture was heated to 100 °C to dissolve the coniferyl alcohol. At 100 °C a solution of Cu(OAc)₂ x 1 H₂O (520 mg, 2.60 mmol) in water (6 ml) was added at once and the mixture was stirred at 100 °C for 45 min. (the color changes from green to orange). After cooling to room temperature, the insoluble copper salts were filtered off and the filtrate was carefully acidified to pH 5 with 1 N HCl. The aqueous phase was extracted five times with diethyl ether (30 ml each) and once with ethyl acetate (30 ml). The combined organic extracts were dried with MgSO₄. After filtering the solvents were removed in vacuo giving a brownish foam. The solid material was dissolved in methanol (10 ml) and the solution was evaporated again to dryness. The methanol dissolving/evaporating procedure was repeated five times to remove the residual boric acid completely as volatile trimethyl borate. Crude yield: 301 mg of a mixture dilignols and higher polydignols together with unreacted starting material.

Separation of the crude product by preparative TLC (acetone/dichloromethane 1:4 (v/v); only one development) led to the dilignols **11** (R_f = 0.06, 60 mg), **13** (R_f = 0.14, 89 mg) and **16** (R_f = 0.49, 21 mg).



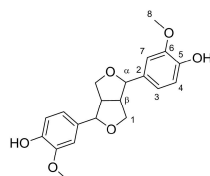
11: ¹H-NMR (400 MHz, Aceton-d₆): δ = 3.69 (m, 1H, Ha-1), 3.77 (m, 1H, Hb-1), 3.80 (m, 1H, OH), 3.81 (s, 3H, H-18), 3.83 (m, 1H, OH), 3.85 (s, 3H, H-8), 4.20 (m, 2H, H-1), 4.30 (m, 1H, H-9), 4.55 (d, *J* = 4.4 Hz, 1H, H-11), 4.89 (t, *J* = 4.8 Hz, 1H, OH), 6.28 (dt, *J* = 5.6 Hz, *J* = 16.0 Hz, 1H, H-β), 6.51 (d, *J* = 16.0 Hz, 1H, H-α), 6.76 (d, *J* = 8.0 Hz, 1H, H-13), 6.89 (m, 3H, H-4, H-14, H-17), 7.09 (m, 1H, H-3), 7.09 (m, 1H, H-7), 7.47 (s, 1H, Ar-OH).

¹³C-NMR (100 MHz, Aceton-d₆): δ = 57.1 (C-18), 57.2 (C-8), 62.8 (C-10), 64.3 (C-1), 74.7 (C-11), 87.6 (C-9), 111.9 (C-17), 112.4 (C-7), 116.1 (C-14), 120.2 (C-4), 121.2 (C-3), 121.4 (C-13), 130.5 (C-β), 130.9 (C-α), 133.8 (C-2), 135.2 (C-12), 147.6 (C-15), 148.9 (C-5), 149.5 (C-16), 152.8 (C-6).



13: ¹H-NMR (400 MHz, Aceton-d₆): δ = 3.53 (m, 1H, H-9), 3.82 (s, 3H, H-8), 3.85 (m, 2H, H-10), 3.85 (m, 1H, OH), 3.86 (s, 3H, H-18), 4.19 (m, 3H, OH, H-1), 5.56 (d, *J* = 6.52 Hz, 1H, H-11), 6.24 (dt, *J* = 5.52 Hz, *J* = 15.8 Hz, 1H, H-β), 6.52 (d, *J* = 15.8 Hz, 1H, H-α), 6.80 (d, *J* = 8.08 Hz, 1H, H-14), 6.88 (dd, *J* = 2.0 Hz, *J* = 8.08 Hz, 1H, H-13), 6.95 (s, 1H, H-3) 6.98 (s, 1H, H-7), 7.03 (d, *J* = 2.0 Hz, 1H, H-17) 7.68 (m, 1H, Ar-OH).

¹³C-NMR (100 MHz, Aceton-d₆): δ = 55.7 (C-9), 57.2 (C-18), 57.3 (C-8), 64.4 (C-1), 65.6 (C-10), 89.5 (C-11), 111.4 (C-7), 112.6 (C-17), 116.7 (C-3), 117.0 (C-14), 120.6 (C-13), 129.3 (C-β), 131.4 (C-α), 131.5 (C-4), 132.9 (C-2), 135.3 (C-12), 144.7 (C-6), 146.1 (C-15), 148.3 (C-16), 149.4 (C-5).



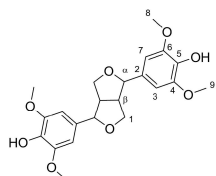
16: ¹H-NMR (400 MHz, Aceton-d₆): δ = 3.08 (m, 2H, H-β), 3.80 (dd, *J* = 4.0 Hz, *J* = 9.0 Hz, 2H, Ha-1), 3.84 (s, 6H, H-8), 4.19 (m, 2H, Hb-1), 4.67 (d, *J* = 4.4 Hz, 2H, H-α), 6.79 (d, *J* = 8.0 Hz, 2H, H-4), 6.83 (dd, *J* = 1.8 Hz, *J* = 8.0 Hz, 2H, H-3), 6.99 (d, *J* = 1.8 Hz, 2H, H-7), 7.59 (s, 2H, Ar-OH).

¹³C-NMR (100 MHz, Aceton-d₆): δ = 56.2 (C-β), 57.2 (C-8), 73.2 (C-1), 87.6 (C-α), 111.5 (C-7), 116.5 (C-4), 120.6 (C-3), 135.1 (C-2), 147.8 (C-5), 149.3 (C-6).

Procedure for 14 and 15. Coniferyl alcohol **20** (180 mg, 1.00 mmol) and sinapyl alcohol **23** (210 mg, 1.00 mmol) were placed in a 100 ml tree necked round bottom flask with magnetic stirr bar and reflux condenser under an atmosphere of dry N₂. A solution of Na₂B₄O₇ x 10 H₂O (50 ml, 0.05 M) was added and the mixture was heated to 100 °C to dissolve the alcohols. At 100 °C, a solution of Cu(OAc)₂ (260 mg, 1.30 mmol) in water (3 ml) was added at once and the mixture was stirred at 100 °C for 10 min (the color changed from green to orange). After cooling to room temperature, the insoluble copper salts were filtered and the filtrate was carefully acidified to pH 5 with 1 N HCl. The aqueous phase was extracted five times with ethyl acetate (30 ml each). The combined organic extracts were dried with MgSO₄. After filtering, the solvents were removed in vacuo giving a brownish foam. The solid material was dissolved in methanol (5 ml) and the solution was evaporated again to dryness. The methanol dissolving/evaporating procedure was repeated five times to remove the residual boric acid completely as volatile

trimethyl borate. Crude yield: 208 mg of a mixture dilignols and higher polygignols together with unreacted starting materials.

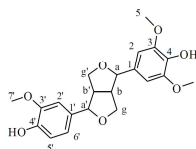
Separation of the crude product by preparative TLC (toluene/petrol ether/acetone 1:1:1 (v/v); four developments) led to the dilignols **14** ($R_f = 0.51$, 23 mg) and **15** ($R_f = 0.91$, 12 mg).



1H, H-5'), 6.68 (s, 2H, H-2), γ'), 3.86-3.84 (m, 2H, H- γ), ppm.

14: $^1\text{H-NMR}$ (400 MHz, Aceton- d_6): $\delta = 3.09$ (m, 2H, H- β), 3.90 (m, 2H, H- α), 3.90 (s, 12H, H-8, H-9), 4.28 (m, 2H, Hb-1), 4.73 (d, $J = 4.4$ Hz, 2H, H- α), 5.50 (s, 2H, Ar-OH), 6.58 (s, 4H, H-3, H-7).

$^{13}\text{C-NMR}$ (100 MHz, Aceton- d_6): $\delta = 54.3$ (C- β), 56.3 (C-8, C-9), 71.8 (C-1), 86.0 (C- α), 102.7 (C-3, C-7), 132.0 (C-2), 134.3 (C-5), 147.1 (C-4, C-6).



15: $^1\text{H-NMR}$ (400 MHz, Aceton- d_6): $\delta = 9.83$ (s, 2H, OH), 7.45-7.44 (m, 2H, H-2' und H-6'), 7.01 (d, $J = 8.0$ Hz, 4.67 (d, $J = 4.4$ Hz, 2H, H- α , H- α'), 4.27-4.21 (m, 2H, H-3.82 (s, 9H, H-5 und H-7'), 3.11-3.08 (m, 2H, H- β , H- β')

Experimental Section

Chemicals and materials

The following chemicals were used for preparation of stationary phases and HPLC eluents: toluene (anhydrous) and acetonitrile (HPLC grade) from Sigma-Aldrich (Steinheim, Germany), dichloromethane (HiPerSolv) and methanol (HPLC grade) from VWR (Darmstadt, Germany); ultra-pure water was generated using an Elga (Celle, Germany) Purelab Ultra purification system. Hydrochloric acid and acetic acid were from an in-house university supply. Sodium acetate (>99%) was from Sigma-Aldrich, triethylamine from Merck (Darmstadt, Germany), (3-bromopropyl)trichlorosilane from ChemPur (Karlsruhe, Germany) and trioctylphosphine from Alfa Aesar (Karlsruhe, Germany). Exchangeable anion species sodium trifluoromethanesulfonate (98%) and sodium hexafluorophosphate (98%) were from Sigma-Aldrich. Acetanilid (Merck) was used as calibration standard for elemental analysis.

Phenol (puriss), uracil (>99%), toluene and ethylbenzene (puriss) from Sigma-Aldrich, and *p*-ethylaniline from Alfa Aesar were used as standards for the Jungheim/Engelhardt test.^{1,2} The standards *p*-coumaric acid ($\geq 98\%$), *trans*-3,5-dimethoxy-4-hydroxycinnamaldehyde (SPA) (98%), *trans*-ferulic acid (99%), homovanillic acid (HVA) (fluorimetric reagent), 4-hydroxybenzaldehyde (4-HB) (98%), DL-*p*-hydroxyphenyllactic acid (DL-HPA) ($\geq 97\%$), sinapic acid ($\geq 98\%$), syringaldehyde (SA) (98%), syringic acid ($\geq 95\%$), vanillin (99%), vanillic acid ($\geq 97\%$) were from Sigma-Aldrich; custom-made dimers guaiacylglycerol- β -coniferyl ether (G- β -O4-G), dehydroniciferyl alcohol (G- β -5-G), pinoresinol (G- β -G), 4-[4-(4-Hydroxy-3-methoxyphenyl)tetrahydro-1H,3H-furo[3,4-c]furan-1-yl]-2,6-dimethoxyphenol (G- β -S) and DL-syringaresinol (S- β -S) were used as a model lignin decomposition standard mixture. The chemical structures of these compounds are provided in the Supporting Information (Figure S5), along with synthesis schemes, procedures and NMR data (Schemes S1 and S2) for the custom-made dimers.

Alkali lignin was purchased from Sigma-Aldrich and triethylammonium methane sulfonate was synthesized as described previously.³ Alkali lignin was degraded as previously reported.⁴

The starting material for the preparation of the stationary phase was Prontosil 120-5-SI (120 Å, 5 μm , 300 $\text{m}^2 \text{g}^{-1}$ BET) from Bischoff (Leonberg, Germany).

Preparation of trioctylpropylphosphonium-based stationary phases

Based on previous work by Qiu *et al.*,⁵ stepwise syntheses were performed as follows:

Activation of Prontosil-120-5-SI (Sil): 3 g Sil were dispersed in 110 mL HCl (37%)/H₂O (1:1 v/v) and stirred under reflux for 2 h. After cooling to room temperature (RT), the activated silica particles were filtered, washed with H₂O until pH of 6-7 was reached for the filtrate, washed with methanol and dried at 60 °C for 18 h.

Preparation of SilPrBr: 3 g activated Sil were dispersed in 120 mL toluene (anhydrous), 1 mL NEt₃ added and stirred in N₂-atmosphere. 3.5 mL (21.9 mmol; $\rho=1.605 \text{ g mL}^{-1}$) (3-bromopropyl)trichlorosilane were added dropwise. The solution was stirred at RT for 7 d. The resulting SilPrBr was filtered, washed four times with acetonitrile and stored in a drying chamber at 60 °C.

Preparation of SilPrPhoBr: 2 g SilPrBr were dispersed in 100 mL toluene (anhydrous). 10 mL (22.4 mmol; $\rho=0.831 \text{ g mL}^{-1}$) trioctylphosphine were added to the dispersion and stirred under reflux for 48 h. After cooling to RT, the resulting SilPrPhoBr was washed three times with water, twice with methanol and stored in a drying chamber at 60 °C.

Preparation of SilPrPhoOTf: 0.8 g SilPrPhoBr were dispersed in 30 mL H₂O. Under stirring, 86.03 mg (0.5 mmol) sodium trifluoromethanesulfonate, which were dissolved in 60 mL H₂O, were added to the dispersion. The resulting mixture was stirred at 70 °C for 48 h. The resulting SilPrPhoOTf was filtered and washed with water multiple times until no precipitation of AgBr after adding concentrated AgNO₃ solution to the filtrate seen. SilPrPhoOTf was then washed twice with water.

Preparation of SilPrPhoPF₆: The same procedure as for SilPrPhoOTf was used.

Column packing

SilPrPho-based material (0.6 g) was dispersed in methanol/dichloromethane (1:2 v/v) and sonicated for 2 min. The quasi-stable dispersion was filled into a blank column (150×2 mm) without air bubbles and slowly overlaid with methanol. The closed packing apparatus was attached to a HPLC pump from Bischoff and methanol constantly pumped through at 380 bar for 30 min. The resulting packed column was flushed with acetonitrile/H₂O (70:30 v/v) for 20 min.

Jungheim/Engelhardt test^{1,2}

Prior to the separations, the respective stationary phase (custom made (SilPrPhoBr, SilPrPhoOTf and SilPrPhoPF₆) + Nucleodur C₁₈ (150×2 mm, 100 Å, 5 µm) and Nucleodur Sphinx RP (150×2 mm, 100 Å, 5 µm) from Macherey-Nagel (Düren, Germany)) were equilibrated for 1 h with eluent (methanol/H₂O 49:51 w/w). The standard mixture (uracil (0.05 g L⁻¹), phenol (1 g L⁻¹), *p*-ethylanilin (1.0 g L⁻¹), toluene (1 g L⁻¹) and ethylbenzene (1 g L⁻¹)), which was dissolved in methanol/H₂O (49:51 w/w), was isocratically separated (eluent: MeOH/H₂O 49:51 w/w; *t*=35 min) on each investigated stationary phase. The following chromatographic parameters were used: void volume/dead time *t*₀ via retention time of uracil, column efficiency via number of theoretical plates for ethylbenzene, hydrophobicity via *k* value of ethylbenzene, CH₂ selectivity via selectivity for separation of ethylbenzene and toluene, silanophilic activity through asymmetry of *p*-ethylaniline, and polar activity via selectivity of separation for of phenol and toluene.

Elemental analysis, HPLC and MS instrumentation

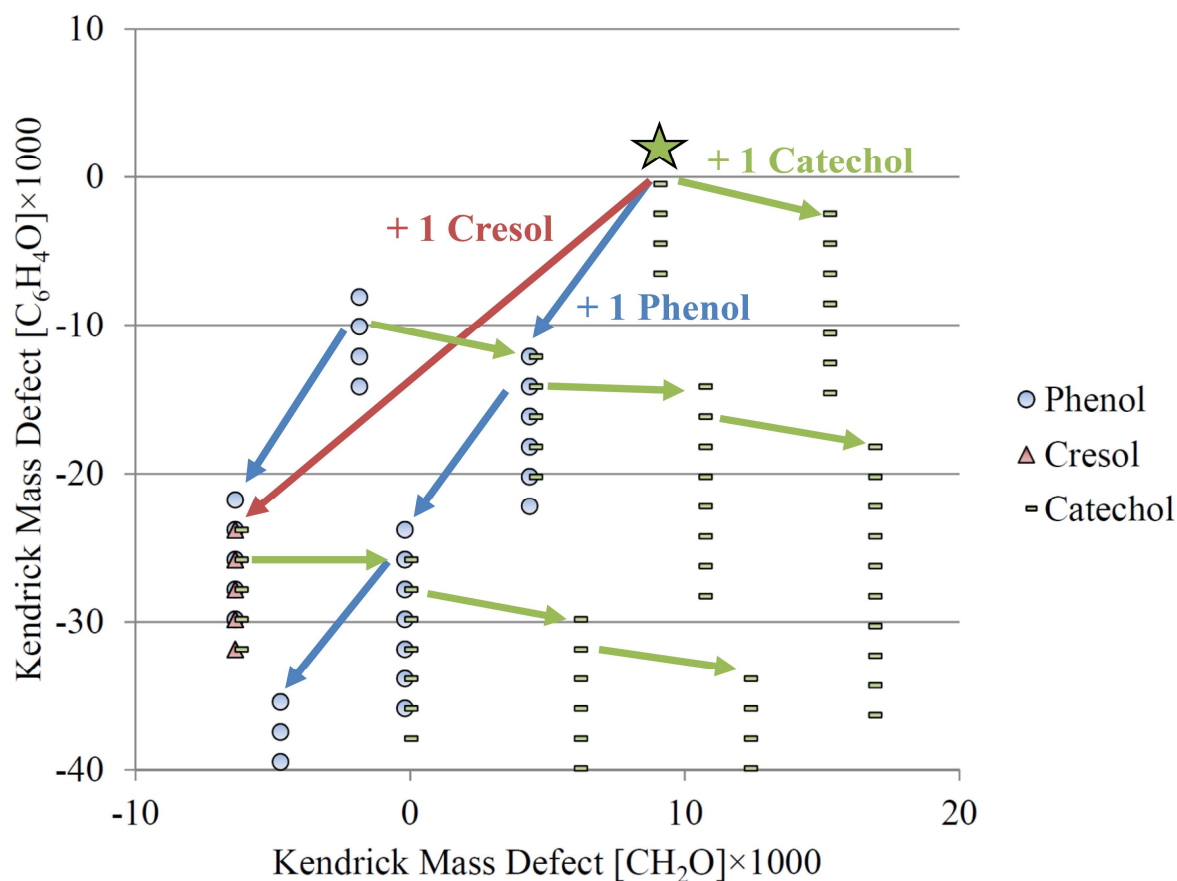
For surface coverage determination of synthesized stationary phases and intermediates, carbon, hydrogen and nitrogen (CHN) content were determined by elemental analysis using a Vario EL analyzer from Elementar (Hanau, Germany). All separations were performed on an Agilent (Waldbronn, Germany) 1100 HPLC system, equipped with binary pump, degasser, autosampler and variable wavelength detector. The columns were heated to 40°C using a Knauer (Berlin, Germany) thermostat. A flow rate of 0.25 mL min⁻¹ and injection volume of 10 µL were used in all chromatographic separations. For experiments using the lignin-related standard mixture and decomposed lignin, samples were dissolved in acetonitrile/H₂O (10:90 v/v) and chromatographically separated on each stationary phase at 40°C using gradient elution with mobile phases water (A) and acetonitrile (B). The regular gradient was as follows: after 10 min equilibration at 10% B, B was increased to 30% within 5 min, held there for 5 min, increased to 80% within 25 min, held there for 5 min, reduced to 10% within 0.1 min and ending with post equilibration for 5 min at 10% B. A second modified gradient (see Results and Discussion) was as follows: after 10 min equilibration at 10% B, B was increased to 30% within 5 min, held there for 5 min, increased to 80% within 25 min, held there for 25 min, reduced to 10% within 0.1 min and ending with post equilibration for 25 min at 10% B. For HPLC-UV, Chemstation A.10.02 software from Agilent was used and resulting chromatograms were exported to Excel spreadsheets. LC-MS experiments were performed in negative ionization mode on a Bruker (Bremen, Germany) Solarix 7 Tesla FTICR instrument equipped with APCI source and Infinity cell. For each spectrum, 2 transients with estimated resolving power of 140,000 at *m/z* 400 were collected and co-added. Mass spectra were externally calibrated using Agilent APCI/APPI tuning mix solution in negative ionization mode. Elemental restrictions for chemical compositions and data analyses using Bruker's Data Analysis 4.2 were adopted from a previous study.⁴

References

- (1) Engelhardt, H.; Jungheim, M. *Chromatographia* **1990**, *29* (1–2), 59–68.
- (2) Engelhardt, H.; Arangio, M.; Lobert, T. *LC GC* **1997**, *15* (9), 856–866.
- (3) Reichert, E.; Wintringer, R.; Volmer, D. A.; Hempelmann, R. *Phys. Chem. Chem. Phys.* **2012**, *14* (15), 5214–5221.
- (4) Dier, T. K. F.; Egele, K.; Fossog, V.; Hempelmann, R.; Volmer, D. A. *Anal. Chem.* **2016**, *88*, 1328–1335.
- (5) Qiu, H.; Jiang, Q.; Wei, Z.; Wang, X.; Liu, X.; Jiang, S. *J. Chromatogr. A* **2007**, *1163* (1–2), 63–69.

Publication 3**Exploring the Potential of High Resolution Mass Spectrometry for the Investigation of Lignin-Derived Phenol Substitutes in Phenolic Resin Syntheses**

T.K.F. Dier, M. Fleckenstein, H. Miltz, D.A. Volmer

Anal. Bioanal. Chem., **2017**, DOI: 10.1007/s00216-017-0282-1

Reprinted with permission from T.K.F. Dier *et al.*, *Anal. Bioanal. Chem.*, **2017**, DOI: 10.1007/s00216-017-0282-1. Copyright (2017) Springer Verlag, Berlin Heidelberg.

Exploring the potential of high resolution mass spectrometry for the investigation of lignin-derived phenol substitutes in phenolic resin syntheses

Tobias K. F. Dier¹ · Marco Fleckenstein² · Holger Militz² · Dietrich A. Volmer¹Received: 16 January 2017 / Revised: 22 February 2017 / Accepted: 27 February 2017
© Springer-Verlag Berlin Heidelberg 2017

Abstract Chemical degradation is an efficient method to obtain bio-oils and other compounds from lignin. Lignin bio-oils are potential substitutes for the phenol component of phenol formaldehyde (PF) resins. Here, we developed an analytical method based on high resolution mass spectrometry that provided structural information for the synthesized lignin-derived resins and supported the prediction of their properties. Different model resins based on typical lignin degradation products were analyzed by electrospray ionization in negative ionization mode. Utilizing enhanced mass defect filter techniques provided detailed structural information of the lignin-based model resins and readily complemented the analytical data from differential scanning calorimetry and thermogravimetric analysis. Relative reactivity and chemical diversity of the phenol substitutes were significant determinants of the outcome of the PF resin synthesis and thus controlled the areas of application of the resulting polymers.

Keywords Bio-oils · Lignin · High resolution mass spectrometry · Mass defect · Phenol formaldehyde resin

Tobias K. F. Dier and Marco Fleckenstein contributed equally to this work.

Electronic supplementary material The online version of this article (doi:10.1007/s00216-017-0282-1) contains supplementary material, which is available to authorized users.

✉ Dietrich A. Volmer
dietrich.volmer@mx.uni-saarland.de

¹ Institute of Bioanalytical Chemistry, Saarland University, Campus B2 2, 66123 Saarbrücken, Germany

² Wood Biology and Wood Products, Georg-August-University Göttingen, Büsgenweg 4, 37077 Göttingen, Germany

Introduction

Phenol resin syntheses and the practical use of phenol formaldehyde (PF) resins were pioneered by Baekeland and Lebach in 1908 [1]. Even today, PF resins are still optimized, in particular to reduce the amounts of hazardous residual free formaldehyde and phenols. In addition, kinetic studies are performed to fully understand the underlying reaction mechanisms during resinification and curing. PF resins are utilized in many applications, in particular as paper coatings, abrasives, packaging lacquer, photoresists, and coupling agents for the rubber industry. Generally, resin synthesis is performed by one of two general procedures: acid-catalyzed novolak synthesis via condensation of the hydroxymethyl cation (molar ratio of phenol/formaldehyde, 1/<1) or base-catalyzed resol resin synthesis by electrophilic aromatic substitution of formaldehyde (molar ratio of phenol/formaldehyde, 1/>1) [2]. Both reactions take place in *ortho* and *para* positions of phenol, where *ortho* is statistically preferred. Other substituted phenols, in particular cresols and xylenols, have been used in PF resin syntheses instead of phenol, with the properties of the resulting resins dependent on the composition of the mono-aromatic phenols and synthesis conditions such as reaction time and temperature [3].

The phenol precursors for PF resin syntheses are mainly produced by the cumene-to-phenol process, which utilizes the petroleum-derived starting materials benzene and polyene [4, 5]. Limited future supplies of fossil resources and steadily increasing demand [6], however, make gradual replacement with renewable, bio-based alternatives essential. Lignin, a major component of lignocellulosic biomass, is a potential sustainable alternative, as it is the most abundant renewable polyphenolic biopolymer [7]. About 80 million tons of lignin are produced annually by the pulp and paper industry as by-product [8], but are mostly only combusted for energy

production [9]. The ample availability of lignin, its low price, and the inherent aromatic core structure of lignin, however, present tremendous commercial opportunities as renewable resources for chemicals and fuels [9, 10]. This has been exploited for phenolic base-chemicals by various lignin depolymerization processes, to generate low molecular weight aromatic precursor compounds [10]. For example, base, acid and metal-catalyzed, ionic liquid-assisted, and supercritical fluid-assisted lignin depolymerizations have been developed [9] as well as pyrolytic cleavages by conventional or microwave heating [11, 12]. The pyrolytic degradation of Kraft lignin resulted in depolymerization of lignin into different substituted mono-aromatic phenols (11.1% of total depolymerized lignin) within 7.5 min [13]. Moreover, Forchheim et al. [14] successfully degraded hydrothermal lignin into mono-aromatic phenols, with and without using a catalyst, resulting in up to 24.9 mg of mono-aromatic degradation products per gram of lignin. Several phenols from lignin as potential substitutes for phenol in PF resin syntheses have been described [15, 16]. Recent investigations of high value bio-oils from lignin conversions mainly utilized mineral bases (NaOH, LiOH, KOH, etc.) or metal catalysts (e.g., Pd, Pt, Ni, SiO₂) in inert gas atmospheres [9]. In particular, lignin depolymerization using NaOH has been widely applied because formation of aromatic compounds was promoted [17]. However, these methods exhibited major disadvantages, such as corrosion, problems with catalyst recovery, and the need for high temperatures and pressures [18]. Consequently, particular emphasis is currently placed on waste valorization methods that avoid these technical drawbacks, to generate high value products such as mono-aromatic phenols.

The phenols can be divided into different groups, based on the chemical functionality, effects of aromatic substituent and associated reactivity compared to formaldehyde. In the resin synthesis, di- and trifunctional phenols have the ability to polymerize in linear or three-dimensional fashion, which is necessary to build a stable network. Positive and negative inductive effects of the substituents attached to the aromatic rings affect the utility of the appropriate phenols for resin synthesis. Sprung tested the relative reactivity of mono- and dimethylated phenol monomers with formaldehyde and showed that the reaction rate of *ortho*- and *para*-cresol was ~30% lower as compared to phenol, but increased by ~770% for 3,5-xyleneol [19, 20].

The exact chemical compositions of lignin phenol/formaldehyde resol resins, which significantly influence the resulting resin properties, often remain unknown. Development of comprehensive analytical characterization methods is therefore crucial. Several analytical methods have been applied for characterization of resin syntheses. For example, differential scanning calorimetry (DSC), thermogravimetric analysis (TGA), and Fourier-transform infrared spectroscopy (FTIR) have provided

important information of the resin's properties; they do not, however, offer the detailed molecular information required to fully characterize the structures of the resins [21–25]. Mass spectrometry (MS), in particular high resolution mass spectrometry (HRMS), and nuclear magnetic resonance (NMR) spectroscopy have enabled detailed structural analyses of the resulting resins [26, 27] or renewable lignin-derived substitutes [28–30]. NMR will often require more elaborate and time-consuming sample preparation (derivatization, lyophilization) and data acquisition routines than MS, making mass spectrometry the preferred choice, in particular in process analysis applications. Pyrolysis gas-chromatography-MS (Py-GC-MS) is a common technique for resol resin analysis. For example, detection of unexpected pyrolysis products has supported the implementation of particular additives to the polymer [31], allowed monitoring of the curing stage of the PF resol resins [32] or provided data on the time-dependent alteration of stored resins [33]. Py-GC-MS degrades the polymers, however, thus preventing identification of the exact source of the pyrolysis products within the polymer. For this purpose, non-destructive analytical methods are required. Here, we considered electrospray ionization (ESI)-MS for structural analysis of PF resol resins, as samples only need to be dissolved in a common solvent for ESI, and analytes usually remain intact during analysis.

In this study, we have investigated effects of common lignin-based di-substituted phenols on the properties of the synthesized bio-based resins. The hypothesis used in this study was that these phenolic mixtures are sustainable substitutes for phenol in PF resin syntheses. To verify the hypothesis, model mixtures of lignin monomers were implemented, with chemical compositions of the mono-aromatic phenols very similar to those obtained from technical lignin degradation processes [14] (Table 1). We restricted the degree of polymerization to low molecular weight oligomers (≤ 1500 Da) to reduce the complexity of the samples, and to exemplify typical technical applications in the wood processing industry, where low molecular weight resins are usually used. The selected monomers were limited to mono-substituted phenols, to control the number of possible oligomers/polymers. Multiply-substituted monomeric phenols (e.g., 4-methyl guaiacol) were not investigated, since single electrophilic substitution with formaldehyde would occupy all possible reaction sides and therefore stop the polymerization. Chemical substitution of the phenols also strongly affects the dissociation of the phenolic hydroxyl group [34]. Since deprotonated hydroxyl groups are required for base-catalyzed polymerization, polymerization kinetics, water solubility, and stability of the synthesized resins are affected by the type and degree of phenol substitution. Because of these multiple influencing parameters, it was important to implement analytical characterization techniques

Table 1 Mass balance of selected mono-aromatic phenols in the artificial bio-oils

Resin	Mono-aromatic content in %					Composition parameters ^a			
	Phenol	Guaiacol	Catechol	<i>o</i> -Cresol	<i>p</i> -Cresol	m_{total} [g]	n_{total} [mol]	V [mL]	c_{total} [mol/L]
A	6.0	22.5	66.2	2.0	3.3	31.78	0.51	37.46	13.61
B	12.0	48.0	36.0	0.0	4.0	34.89	0.55	40.08	13.72
C	18.2	45.5	36.4	0.0	0.0	33.02	0.52	38.6	13.47
D	54.7	0.0	1.8	4.9	38.6	29.88	0.51	39.82	12.81
E	57.8	0.6	0.0	4.2	37.3	29.65	0.52	41.00	12.68
F	100.0	0.0	0.0	0.0	0.0	26.68	0.48	38.55	12.45

^aThe total amount of added formaldehyde was included in the calculations

that were able to provide comprehensive, real-time data on the polymerization process, to fully understand the reaction mechanisms of the formed PF resol resin networks. Here, mass spectrometry, in particular HRMS, enabled rapid compound assignments of the PF resol resins. Complementary results from DSC and TGA provided information on resin properties. The combination of HRMS and DSC/TGA data then enabled systematic correlations of oligomer distributions/degree of substitution with the properties of the resulting lignin-based model resins.

Experimental

Chemicals

Methanol (HPLC grade) was purchased from VWR (Darmstadt, Germany) and sodium hydroxide (99%) from Grüssing (Filsun, Germany). Trifluoroacetic acid ($\geq 99\%$) was from Sigma-Aldrich (Munich, Germany). Ultra-pure water was generated using an Elga (Celle, Germany) Purelab Ultra purification system. Technical grade phenol ($>99\%$), catechol ($>99\%$), *o*-cresol ($>99\%$), *p*-cresol ($>99\%$) and guaiacol ($>99\%$), formalin (37% aqueous formaldehyde solution), and sodium hydroxide (50% aqueous solution) were from Sigma-Aldrich.

Synthesis of model resins

The lignin model resins were synthesized in a 500-mL four-neck flask equipped with a water-cooled condenser, thermometer, teflon stirrer, and dropping funnel for adding formaldehyde. The yields of selected mono-aromatic phenols after hydrothermal lignin depolymerization based on Forchheim et al. [14] served as reference for the lignin-derived model mixtures resulting in the resin solutions A to F (Table 1). Hydroxymethylation of the model mixtures was implemented using a molar ratio of mono-aromatic phenols to formaldehyde to sodium hydroxide of 1:1.5:0.1. Sodium

hydroxide was added to increase the pH value to 11, to enable base-catalyzed resin synthesis. Approx. 5 g of ethanol was added to improve solubility. After heating the solution to 65 °C, the required amount of formaldehyde was added dropwise to the stirred solutions. After 4 h of resinification reaction, the flask was cooled with ice water to room temperature, to stop hydroxymethylation and polymerization reactions.

Characterization of resins

Ten microliters of the resol resin solutions at concentrations between 12.45 and 13.72 mol/L in H₂O/ethanol 90:10 v/v was diluted with ethanol to give 1 mL working solutions. The working solutions were analyzed by direct infusion ESI-high resolution mass spectrometry in negative ionization mode using a Bruker (Bremen, Germany) solariX 7 T Fourier-transform ion cyclotron resonance (FTICR) instrument. Deprotonation of precursor species to [M-H]⁻ ions was enhanced in the working solutions at basic pH from remaining sodium hydroxide of the basic resol resin stock solutions. The following instrument settings were used: m/z range, 50–1250; drying gas flow, 4.0 L/min; drying gas temperature, 200 °C; nebulizer gas flow, 1.0 bar, syringe flow, 2.0 μ L/min; capillary voltage, 4500 V; endplate offset, -500 V; skimmer 1, -25.0 V; sidekick offset, 3.0 V; ion accumulation time, 0.1 s; flight time to acquisition cell, 0.65 ms. For the extended m/z range of 50 to 2500, a slightly longer flight time to the acquisition cell of 1 ms was used. Sixteen transients with estimated resolving power of 280,000 at m/z 400 were collected and co-added. Mass spectra were externally calibrated using a freshly prepared 100 ng/mL solution of sodium trifluoroacetate. Chemical formulae were determined using the Bruker Data Analysis 4.2 software with mass tolerance of ± 5 ppm; m/z signals were exported to Excel spreadsheets for further processing. Mass scale conversion to scales representing formaldehyde (CH₂O) and

phenol repeat units (C_6H_4O) was adopted from a previously reported procedure [35–37], leading to the corresponding Kendrick masses (KM) [38]:

$$CH_2O: \quad KM [CH_2O] = m/z(IUPAC) \times (30/30.010565) \quad (1)$$

$$C_6H_4O: \quad KM [C_6H_4O] = m/z(IUPAC) \times (92/92.026215) \quad (2)$$

The corresponding Kendrick mass defects (KMD) were calculated as follows:

$$CH_2O: \quad KMD [CH_2O] = (\text{nominal } m/z(IUPAC) - KM [CH_2O]) \times 1000 \quad (3)$$

$$C_6H_4O: \quad KMD [C_6H_4O] = (\text{nominal } m/z(IUPAC) - KM [C_6H_4O]) \times 1000 \quad (4)$$

The relative content of oligomers in the mixtures was estimated from the normalized peak areas for each relevant m/z signal.

The curing of the synthesized resins was measured using a Netzsch (Selb, Germany) differential scanning calorimeter DSC 200 F3. Twenty milligrams of the appropriate resin sample was placed in a high pressure gold crucible. An empty crucible served as reference. Under nitrogen, the crucibles were heated from 0 to 250 at 20 °C/min. For TGA, 10 mg of the appropriate resin sample was heated from room temperature to 500 at 10 °C/min under a nitrogen flow of 50 mL/min using a Netzsch TG 209 F1 TGA instrument. The free formaldehyde content in the synthesized resins after resinification was determined according to the standard method EN9397 [39].

Reactivity of the phenols with formaldehyde

Phenol, guaiacol, catechol, *o*-cresol, and *p*-cresol were activated with formaldehyde. Resin synthesis was performed as described above. After heating the solution to 65 °C, formaldehyde was added drop-by-drop within 5 min. Approximately 10 g of samples was taken out of the flask after 0.5, 1, 1.5, 2, 3, and 4 h resinification times. The amount of free formaldehyde was measured using the EN9397 method. Based on the detected amount of free formaldehyde in the solution, the formaldehyde consumption by the phenols was calculated.

Results and discussion

PF resol resin polymerization reaction

As mentioned in the “Introduction,” the primary aim of this work was the investigation of lignin-derived di-substituted

phenols for PF resol resin polymerization as substitutes for phenol, and their impact on the properties of the resulting resins. Therefore, as reference, the polymerization was initially conducted using 100% phenol (resin F, Table 1), as described in the “Experimental” section, and characterized via gel permeation chromatography (GPC). This reaction exhibited the expected formation of low molecular weight PF resol resin oligomers ($M_w=388$ g/mol; $M_p=348$ g/mol; polydispersity index, PDI=1.30; the molecular weight distribution is shown in the Electronic Supplementary Material (ESM), Fig. S1). For estimating the molecular weight distributions for the lignin-derived model mixtures, an experiment was conducted to determine the relative reactivities of each of the respective monomers (Fig. 1 and Table 1). After 0.5 h, the amount of formaldehyde consumed differed significantly between the model mixtures. Substituted phenols that exhibited positive mesomeric effects increased the electron density at the aromatic ring and thus accelerated hydroxymethylation, in particular catechol and guaiacol. Cresol’s positive inductive effect also increased the electron density at the ring, but the rate of formaldehyde consumption was significantly lower as compared to phenol. Deprotonation of catechol is possible at either one of the two hydroxyl functionalities, thus increasing the number of reaction sites from 3 to 4 as compared to phenol. Conversely, the additional methoxy (guaiacol) or methyl (cresol) groups occupy one potential reaction site, thereby reducing this number to 2. We assume that the different numbers of reaction sites are the primary reason for the different formaldehyde consumption rates seen in Fig. 1. After 4 h, formaldehyde consumption was virtually identical for all studied systems and this can be readily explained by the maximal available formaldehyde amount of 0.296 mol during resinification.

A blank control reaction without any phenol showed an insignificant decrease (<1%) of formaldehyde during 4 h

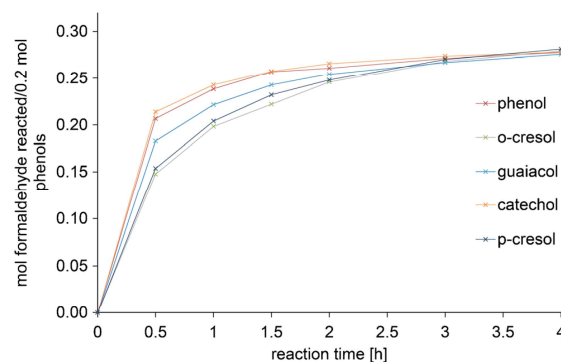


Fig. 1 Kinetics for the reactions of various phenols with formaldehyde (FA)

reaction time, thus excluding the occurrence of intermolecular reactions of formaldehyde, in particular the Cannizzaro reaction. This small decrease was likely due to evaporative losses of formaldehyde.

As a result, the relative reaction rates for each model monomer mixture differed from the reference F. The narrow molecular weight distribution of reference F (PDI=1.30) and the measured relative reaction rates of the respective monomers allowed us to assume primary formation of low molecular weight oligomers. The recorded mass spectra for each model mixture confirmed this assumption because neither multiply-charged oligomers nor features with $m/z \geq 1500$, which matched characteristics of the structural Pf resol resin, were seen (see Fig. S2 and S3, and data file ESM_2.xlsx in the ESM). Therefore, the development of a graphical visualization tool for the low molecular weight oligomers using mass defect filtering (MDF) techniques was used to elucidate the mechanisms further.

Characterization of individual species during polymerization

Enhanced MDF plots [35–37], which were individually modified for PF resol resins, readily identified the predominant species during the polymerization reactions as well as the resulting degrees of polymerization (Figs. 2 and 3). In these MDF plots, the data points along the y -axis belong to the same polymer category with varying number of formaldehyde units (decreasing Kendrick mass defect (KMD) $[C_6H_4O] \equiv$ increasing number of formaldehyde units). KMD $[C_6H_4O]$ also provides information on the degree of polymerization: the lower the KMD, the higher the degree of polymerization for the respective polymer backbone (Fig. 2). For example, starting

at the KMD for an unsubstituted catechol monomer (★) and following the line vertically along the y -axis, four subsequent m/z features follow the straight line. Each of these m/z features belongs to increasingly formaldehyde-substituted catechol monomers; that is, the fifth (last) m/z feature in the line represents the fourfold formaldehyde-substituted catechol monomer. The same procedure was valid for all vertically aligned feature sequences along the y -axis in the 2D-MDF plots, where the first m/z feature of a linked group always represented the unsubstituted monomer/oligomer. Addition of one formaldehyde to the monomer is the requirement for subsequent polymerization of multiple monomers, leading from the unsubstituted catechol monomer (★) to the first m/z feature below the starting point. The polymerization reaction of a singly formaldehyde-substituted monomer with an unsubstituted monomer triggered a significant change in the KMD $[CH_2O]$ direction. In our plots, the additional catechol monomer significantly increased KMD $[CH_2O]$ (see green-colored arrow in Fig. 2a), while additional phenol or cresol moieties considerably decreased KMD $[CH_2O]$. This behavior will depend on the chosen KMD base units and therefore has to be adapted if base units are changed. Furthermore, going horizontally from the first m/z feature underneath the start point to the initial member of the adjacent group of m/z features with similar KMD $[C_6H_4O]$ represents the polymerization reaction between singly formaldehyde-substituted catechol and catechol (\equiv green arrow Fig. 2b). For phenol or cresol addition, the pathway starts at the same point, which was used for the catechol addition. The blue arrow in Fig. 2b symbolizes the addition of a phenol unit, and the red arrow in Fig. 2b denotes the addition of a cresol unit. The interpretation of the cresol and phenol pathways is analogous to the catechol pathway (see Fig. 2a). Therefore, measured m/z signals can be quickly assigned to the predominant mono-aromatic species

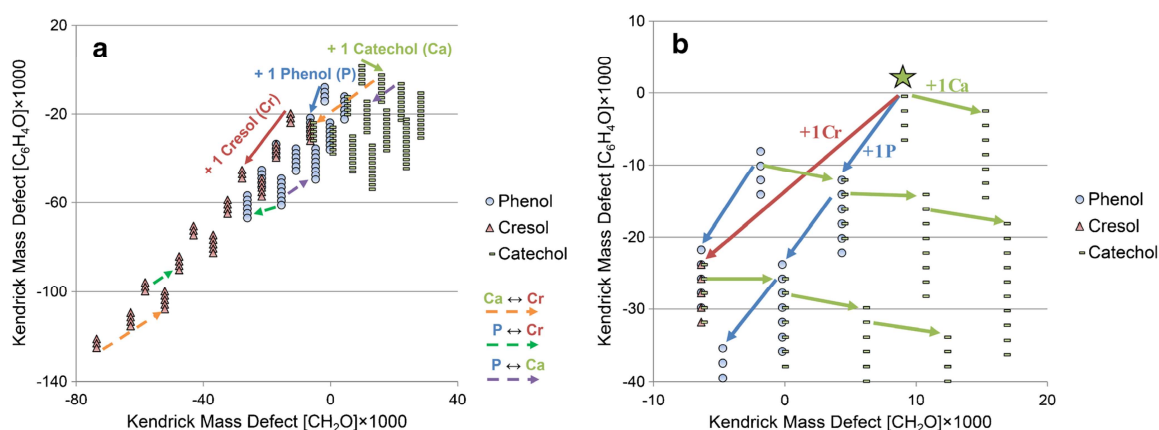


Fig. 2 **a** Enhanced MDF plot for PF resol resins. Data sets represent the dominant species in the polymer; *solid lines* represent addition of one mono-aromatic unit; *dashed lines* represent the exchange of a mono-

aromatic unit in the polymer. **b** Enlarged area of the catechol-rich region. The *star symbol* is the starting point of the example of MDF plots explained in the text

in the polymer and the degree of polymerization. Enhanced MDF plots for PF oligomers clearly highlighted the dominant species for polymerization in each of the studied bio-oil model systems for polymerization (Fig. 3). The data points in Fig. 3 were restricted to m/z features matching the structural characteristics of PF resol resins; that is, using characteristic double bond equivalents (regular PF resol resins, DBE = multiples of 4; quinones,

DBE = 5 + multiples of 4) and O/C ratios from 0.1 to 0.6 for low molecular weight oligomers. The 2D-MDF plots of all measured m/z features are summarized in Fig. S4 (ESM).

High resolution mass spectrometry, however, could not distinguish between structural isomers; that is, guaiacol was included in the phenol data sets in our analyses, as the atomic difference between guaiacol and phenol is the same as a

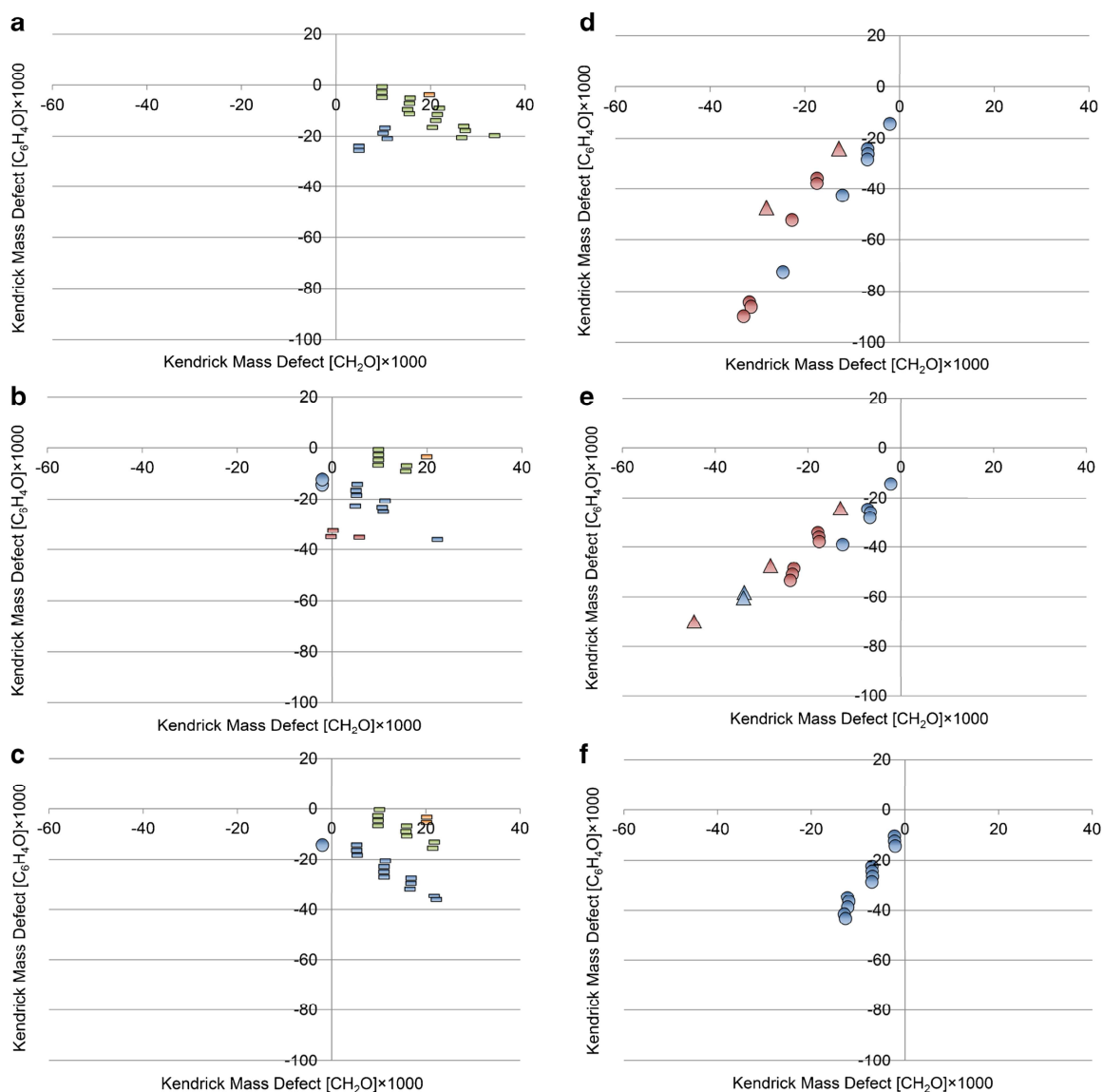


Fig. 3 Enhanced MDF plots of the PF resol resin model systems A to F (Table 1). Symbols represent the dominant mono-aromatic species: circle, phenol; triangle, cresol; rectangle, catechol. Colors correspond to the exchange of one mono-aromatic unit in the polymer: blue, phenol; red,

cresol; green, catechol. Quinones are orange-colored (m/z range 50 to 1250; note: only those m/z features relevant for PF resol resins are shown in the diagrams)

formaldehyde-substituted phenol. To enable straightforward data interpretation, only the exchange of one mono-aromatic species was considered in this study.

More detailed examination of polymerization products

The polymerization of the catechol and cresol-containing model mixtures with formaldehyde proceeded via the expected electrophilic aromatic substitution reaction, resulting in methylene-ether-linked aromatic oligomers. Faster polymerization reactions were seen for catechol-containing resins as compared to the PF resol resin reference (F), however, except for solution B, as evidenced by the higher degrees of polymerization. In addition, quinones (formed by autooxidation of the starting material [40]) were only detected in the catechol-containing solutions. The presence of quinones reduces the number of suitable reactants for polymerization of the resol resin network, by preventing formaldehyde substitution on the corresponding aromatic units and can therefore impair the stability of the resin network. For model systems D and E, the degrees of polymerization as well as the number of formaldehyde substitutions for the corresponding oligomers were comparable to the reference solution F. As seen in Fig. 3, the presence of cresol in solutions D and E enabled the formation of cresol-containing oligomers. The hexamer formation for solution D, however, was not fully understood and has therefore not been considered here; this will require more detailed analysis in the future. The similarities seen for solutions D, E, and F with respect to the degree of polymerization and number of formaldehyde substitutions made sense, since the relative reactivities of phenol and cresol with formaldehyde are only slightly different [19]. For model systems A–C, the majority of observed m/z signals in the mass spectra of the reaction mixtures originated from catechol-rich polymer species. As a result, 2D-MDF plots readily enabled assignments of the resulting PF resol resin oligomers. In addition, a more detailed interrogation of the relative abundances of the oligomers with respect to the degree of polymerization and formaldehyde substitution further substantiated the characterization of the formed PF resol resins. Figure 4 shows the oligomer distribution of the different resin solutions, where the relative content of each oligomer was determined from the normalized peak areas of the corresponding m/z features in the HRMS spectra. The relative abundances of oligomers of resins A to C demonstrated that the catechol/cresol ratio had significant influence on the resulting degrees of polymerization, and that higher amounts of cresol suppressed the polymerization. Higher percentages of catechol led to larger oligomers during resin synthesis.

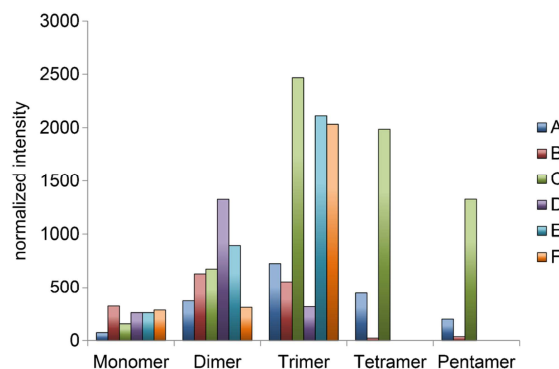


Fig. 4 Relative abundances of synthesized oligomers for models A to F (from direct infusion experiments using ESI in negative ionization mode; m/z range 50–1250)

This is consistent with TGA data (see below) and literature results [41], as electron densities at ring positions 3, 4, 5, and 6 were increased for these compounds and therefore electrophilic substitution was favored. The polymerization of resin B predominantly resulted in formation of dimers and trimers, indicating comparable oligomer distributions to resins D, E and reference F.

From this initial proof-of-concept data, it is clear that solutions B, D, and E were promising sustainable alternatives for common PF resol resin applications.

Importantly, the oligomer distribution is only one factor that influences resin syntheses. The degree of substitution plays an equally important role in the resins' stability in water. Li et al. demonstrated that successive formaldehyde substitutions increased the resin's polarity, which also depended on the position of the terminal hydroxymethyl groups [42]. The determination of the number of terminal hydroxymethyl groups was readily visible from the MDF plots. In combination with the normalized intensities of the corresponding m/z features, the relative abundances of PF oligomers were determined and the total polarity of the respective resin mixture estimated, which determines the stabilities in water. Table 2 summarizes the relative abundances of formaldehyde-substituted oligomers. Highly substituted PF oligomers reduced the resol resin's stability in water. Resins D and E exhibited predominant formations of lower-substituted oligomers, with water stability remaining comparable to reference F. The catecholic resins (A to C) exhibited strong formaldehyde substitution and therefore significant polarity increase of the resins, with possible deficits with respect to stability in water. As a result, introduction of catechol to PF resol resin synthesis was not seen as a sustainable alternative to existing phenols. The introduction of cresol from lignin degradation mixtures into the PF resol resin synthesis, on the other hand, exhibited strong potential [2].

Table 2 Relative abundances of terminal formaldehyde substitutions of oligomers relevant for chemical modification (direct infusion ESI in negative ionization mode; m/z range 50–1250; flow rate, 2 $\mu\text{l}/\text{min}$)

Terminal formaldehyde	Monomer	Dimer	Trimer	Tetramer	Monomer	Dimer	Trimer	Tetramer
	A				B			
0	0	36.6	0	0	0	28.7	0	0
1	46	38.6	119.1	0	53.8	102.3	0	0
2	13	45.7	164.5	212.5	175.1	50.5	0	0
3	15.6	83.8	232.5	194.3	75.1	115.7	261.8	23.7
4	0	165.4	152.1	37.2	17.7	20.6	105.3	0
5	0	0	0	0	0	0	70.4	0
6	0	0	0	0	0	0	0	0
	C				D			
0	0	229.5	0	0	0	0	0	0
1	106.2	444.7	0	0	0	494.4	0	0
2	117.5	271.7	0	0	129	290.4	0	0
3	261.7	303.5	1128.1	0	130.2	226.9	630.7	0
4	145.1	242	923.8	668.2	0	0	0	0
5	0	0	67.9	618.4	0	0	0	0
6	0	0	347.6	699.2	0	0	0	0
	E				F			
0	0	203.3	0	0	0	191.2	847.2	0
1	0	464.8	1186.3	0	102	71.3	565.1	0
2	129	150.3	609.2	0	116.3	27.8	306.1	0
3	130.2	77	316.3	0	66.7	19.3	314.1	0
4	0	0	0	0	0	0	0	0
5	0	0	0	0	0	0	0	0
6	0	0	0	0	0	0	0	0

In conclusion, the structural information obtained from 2D-MDF analysis allowed a preliminary assessment of key properties for each model mixture from simple compound assignments and relative abundances. The comparison of well-established analytical methods, commonly used in the field of resol resins, can enhance the interpretation and characterization of the model mixtures and can confirm these preliminary assessments, as shown below.

Resin curing as a function of model mixture composition

The combined information from mass spectrometry and reaction kinetics measurements clearly demonstrated the influential role of the type of substituted phenol on the degree of polymerization and the resulting resin polarity. We studied this influence further for lignin-derived model mixtures, by evaluating the resin curing by DSC. The resin curing comprises two reactions, which are detectable with DSC. In the first step, free formaldehyde in solution is added to the phenolic rings at lower temperatures (hydroxymethylation), to form the resin, which then undergoes condensation reactions at higher temperatures [43]. Condensation reactions depend on the number of

free *ortho* and *para* positions available on the aromatic rings and inductive effects of substituents [3].

Resins A, B and C exhibited lower onset, peak, and end temperatures as compared to reference PF resin (F) (Table 3). Lower onset temperatures can be readily explained by higher amounts of free formaldehyde in resins A, B, and C, viz. 0.5, 1.4 and 1.3%, respectively. The more reactive catechol and guaiacol as compared to phenol resulted in faster hydroxymethylations and polymerizations (Fig. 2), illustrated by the decreased peak height and end temperature in comparison to resin F. Higher catechol-content therefore benefited the polymerization rate and

Table 3 DSC results for uncured resins with different composition of bio-oil model mixtures

Resin	Onset [$^{\circ}\text{C}$]	Peak [$^{\circ}\text{C}$]	End [$^{\circ}\text{C}$]
A	79.3	136.9	193.8
B	78.7	145.9	223.9
C	81.1	146.2	219.2
D	101.3	168.6	222.6
E	103.5	168.2	224.1
F	87.1	168.0	225.4

Investigating lignin-derived phenol substitutes in phenolic resins

Table 4 Two-step mass losses (ML) of the synthesized resins at temperature up to 500 °C

Resin	ML1		ML2		Residual mass [%]
	Temperature range [°C]	Mass loss [%]	Temperature range [°C]	Mass loss [%]	
A	21–152	62.5	153–498	12.5	25.0
B	21–133	62.2	134–498	12.1	25.7
C	21–147	62.9	148–498	12.6	24.5
D	21–172	61.4	173–498	11.1	27.5
E	21–139	61.2	140–498	10.9	27.9
F	21–155	62.7	156–498	10.6	26.7

made the polymerization process more energy-efficient. On the other hand, cresol reduced the polymerization rate, as the end temperature was significantly higher for resin B than for the other two catechol-dominant resins (A and C). This is consistent with the reactivity of cresol [19] as discussed above. Exchange of cresol with phenol and guaiacol leads to the expected lower end temperature for resin C and increased polymerization rate as well as the number of hydroxymethyl groups. DSC results of resins D and E were comparable to F, except for the increased onset temperature. This can be explained by the lower reactivity of the bifunctional cresols (approx. 43% in the bio-oil) as compared to formaldehyde [19], even though the free formaldehyde content in resins D and E increased by approximately 0.5 and 0.3%, respectively. The comparable resin curing of D and E in comparison to F illustrated the potential of cresol as sustainable phenol alternative. The DSC results therefore permitted similar interpretations of the polymerization process than the results from enhanced MDF plots. With respect to the polymerization rate, MDF plots can be used as viable and rapid alternative or as complement to DSC experiments.

Stabilities of resins as a function of model mixture composition

To evaluate the stability of the synthesized resins, TGA was performed.

The TGA results (Table 4) showed a two-step mass loss for all phenolic resins in an inert atmosphere. The mass reduction during mass loss 1 (ML1) was largely due to the loss of water, with a small contribution from evaporation of non-hydroxymethylated phenols and free formaldehyde. Resins A, B, C and F exhibited virtually identical mass losses. However, mass losses of resins D and E decreased by ca. 1.5%, which was consistent with cresol’s previously described lower reactivity and the resulting reduced amount of formed water during the polymerization. The mass loss 2 (ML2) of the phenolic resins at temperatures up to 498 °C can be explained by three phenomena: (1) transformation of ether to

methylene bridges at temperatures between 164 and 237 °C, including simultaneous release of formaldehyde, which is common for low temperature-synthesized resol resins, (2) breakdown of methylene linkages above 475 °C, and (3) polymer degradation [3, 44]. Resins A, B, and C showed the strongest mass losses and therefore exhibited the least stable resin networks as compared to reference F, whereas resins D and E exhibited higher residual mass and therefore more stable resin networks. The same conclusion was previously drawn from the structural information of 2D-MDF analysis (*vide supra*). As a result, cresol and catechol had significant influence on the polymerization, substitution, and therefore the stability of the resulting resin networks. Catechol-rich resins were highly substituted and polymerized to a higher degree than the reference or the cresol-dominant resins, unless the cresol content in catechol-rich resins was increased. The resin’s stability always depended on the dominant precursor and therefore determined the possible technical application fields of the PF resol resins.

Conclusions

PF resol resins were successfully synthesized from lignin-derived model mixtures and subsequently characterized by detailed mass defect analysis based on characteristic structural elements of the resins. This structural information readily allowed preliminary assessment of key properties of each respective model mixture. Cresol-containing polymers exhibited comparable properties to crude oil-based PF resol resins. Therefore, the synthesized cresol-rich resins were suitable sustainable alternatives to common PF resol resins. Obviously, the chemical composition of the model mixture strongly influences resinification and curing behavior of the resins. This effect was readily observed by the combined use of 2D-MDF plots (to obtain the structural information) and DSC/TGA (to evaluate the resulting physical and mechanical resin properties). In addition, the degree of formaldehyde substitution had strong impact on stability parameters as determined by DSC and TGA.

Detailed 2D-MDF analysis has the potential to strongly support the characterization of complex, low molecular weight lignin-derived model mixtures with mostly unknown structural compositions. Future studies will focus on the development of improved MDF procedures to enable characterization of bio-oil samples from lignin wastes as well as samples of higher molecular weight polymers.

Acknowledgements The authors acknowledge the Alfred Krupp von Bohlen und Halbach-Stiftung, the German Research Foundation (DFG VO 1355/4-1 and FTICR-MS Facility, DFG INST 256/356-1) and “Niedersächsisches Ministerium für Wissenschaft und Kultur” for financial support. The authors thank Allnex S.à.r.l. (Luxembourg) for the GPC experiments.

Author contributions The manuscript was written through contributions of all authors.

Compliance with ethical standards

Conflict of interest The authors declare that they have no competing financial or non-financial interests.

References

- Megson NJL. Aldehyde phenolic condensations from a chemical standpoint. *Trans Faraday Soc.* 1935;336–345.
- Knop A, Pilato LA. Phenolic resins: chemistry, applications and performance. Berlin Heidelberg: Springer-Verlag; 2013.
- Hultsch K. *Chemie der Phenolharze*. Berlin Heidelberg: Springer-Verlag; 1950.
- Gardziella A, Pilato L, Knop A. Phenolic resins: chemistry, applications, standardization, safety, and ecology. Berlin Heidelberg: Springer-Verlag; 2013.
- Pilato LA. Phenolic resins: a century of progress. Berlin Heidelberg: Springer-Verlag; 2010.
- BP. Statistical review of world energy. 2016;1–48.
- Ragauskas AJ, Beckham GT, Biddy MJ, Chandra R, Chen F, Davis MF, et al. Lignin valorization: improving lignin processing in the biorefinery. *Science*. 2014;344:1246843.
- Pradhan SK, Chakraborty I, Kar BB. Chemically modified lignin—a potential resource material for composites with better stability. *Int J Sci Environ Technol*. 2015;4:183–9.
- Wang H, Tucker M, Ji Y. Recent development in chemical depolymerization of lignin: a review. *J Appl Chem*. 2013;2013:1–9.
- Pandey MP, Kim CS. Lignin depolymerization and conversion: a review of thermochemical methods. *Chem Eng Technol*. 2011;34:29–41.
- de Wild PJ, Huijgen WJJ, Gosselink RJA. Perspective: lignin pyrolysis for profitable lignocellulosic biorefineries. *Biofuels, Bioprod Biorefining*. 2012;6:246–56.
- Mudraboyina BP, Fu D, Jessop PG. Supercritical fluid rectification of lignin microwave-pyrolysis oil. *Green Chem*. 2015;17:169–72.
- Jegers HE, Klein MT. Primary and secondary lignin pyrolysis reaction pathways. *Ind Eng Chem Process Des Dev*. 1985;24:173–83.
- Forchheim D, Hornung U, Kempe P, Kruse A, Steinbach D. Influence of RANEY nickel on the formation of intermediates in the degradation of lignin. *Int J Chem Eng*. 2012;2012:589749.
- Stewart D. Lignin as a base material for materials applications: chemistry, application and economics. *Ind Crops Prod*. 2008;27:202–7.
- Kleinert M, Barth T. Phenols from lignin. *Chem Eng Technol*. 2008;31:736–45.
- Pineda A, Lee AF. Heterogeneously catalyzed lignin depolymerization. *Appl Petrochem Res*. 2016;6:1–14.
- Deepa AK, Dhepe PL. Lignin depolymerization into aromatic monomers over solid acid catalysts. *ACS Catal*. 2015;5:365–79.
- Sprung MM. Reactivity of phenols toward paraformaldehyde. *J Am Chem Soc*. 1941;63:334–43.
- Mitsunaga T, Conner AH, Hill CG. Reaction of formaldehyde with phenols: a computational study. *Wood Adhes*. 2000;147–154.
- Cheng S, Yuan Z, Leitch M, Anderson M, Xu CC. Highly efficient de-polymerization of organosolv lignin using a catalytic hydrothermal process and production of phenolic resins/adhesives with the depolymerized lignin as a substitute for phenol at a high substitution ratio. *Ind Crops Prod*. 2013;44:315–22.
- Feng S, Yuan Z, Leitch M, Shui H, Xu CC. Effects of bark extraction before liquefaction and liquid oil fractionation after liquefaction on bark-based phenol formaldehyde resoles. *Ind Crops Prod*. 2016;84:330–6.
- Moubarik A, Grimi N, Boussetta N, Pizzi A. Isolation and characterization of lignin from Moroccan sugar cane bagasse: production of lignin-phenol-formaldehyde wood adhesive. *Ind Crops Prod*. 2013;45:296–302.
- Turunen M, Alvila L, Pakkanen TT, Rainio J. Modification of phenol-formaldehyde resol resins by lignin, starch, and urea. *J Appl Polym Sci*. 2003;88:582–8.
- Wang M, Leitch M, Xu C. Synthesis of phenol-formaldehyde resol resins using organosolv pine lignins. *Eur Polym J*. 2009;45:3380–8.
- Yuan FY, Zhang HB, Li X, Ma HL, Li XZ, Yu ZZ. In situ chemical reduction and functionalization of graphene oxide for electrically conductive phenol formaldehyde composites. *Carbon*. 2014;68:653–61.
- Liu C, Li K, Li H, Zhang S, Zhang Y. The effect of zirconium incorporation on the thermal stability and carbonized product of phenol-formaldehyde resin. *Polym Degrad Stab*. 2014;102:180–5.
- Yang S, Zhang Y, Yuan T-Q, Sun R-C. Lignin-phenol-formaldehyde resin adhesives prepared with biorefinery technical lignins. *J Appl Polym Sci*. 2015;132:42493.
- Tachon N, Benjelloun-Mlayah B, Delmas M. Organosolv wheat straw lignin as a phenol substitute for green phenolic resins. *BioResources*. 2016;11:5797–815.
- Hoong YB, Pizzi A, Chuah LA, Harun J. Phenol-urea-formaldehyde resin co-polymer synthesis and its influence on elaeis palm trunk plywood mechanical performance evaluated by ¹³C NMR and MALDI-TOF mass spectrometry. *Int J Adhes Adhes*. 2015;63:117–23.
- Wang J, Jiang H, Jiang N. Study on the pyrolysis of phenol-formaldehyde (PF) resin and modified PF resin. *Thermochim Acta*. 2009;496:136–42.
- Sobera M, Hetper J. Pyrolysis-gas chromatography-mass spectrometry of cured phenolic resins. *J Chromatogr A*. 2003;993:131–5.
- Strzemiescka B, Voelkel A, Zieba-Palus J, Lachowicz T. Assessment of the chemical changes during storage of phenol-formaldehyde resins pyrolysis gas chromatography mass spectrometry, inverse gas chromatography and Fourier transform infra red methods. *J Chromatogr A*. 2014;1359:255–61.
- Santos RM B, Martinho Simões JA. Energetics of the O-H bond in phenol and substituted phenols: a critical evaluation of literature data. *J Phys Chem Ref Data*. 1998;27:707–39.
- Dier TKF, Egele K, Fossog V, Hempelmann R, Volmer DA. Enhanced mass defect filtering to simplify and classify complex mixtures of lignin degradation products. *Anal Chem*. 2016;88:1328–35.
- Qi Y, Hempelmann R, Volmer DA. Two-dimensional mass defect matrix plots for mapping genealogical links in mixtures of lignin depolymerisation products. *Anal Bioanal Chem*. 2016;408:4835–43.
- Qi Y, Hempelmann R, Volmer DA. Shedding light on the structures of lignin compounds: photo-oxidation under artificial UV light and

Investigating lignin-derived phenol substitutes in phenolic resins

- characterization by high resolution mass spectrometry. *Anal Bioanal Chem.* 2016;408:8203–10.
38. Kendrick E. A mass scale based on CH₂ = 14. 0000 for high resolution mass spectrometry of organic compounds. *Anal Biochem.* 1963;35:2146–54.
 39. Determination of free-formaldehyde content by hydroxylamine hydrochloride method (ISO 9397:1995). 1997. <https://www.beuth.de/norm/din-en-iso-9397/2973638>.
 40. Hathway DE, Seakins JWT. Autoxidation of catechin. *Nature.* 1955;176:218.
 41. Pekala RW. Organic aerogels from the polycondensation of resorcinol with formaldehyde. *J Mater Sci.* 1989;24:3221–7.
 42. Li P, Coleman DW, Spaulding KM, McClennen WH, Stafford PR, Fife DJ. Fractionation and characterization of phenolic resins by high-performance liquid chromatography and gel-permeation chromatography combined with ultraviolet, refractive index, mass spectrometry and light-scattering detection. *J Chromatogr A.* 2001;914:147–59.
 43. Christiansen AW, Gollob L. Differential scanning calorimetry of phenol-formaldehyde resols. *J Appl Polym Sci.* 1985;30:2279–89.
 44. Khan MA, Ashraf SM, Malhotra VP. Eucalyptus bark lignin substituted phenol formaldehyde adhesives: a study on optimization of reaction parameters and characterization. *J Appl Polym Sci.* 2004;92:3514–23.

Analytical and Bioanalytical Chemistry

Electronic Supplementary Material

Exploring the potential of high resolution mass spectrometry for the investigation of lignin-derived phenol substitutes in phenolic resin syntheses

Tobias K.F. Dier, Marco Fleckenstein, Holger Militz, Dietrich A. Volmer

Additional file available under „Supplementary material”

Table of contents:

Fig. S1. Molecular weight distribution for reference resin F from GPC analysis.....2

Fig. S2. FTICR mass spectra of working solution of resin C in negative ESI mode.....3

Fig. S3. FTICR mass spectra of working solution of resin F in negative ESI mode.....4

Fig. S4. Enhanced mass defect filtering plots for (a) resin C and (b) resin F.....5

ESM_2.xlsx see separate data file

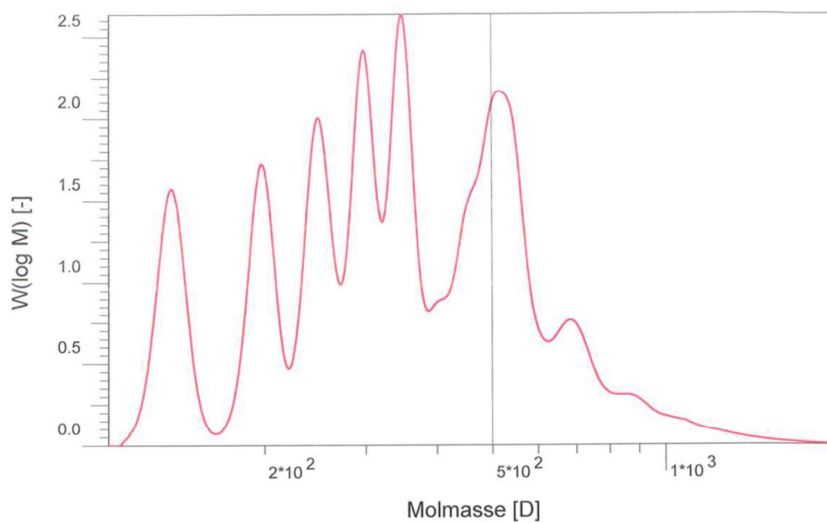


Fig. S1 Molecular weight distribution of reference resin F from GPC analysis. GPC conditions: solvent, stabilized tetrahydrofuran; flow rate, 1 mL/min, column temperature, 40°C, injection volume, 25 µL

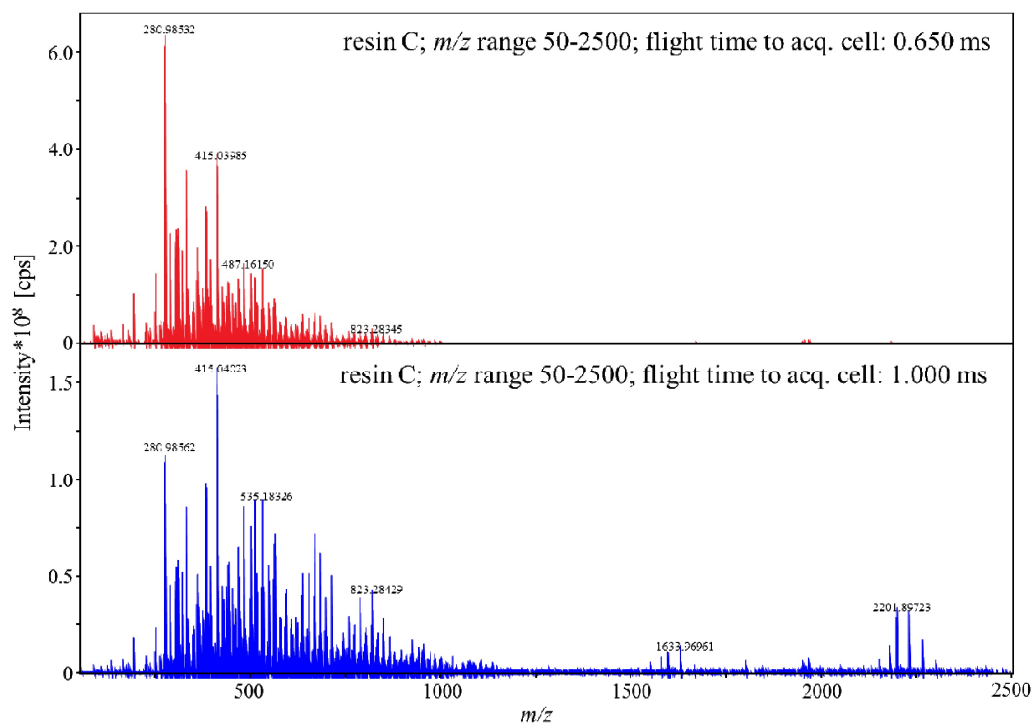


Fig. S2 FTICR mass spectra of working solution of resin C in negative ESI mode for different flight times to acquisition cell. Flow rate: 2 $\mu\text{L}/\text{min}$; m/z range: 50-2500; 16 transients collected and co-added

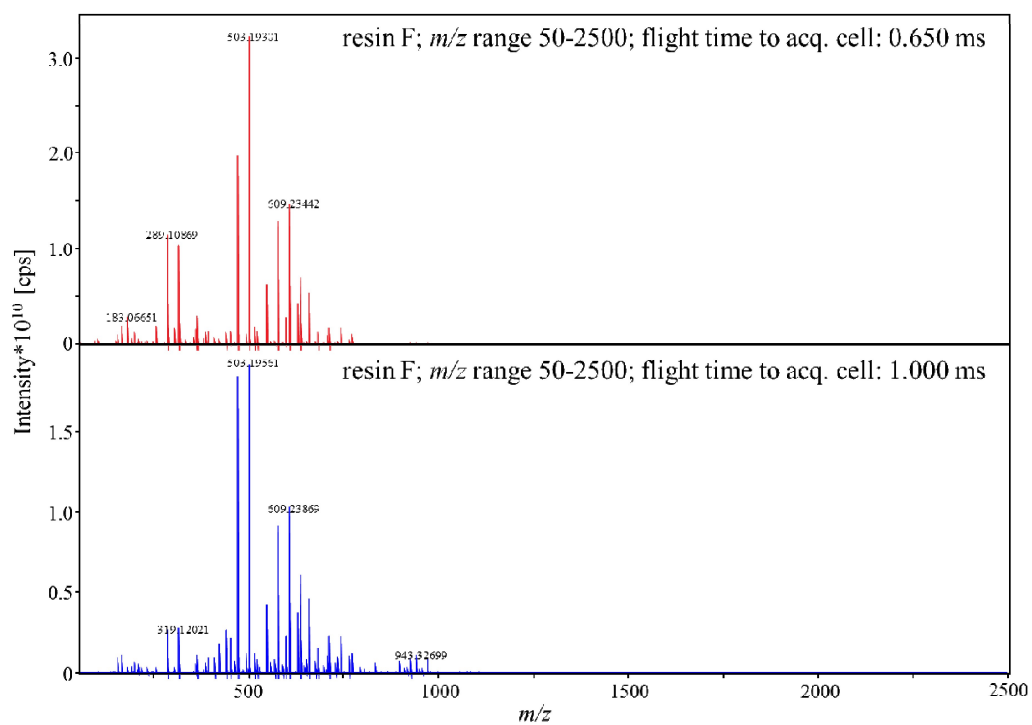


Fig. S3 FTICR mass spectra of working solution of resin F in negative ESI mode for different flight times to acquisition cell. Flow rate: 2 $\mu\text{L}/\text{min}$; m/z range: 50-2500; 16 transients collected and co-added

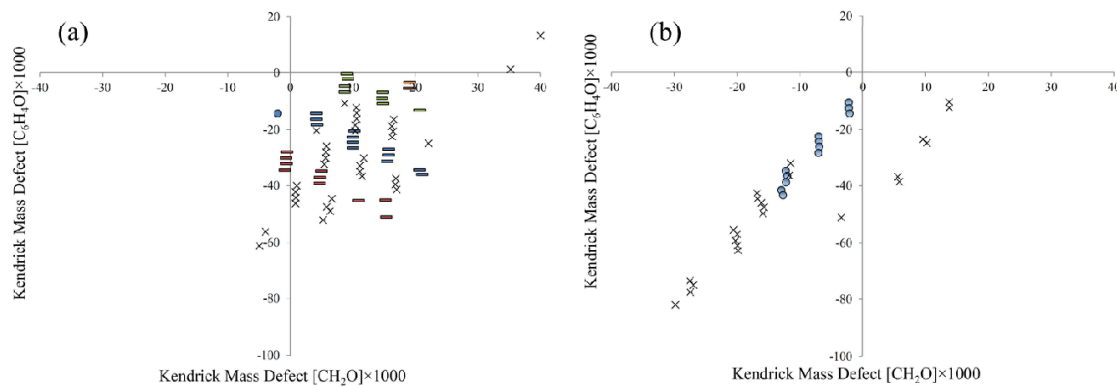


Fig. S4 Enhanced mass defect filtering plot for (a) resin C and (b) resin F showing all m/z features (m/z range, 50-2500). Symbols represent the dominant mono-aromatic species: ● phenol and — catechol. All m/z features that do not match the structural PF resol resin characteristics are marked with a cross (×). Colors correspond to the exchange of one mono-aromatic unit in the polymer: blue, phenol; red, cresol; green, catechol. Quinones are orange-colored

VI. Summary and Conclusions

The objectives of the thesis were successfully achieved. The developed analytical technique allowed a comprehensive analysis of electrochemically decomposed lignin, including structure elucidation and compositional analysis¹³⁹ as well as an unique possibility for chromatographic separation¹⁴⁰. Its easy modifiability also allowed its usage in related fields such as the analysis of sustainable phenol-formaldehyde resin synthesis.¹⁴¹ Nevertheless, the developed analytical technique can still benefit from further improvements, since several other objectives and scientific issues arose from the given results. In the following, previously mentioned main objectives are discussed in more detail and subsequent objectives will be defined.

6.1 Product Coverage by MS

The choice of a suitable ionization technique providing as much information about the chemical composition as possible was one of the primary objectives for characterizing electrochemically decomposed lignin. For this specific and fairly unknown degradation process due to the utilization of ionic liquids as electrolyte, atmospheric pressure ionization techniques such as APCI and APPI provided the most comprehensive results.¹³⁹ The number of detectable m/z features as well as the expected mass range were comparable to other lignin studies.^{31,61,62,76,78,102,130} Common homologous series like the β -O-4 substance class as well as product clusters that were unique for electrochemically degraded lignin were detectable by both ionization techniques. Fast feasibility in the matter of sample preparation and analysis duration additionally gave an advantage to the developed MS-based application over NMR-based analysis. However, expected low molecular weight products, commonly verifiable by GC/MS^{18,44,57,68,71,76}, were rarely detectable or even non-detectable. This lack of detection can be caused by two different reasons. The most common reason was seen in an incomplete electrochemical lignin degradation. It is very likely that the electrochemical degradation process itself was not yet optimized, so that not all interlinkage bonds between the lignin monomers/oligomers were cleavable. The second reason was seen in possible ion suppression of the low molecular weight fraction. Even for atmospheric pressure ionization techniques such as APCI and APPI, ion suppression or enhancement effects can influence the ion formation significantly.¹⁴²⁻¹⁴⁴ It is therefore to be expected that the ionization process of certain degradation products is either enhanced or suppressed. Furthermore, the electrochemical degradation as well as the analytical technique were only performed on one specific, commercially available lignin. It is possible that major modifications in terms of degradation and analysis are necessary to provide sufficient results. Nevertheless, it can be expected that the analytical method provides similar results due to the structural similarities between different lignins.

6.2 Data simplification strategy

The complex data sets were significantly simplified by using an enhanced version of the Kendrick mass defect (KMD) plot. The data visualization of two different KMD's in one graphical illustration provided compositional as well as structural information on electrochemically decomposed lignin.¹³⁹ Depending on the analytical interests, experiments and data evaluation can be easily adjusted to provide the requested information. The arrangement of m/z features allowed clear allocation of the respective degradation products to typical lignin-related substance classes.¹³⁹ In addition, the received information surpassed the information gathered from classical data simplification strategies, namely van Krevelen and Kendrick plot. The enhanced mass defect filtering plot allowed the classification of distinct data point regions to specific substance classes comparable to the van Krevelen plot. However, the information about the molecular weight of the considered data point or rather the considered m/z feature was not completely lost. Studies utilizing the van Krevelen plot^{76,78,82,130} could therefore benefit from the utilization of the enhanced mass defect filtering technique to reveal additional compositional information of the considered sample. Chemical transformations can also be visualized by suitable KMD distance calculations, comparable to the van Krevelen plot. Furthermore, data interpretation of a classical KMD approach can also significantly benefit from its enhanced version. Multiple chemical affiliations can be observed and could consequently improve the data interpretation of other studies.^{82,102} Minor modifications of the used KMD parameters allowed clear assignments of all m/z features from samples with known complexity.¹⁴¹ The overall picture of electrochemically decomposed lignin using the enhanced mass defect filtering illustrated that the degradation products were extensively and intricately linked. These degradation product linkages gave a further hint to the presumed ordered lignin structure.¹⁴⁵ As a result, the developed mass defect filtering strategy can be used as a suitable platform to support the interpretation of complex samples using Morreel's sequencing approach.⁸¹ The verification of further MS-based sequences for lignin oligomers can be visualized by suitably adjusting the KMD parameters. However, the enhanced mass defect filtering plot in its current state has to make compromises. The molecular weight of each respective m/z feature can only be estimated by the position of the data point or rather the resulting KMD [CH₂] value. The introduction of a third dimension suitable for illustrating the accurate mass of respective m/z features could counterbalance this drawback, but could also significantly increase the complexity of the data simplification strategy.

The enhanced mass defect filtering technique can also be used for structure elucidation. The major advantage here lies in the possible simultaneous structure elucidation from a complete set of m/z features by performing collision induced dissociation (CID) experiments on a single m/z feature from the corresponding homologous series.¹³⁹ Therefore, the enhanced mass defect filtering technique can provide structural information about the analyzed lignin sample comparable to MS-based^{44,70,71,81,101} and NMR-based applications^{45,55,61,62} or even extend the information.

VI. Summary and Conclusions

The short analysis duration can be treated as a major advantage of the enhanced mass defect filtering approach over NMR analyses. However, this major advantage can change into a drawback if the complexity of the analyzed sample exceeds a critical number of independent products/product clusters, so that a tremendous amount of CID experiments is necessary to characterize the structural composition of the analyzed sample. Resulting data points of the enhanced mass defect filtering plot are only connected to elemental compositions. It is therefore possible that members of linked elemental compositions do not share the same structural framework. Nevertheless, the enhanced mass defect filtering technique provided essential structural information of fairly unknown degradation products whose exact structural composition would be difficult to determine by e.g. NMR spectroscopy.¹³⁹

In its current state, the data simplification strategy is limited to samples with carbon, hydrogen and oxygen content. Other sample types such as crude oil^{110,111,113,114} or natural organic matter^{115–123} require the consideration of additional elements such as sulfur, nitrogen or phosphorus. However, the unique mass defect of each respective element creates distinct and distinguishable elemental compositions, so that a clear assignment is possible. Reliability of the elemental composition assignment of course depends on the mass accuracy given by the analytical instrument used. In addition, considering Fiehn's golden rules¹⁴⁶ and subsequent work^{147,148} the amount of possible elemental compositions for each detected m/z feature can be significantly reduced. Suitable modifications of the enhanced mass defect filtering technique can consequently make the simplification strategy applicable in other scientific fields.

6.3 Chromatographic separation

Utilizing immobilized ionic liquids as stationary phases provided an unique separation behavior for lignin analysis.¹⁴⁰ The degradation products were separated according to the chemical functionalities in the side chains of the considered chemical compound. As a result, the chromatographic separation revealed the present isobaric content of the complex sample. The separation behavior of the custom-made stationary phase was different to the separation behavior of common reversed phase (RP) stationary phases. However, the custom-made stationary phases were comparable and were able to compete with common RP stationary phases such as C₁₈^{44,74,77} or other materials.⁴² The custom-made stationary phases can be used to purify certain chemical functionalities that are useful for subsequent processes. For example, purified lignin-related side chain hydroxyls can be electrochemically oxidized by stable 2,2'-azinobis-(3-ethylbenzthiazoline-6-sulfonate) (ABTS) dications (chemical structure of ABTS see Figure 6.1) to lignin-related side chain aldehydes.^{15,149} It is therefore presumed that the development of similar electrochemical transformations using suitable mediators provide the production of valuable chemicals or even chemical energy from further substance classes.

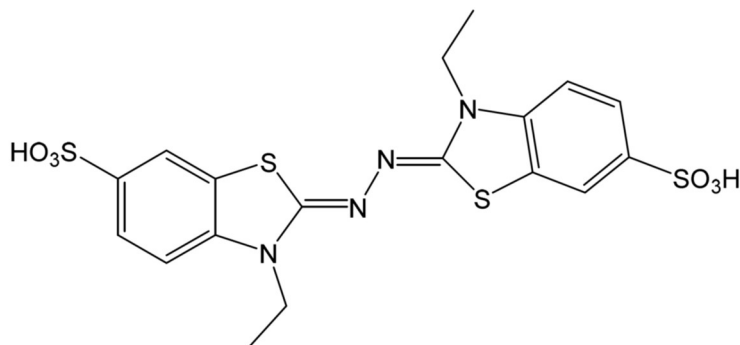


Figure 6.1. Chemical structure of 2,2'-azinobis-(3-ethylbenzthiazoline-6-sulfonate).

The development of the custom-made stationary phase is unfortunately in a very early stage. Several parameters are still not optimized and need further improvements to allow a more precise characterization of degraded lignin or even other complex samples. In addition, the exact interaction mechanisms of the custom-made stationary phases are not fully understood. Optimizing chromatographic separation parameters such as surface coverage or number of theoretical plates enable a more precise evaluation of the stationary phase materials and providing a more concrete description of present interaction mechanisms. In contrary to classic RP phases, multiple interaction mechanisms are present. The interpretation of resulting interactions with different compound classes is therefore complicated. For example, lignin oligomers with a variable number of different side chain functionalities interact with multiple parts of the stationary phase. The resulting primary interaction mechanism therefore has to be determined by additional experiments using a mix of well-known oligomers. As a result, the developed custom-made stationary phase provided unique information about degraded lignin and enabled a special fractionation/purification approach, but left great potential of improvement.

6.4 Electrochemical reaction mechanisms

Understanding the mechanisms of the degradation process is a non-trivial objective. The electrochemical degradation is a merger of several complex reaction mechanisms. The enhanced mass defect filtering technique revealed several hints on present electrochemical reactions.¹³⁹ Single electron transfer (SET) reactions in an oxidative or reductive way were the primary reaction mechanisms, that were clearly identifiable and were confirmed by other studies.^{17,18} In addition, visualized product clusters and homologous series with lower double bond equivalents indicated possible electrochemical hydrogenation of certain substance classes. Furthermore, demethoxylated and dehydroxylated product clusters were detectable, so that the electrochemical degradation in ionic liquids was able to transform the functional groups at the aromatic core. Origin and requirements of the mentioned chemical reactions are not yet fully understood. The combination of both, high-resolution mass spectrometry and chromatographic separation, also revealed hitherto unknown substance classes.¹⁴⁰ Polycyclic hydrocarbons are uncommon components of a lignin sample.

VI. Summary and Conclusions

So-called resin acids are usually the only polycyclic hydrocarbons that can be found in an extracted lignin sample.¹⁵⁰ Therefore, electrochemical cyclisation reactions had to be taken into account, since the abundance of these uncommon polycyclic hydrocarbons significantly increased after electrochemical treatment. Further experiments using a set of well-known standards need to be performed to confirm the presumed electrochemical reactions and to identify the requirements for a successful electrochemical modification/degradation.

6.5 Outlook

The developed analytical method in its current state significantly enhanced the characterization of electrochemically degraded lignin and supported the interpretation of the electrochemical degradation process. Several product clusters unique for an electrochemical degradation were determined. Structure elucidation of the determined product clusters and chromatographic separation provided information on the chemical composition of the complex sample. Nevertheless, several parameters still have to be optimized. The modification of the enhanced mass defect filtering technique, e.g. the consideration of additional elements can extend its applicability. Synthesis and column packing process of the custom-made stationary phase have to be further investigated to allow a precise evaluation of the synthesized stationary phase material. In addition, ideally packed columns enable the possibility to determine physical and chemical influences for the chromatographic separation in a more accurate manner. After processing on these two major objectives the interpretation and the performance of the electrochemical degradation process can be further improved, so that a controlled production of valuable chemicals can be developed.

VII. References

- (1) Logan, B. Y. K. J.; Barry, A. *New Phytol.* **1987**, *105*, 157–173.
- (2) Vanholme, R.; Demedts, B.; Morreel, K.; Ralph, J.; Boerjan, W. *Plant Physiol.* **2010**, *153* (3), 895–905.
- (3) Baltierra-Trejo, E.; Sánchez-Yáñez, J. M.; Buenrostro-Delgado, O.; Márquez-Benavides, L. *Bioresour. Technol.* **2015**, *196*, 418–425.
- (4) Beauchet, R.; Monteil-Rivera, F.; Lavoie, J. M. *Bioresour. Technol.* **2012**, *121*, 328–334.
- (5) Chen, Y.; Zheng, Y.; Li, M.; Zhu, X. *Fuel Process. Technol.* **2015**, *134*, 46–51.
- (6) de la Torre, M. J.; Moral, A.; Hernández, M. D.; Cabeza, E.; Tijero, A. *Ind. Crops Prod.* **2013**, *45*, 58–63.
- (7) Gosselink, R. J. A.; Teunissen, W.; van Dam, J. E. G.; de Jong, E.; Gellerstedt, G.; Scott, E. L.; Sanders, J. P. M. *Bioresour. Technol.* **2012**, *106*, 173–177.
- (8) Johnson, C. W.; Beckham, G. T. *Metab. Eng.* **2015**, *28*, 240–247.
- (9) Jung, K. A.; Woo, S. H.; Lim, S.-R.; Park, J. M. *Chem. Eng. J.* **2015**, *259*, 107–116.
- (10) Kong, J.; He, M.; Lercher, J. A.; Zhao, C. *Chem. Commun.* **2015**, 3–6.
- (11) Shen, D.; Zhao, J.; Xiao, R.; Gu, S. *J. Anal. Appl. Pyrolysis* **2015**, *111*, 47–54.
- (12) Vardon, D. R.; Franden, M. A.; Johnson, C. W.; Karp, E. M.; Guarnieri, M. T.; Linger, J. G.; Salm, M. J.; Strathmann, T. J.; Beckham, G. T. *Energy Environ. Sci.* **2015**, *8* (2), 617–628.
- (13) Zainol, M. M.; Amin, N. A. S.; Asmadi, M. *Bioresour. Technol.* **2015**, *190*, 44–50.
- (14) Zhang, J.; Chen, Y.; Sewell, P.; Brook, M. a. *Green Chem.* **2015**, *17* (3), 1811–1819.
- (15) Eshtaya, M.; Ejigu, A.; Stephens, G.; Walsh, D. A.; Chen, G. Z.; Croft, A. K. *Faraday Discuss.* **2016**, *0*, 1–19.
- (16) Stiefel, S.; Schmitz, A.; Peters, J.; Di Marino, D.; Wessling, M. *Green Chem.* **2016**.
- (17) Schmitt, D.; Regenbrecht, C.; Hartmer, M.; Stecker, F.; Waldvogel, S. R. *Beilstein J. Org. Chem.* **2015**, *11*, 473–480.
- (18) Reichert, E.; Wintringer, R.; Volmer, D. A.; Hempelmann, R. *Phys. Chem. Chem. Phys.* **2012**, *14* (15), 5214–5221.

VII. References

- (19) Ralph, J.; Lundquist, K.; Brunow, G.; Lu, F.; Kim, H.; Schatz, P. F.; Marita, J. M.; Hatfield, R. D.; Ralph, S. A.; Christensen, J. H.; Boerjan, W. *Phytochem. Rev.* **2004**, 3 (1–2), 29–60.
- (20) Hatfield, R.; Ralph, J.; Grabber, J. H. *Planta* **2008**, 228 (6), 919–928.
- (21) Franke, R.; Hemm, M. R.; Denault, J. W.; Ruegger, M. O.; Humphreys, J. M.; Chapple, C. *Plant J.* **2002**, 30 (1), 47–59.
- (22) Franke, R.; McMichael, C. M.; Meyer, K.; Shirley, A. M.; Cusumano, J. C.; Chappie, C. *Plant J.* **2000**, 22 (3), 223–234.
- (23) Boerjan, W.; Ralph, J.; Baucher, M. *Annu. Rev. Plant Biol.* **2003**, 54 (1), 519–546.
- (24) Tolbert, A.; Akinosho, H.; Khunsupat, R.; Naskar, A. K.; Ragauskas, A. J. *Biofuels, Bioprod. Biorefining* **2014**, 8 (6), 836–856.
- (25) Nagarathnamma, R.; Bajpai, P.; Bajpai, P. K. *Process Biochem.* **1999**, 34 (9), 939–948.
- (26) Johansson, E.; Ljunggren, S. *J. Wood Chem. Technol.* **1994**, 14 (4), 507–525.
- (27) Gierer, J. *Wood Sci. Technol.* **1980**, 14 (4), 241–266.
- (28) Gellerstedt, G.; Giever, J.; Szabo-lin, E. P. I. *Liebigs Ann. Chem.* **1976**, 2021–2036.
- (29) Gellerstedt, G.; Agnemo, R.; Mannervik, B.; von Bahr, C.; Glaumann, H. *Acta Chemica Scandinavica*. 1980, 461–462.
- (30) Gellerstedt, G.; Gierer, J.; Pettersson, E.-L.; El-Feraly, F. S.; Nørskov, L.; Schroll, G. *Acta Chemica Scandinavica*. 1977, 735–741.
- (31) Froass, P. M.; Ragauskas, A. J.; Jiang, J. *J. Wood Chem. Technol.* **1996**, 16 (4), 347–365.
- (32) Lupoi, J. S.; Singh, S.; Parthasarathi, R.; Simmons, B. A.; Henry, R. J. *Renew. Sustain. Energy Rev.* **2015**, 49, 871–906.
- (33) Banoub, J.; Delmas, G.-H.; Joly, N.; Mackenzie, G.; Cachet, N.; Benjelloun-Mlayah, B.; Delmas, M. *J. Mass Spectrom.* **2015**, 50, 5–48.
- (34) Fox, S. C.; McDonald, A. G. *BioResources* **2010**, 5, 990–1009.
- (35) Azadi, P.; Inderwildi, O. R.; Farnood, R.; King, D. A. *Renew. Sustain. Energy Rev.* **2013**, 21, 506–523.
- (36) Ragauskas, A. J.; Beckham, G. T.; Biddy, M. J.; Chandra, R.; Chen, F.; Davis, M. F.; Davison, B. H.; Dixon, R. A.; Gilna, P.; Keller, M.; Langan, P.; Naskar, A. K.; Saddler, J. N.; Tschaplinski, T. J.; Tuskan, G. A.; Wyman, C. E. *Science* **2014**, 344 (6185), 1246843.
- (37) Griffiths, P. R.; de Haseth, J. A. *Fourier Transform Infrared Spectrometry*, Second Edi.; John Wiley & Sons, 2007.

-
- (38) Faix, O. Springer Berlin Heidelberg, 1992; 83–109.
- (39) Kubo, S.; Kadla, J. F. *Biomacromolecules* **2005**, *6* (5), 2815–2821.
- (40) Feng, S.; Yuan, Z.; Leitch, M.; Shui, H.; Xu, C. C. *Ind. Crops Prod.* **2016**, *84*, 330–336.
- (41) Ghaffar, S. H.; Fan, M. *Biomass and Bioenergy* **2013**, *57*, 264–279.
- (42) Balan, V.; Sousa, C.; Chundawat, S. P. S.; Marshall, D.; Lansing, E.; Sharma, L. N.; Chambliss, C. K.; Dale, B. E. *Biotechnol. Prog.* **2009**, *25* (2), 365–375.
- (43) Brebu, M.; Tamminen, T.; Spiridon, I. *J. Anal. Appl. Pyrolysis* **2013**, *104*, 531–539.
- (44) Deepa, A. K.; Dhepe, P. L. *ACS Catal.* **2015**, *5* (1), 365–379.
- (45) Joffres, B.; Lorentz, C.; Vidalie, M.; Laurenti, D.; Quoineaud, A.-A.; Charon, N.; Daudin, A.; Quignard, A.; Geantet, C. *Appl. Catal. B Environ.* **2014**, *145*, 167–176.
- (46) Ke, J.; Singh, D.; Yang, X. W.; Chen, S. L. *Biomass Bioenergy* **2011**, *35* (8), 3617–3626.
- (47) Ke, J.; Laskar, D. D.; Chen, S. *Biomacromolecules* **2011**, *12*, 1610–1620.
- (48) Ma, Z.; Sun, Q.; Ye, J.; Qiufang, Y.; Zhao, C. *J. Anal. Appl. Pyrolysis* **2015**, *117*, 116–124.
- (49) Pradhan, S. K.; Chakraborty, I.; Kar, B. B. *Int. J. Sci. Environ. Technol.* **2015**, *4* (1), 183–189.
- (50) Kåldström, M.; Meine, N.; Farès, C.; Rinaldi, R.; Schüth, F. *Green Chem.* **2014**, *16* (5), 2454–2462.
- (51) Bloch, F.; Hansen, W. W.; Packard, M. *Phys. Rev.* **1946**, *70* (7–8), 474–485.
- (52) Bloch, F. *Phys. Rev.* **1946**, *70* (7–8), 460–474.
- (53) Purcell, E. M. *Science* **1953**, *118* (3068), 431–436.
- (54) Purcell, E. M.; Torrey, H. C.; Pound, R. V. *Phys. Rev.* **1946**, *69* (1–2), 37–38.
- (55) Constant, S.; Wienk, H. L. J.; Frissen, A. E.; Peinder, P. de; Boelens, R.; van Es, D. S.; Grisel, R. J. H.; Weckhuysen, B. M.; Huijgen, W. J. J.; Gosselink, R. J. A.; Bruijninx, P. C. A. *Green Chem.* **2016**, *18* (9), 2651–2665.
- (56) Tachon, N.; Benjelloun-Mlayah, B.; Delmas, M. *BioResources* **2016**, *11* (3), 5797–5815.
- (57) Cheng, S.; Wilks, C.; Yuan, Z.; Leitch, M.; Xu, C. *Polym. Degrad. Stab.* **2012**, *97* (6), 839–848.
- (58) Levin, L.; Villalba, L.; Da Re, V.; Forchiassin, F.; Papinutti, L. *Process Biochem.* **2007**, *42* (6), 995–1002.
-

VII. References

- (59) Kim, H.; Ralph, J. *Org. Biomol. Chem.* **2010**, *8* (3), 576–591.
- (60) Rencoret, J.; Gutiérrez, A.; Nieto, L.; Jiménez-Barbero, J.; Faulds, C. B.; Kim, H.; Ralph, J.; Martínez, A. T.; Del Río, J. C. *Plant Physiol.* **2011**, *155* (2), 667–682.
- (61) Van den Bosch, S.; Schutyser, W.; Vanholme, R.; Driessen, T.; Koelewijn, S.-F.; Renders, T.; De Meester, B.; Huijgen, W. J. J.; Dehaen, W.; Courtin, C.; Lagrain, B.; Boerjan, W.; Sels, B. F. *Energy Environ. Sci.* **2015**, *8*, 1748–1763.
- (62) Wagner, A.; Tobimatsu, Y.; Phillips, L.; Flint, H.; Geddes, B.; Lu, F.; Ralph, J. *Proc. Natl. Acad. Sci. U. S. A.* **2015**, *112* (19), 6218–6223.
- (63) Wen, J. L.; Sun, S. L.; Xue, B. L.; Sun, R. C. *Materials (Basel)*. **2013**, *6* (1), 359–391.
- (64) Ralph, S.; Ralph, J. NMR Database of Lignin and Cell Wall Model Compounds https://www.glbrc.org/databases_and_software/nmrdatabase/NMR_DataBase_2009_Complete.pdf.
- (65) Bai, X.; Kim, K. H.; Brown, R. C.; Dalluge, E.; Hutchinson, C.; Lee, Y. J.; Dalluge, D. *Fuel* **2014**, *128*, 170–179.
- (66) de Wild, P.; Van der Laan, R.; Kloekhorst, Ka.; Heeres, E. *Environ. Prog. Sustain.* **2009**, *28* (3), 461–469.
- (67) Di Marino, D.; Stöckmann, D.; Kriescher, S.; Stiefel, S.; Wessling, M. *Green Chem.* **2016**, *18*, 6021–6028.
- (68) Dong, C.; Feng, C.; Liu, Q.; Shen, D.; Xiao, R. *Bioresour. Technol.* **2014**, *162*, 136–141.
- (69) El Fels, L.; Lemee, L.; Ambles, A.; Hafidi, M. *Int. Biodeterior. Biodegrad.* **2014**, *92*, 26–35.
- (70) Eom, I.-Y.; Kim, K.-H.; Kim, J.-Y.; Lee, S.-M.; Yeo, H.-M.; Choi, I.-G.; Choi, J.-W. *Bioresour. Technol.* **2012**, *102* (3), 3437–3444.
- (71) Garcia-Perez, M.; Wang, S.; Shen, J.; Rhodes, M.; Lee, W. J.; Li, C. Z. *Energy and Fuels* **2008**, *22* (3), 2022–2032.
- (72) Hauptert, L. J.; Owen, B. C.; Marcum, C. L.; Jarrell, T. M.; Pulliam, C. J.; Amundson, L. M.; Narra, P.; Aqueel, M. S.; Parsell, T. H.; Abu-Omar, M. M.; Kenttämaa, H. I. *Fuel* **2012**, *95*, 634–641.
- (73) Humpala, J. F.; Chundawat, S. P. S.; Vismeh, R.; Jones, A. D.; Balan, V.; Dale, B. E. *J. Chromatogr. B. Analyt. Technol. Biomed. Life Sci.* **2011**, *879* (13–14), 1018–1022.
- (74) Jarrell, T. M.; Marcum, C. L.; Sheng, H.; Owen, B. C.; O’Lenick, C. J.; Maraun, H.; Bozell, J. J.; Kenttämaa, H. I. *Green Chem.* **2014**, *16* (5), 2713–2727.
- (75) Kekäläinen, T.; Venäläinen, T.; Jänis, J. *Energy Fuels* **2014**, *28* (7), 4596–4602.

-
- (76) Kim, J.-Y.; Park, J.; Hwang, H.; Kim, J. K.; Song, I. K.; Choi, J. W. *J. Anal. Appl. Pyrolysis* **2014**, *113*, 99–106.
- (77) Kiyota, E.; Mazzafera, P.; Sawaya, A. C. H. F. *Anal. Chem.* **2012**, *84* (16), 7015–7020.
- (78) Kloekhorst, A.; Shen, Y.; Yie, Y.; Fang, M.; Heeres, H. J. *Biomass and Bioenergy* **2015**, *80* (0), 147–161.
- (79) Lazzari, E.; Schena, T.; Primaz, C. T.; da Silva Maciel, G. P.; Machado, M. E.; Cardoso, C. A. L.; Jacques, R. A.; Caramão, E. B. *Ind. Crops Prod.* **2016**, *83*, 529–536.
- (80) Liu, D.; Song, L.; Wu, P.; Liu, Y.; Li, Q.; Yan, Z. *Bioresour. Technol.* **2014**, *155*, 152–160.
- (81) Morreel, K.; Dima, O.; Kim, H.; Lu, F.; Niculaes, C.; Vanholme, R.; Dauwe, R.; Goeminne, G.; Inze, D.; Messens, E.; Ralph, J.; Boerjan, W. *Plant Physiol.* **2010**, *153* (4), 1464–1478.
- (82) Ohno, T.; Parr, T. B.; Gruselle, M.-C. I.; Fernandez, I. J.; Sleighter, R. L.; Hatcher, P. G. *Environ. Sci. Technol.* **2014**, *48*, 7729–7236.
- (83) Tamburini, D.; Lucejko, J. J.; Ribechini, E.; Colombini, M. P. *J. Mass Spectrom.* **2015**, *50* (10), 1103–1113.
- (84) Striegel, A. M.; Yau, W. W.; Kirkland, J. J.; Bly, D. D. *Modern Size-Exclusion Liquid Chromatography: Practice of Gel Permeation and Gel Filtration Chromatography*, Second Edi.; Wiley, 2009.
- (85) Cox, B. J.; Ekerdt, J. G. *Bioresour. Technol.* **2012**, *118*, 584–588.
- (86) Forchheim, D.; Hornung, U.; Kempe, P.; Kruse, A.; Steinbach, D. *Int. J. Chem. Eng.* **2012**, *2012*, 589749.
- (87) Nicoletti, I.; Martini, D.; De Rossi, A.; Taddei, F.; D'Egidio, M. G.; Corradini, D. *J. Agric. Food Chem.* **2013**, *61* (48), 11800–11807.
- (88) Thomson, J. J. *P. Roy. Soc. Lond. A Mat.* **1913**, *89* (607), 1–20.
- (89) Squires, G. *J. Chem. Soc. Dalt. Trans* **1998**, 3893–3899.
- (90) Goldstein, E. *Philos. Mag. Ser. 5* **1877**, *4* (26), 353–363.
- (91) Anderson, R. J.; Bendell, D. J.; Groundwater, P. W. In *Organic Spectroscopic Analysis*; The Royal Society of Chemistry, 2004; pp 120–148.
- (92) McLafferty, F. W.; Tureček, F. *Interpretation of Mass Spectra*, Fourth Edi.; University Science Books, 1993.
- (93) Yamashita, M.; Fenn, J. B. *J Phys. Chem.* **1984**, *88* (20), 4451–4459.
- (94) Carroll, D. I.; Dzidic, I.; Stillwell, R. N.; Horning, M. G.; Horning, E. C. *Anal. Chem.* **1974**, *46* (6), 706–710.
-

VII. References

- (95) Karas, M.; Bachmann, D.; Hillenkamp, F. *Anal. Chem.* **1985**, *57* (14), 2935–2939.
- (96) Tanaka, K.; Waki, H.; Ido, Y.; Akita, S.; Yoshida, Y.; Yoshida, T.; Matsuo, T. *Rapid Commun. Mass Spectrom.* **1988**, *2* (8), 151–153.
- (97) Hrabák, J.; Chudáčková, E.; Walková, R. *Clin. Microbiol. Rev.* **2013**, *26* (1), 103–114.
- (98) Clark, A. E.; Kaleta, E. J.; Arora, A.; Wolk, D. M. *Clin. Microbiol. Rev.* **2013**, *26* (3), 547–603.
- (99) Cillero-Pastor, B.; Heeren, R. M. A. *J. Proteome Res.* **2014**, *13* (2), 325–335.
- (100) Harvey, D. J. *Mass Spectrom. Rev.* **2015**, *34*, 268–422.
- (101) Araújo, P.; Ferreira, M. S.; de Oliveira, D. N.; Pereira, L.; Sawaya, A. C. H. F.; Catharino, R. R.; Mazzafera, P. *Anal. Chem.* **2014**, *86*, 3415–3419.
- (102) D'Auria, M.; Emanuele, L.; Racioppi, R. *Nat. Prod. Res.* **2012**, *26* (15), 1368–1374.
- (103) Zhang, G.; Annan, R. S.; Carr, S. A.; Neubert, T. A. *Curr. Protoc. Mol. Biol.* **2014**, 1–27.
- (104) Chapman, J. D.; Goodlett, D. R.; Masselon, C. D. *Mass Spectrom. Rev.* **2014**, *33* (0), 452–470.
- (105) Kailemia, M. J.; Ruhaak, L. R.; Lebrilla, C. B.; Amster, I. J. *Anal. Chem.* **2014**, *86* (1), 196–212.
- (106) Hu, H.; Khatri, K.; Klein, J.; Leymarie, N.; Zaia, J. *Glycoconj. J.* **2016**, *33* (3), 285–296.
- (107) Marshall, A. G.; Hendrickson, C. L.; Jackson, G. S. *Mass Spectrom. Rev.* **1998**, *17*, 1–35.
- (108) Marshall, A. G.; Rodgers, R. P. *Acc. Chem. Res.* **2004**, *37*, 53–59.
- (109) Zubarev, R. A.; Makarov, A. *Anal. Chem.* **2013**, *85* (11), 5288–5296.
- (110) Headley, J. V.; Peru, K. M.; Fahlman, B.; Colodey, A.; McMartin, D. W. *Int. J. Mass Spectrom.* **2013**, *345–347*, 104–108.
- (111) Lababidi, S.; Panda, S. K.; Andersson, J. T.; Schrader, W. *Anal. Chem.* **2013**, *85*, 9478–9485.
- (112) Pomerantz, A. E.; Mullins, O. C.; Paul, G.; Ruzicka, J.; Sanders, M. *Energy and Fuels* **2011**, *25* (7), 3077–3082.
- (113) Romão, W.; Tose, L. V.; Vaz, B. G.; Sama, S. G.; Lobinski, R.; Giusti, P.; Carrier, H.; Bouyssiére, B. *J. Am. Soc. Mass Spectrom.* **2016**, *27* (1), 182–185.
- (114) Schrader, W.; Xuan, Y.; Gaspar, A. *Eur. J. Mass Spectrom.* **2014**, *20* (1), 43–49.

-
- (115) Grinhut, T.; Hertkorn, N.; Schmitt-Kopplin, P.; Hadar, Y.; Chen, Y. *Environ. Sci. Technol.* **2011**, *45* (7), 2748–2754.
- (116) Hawkes, J. A.; Dittmar, T.; Patriarca, C.; Tranvik, L.; Bergquist, J. *Anal. Chem.* **2016**, *88* (15), 7698–7704.
- (117) Kim, S.; Kramer, R. W.; Hatcher, P. G. *Anal. Chem.* **2003**, *75* (20), 5336–5344.
- (118) Mann, B. F.; Chen, H.; Herndon, E. M.; Chu, R. K.; Tolic, N.; Portier, E. F.; Roy Chowdhury, T.; Robinson, E. W.; Callister, S. J.; Wullschleger, S. D.; Graham, D. E.; Liang, L.; Gu, B. *PLoS One* **2015**, *10* (6), e0130557.
- (119) Mead, R. N.; Mullaugh, K. M.; Brooks Avery, G.; Kieber, R. J.; Willey, J. D.; Podgorski, D. C. *Atmos. Chem. Phys.* **2013**, *13* (9), 4829–4838.
- (120) Phungsai, P.; Kurisu, F.; Kasuga, I.; Furumai, H. *Water Res.* **2016**, *100*, 526–536.
- (121) Reemtsma, T. *J. Chromatogr. A* **2009**, *1216* (18), 3687–3701.
- (122) Stenson, A. C.; Landing, W. M.; Marshall, A. G.; Cooper, W. T. *Anal. Chem.* **2002**, *74* (17), 4397–4409.
- (123) Wu, Z.; Rodgers, R. P.; Marshall, A. G. *Anal. Chem.* **2004**, *76* (9), 2511–2516.
- (124) Van Krevelen, D. W. *Fuel* **1950**, *29* (11), 269–285.
- (125) Kendrick, E. *Anal. Biochem.* **1963**, *35* (13), 2146–2154.
- (126) Hodgkins, S. B.; Tfaily, M. M.; McCalley, C. K.; Logan, T. A.; Crill, P. M.; Saleska, S. R.; Rich, V. I.; Chanton, J. P. *Proc. Natl. Acad. Sci. U. S. A.* **2014**, *111* (16), 5819–5824.
- (127) Islam, A.; Cho, Y.-J.; Ahmed, A.; Kim, S.-H. *Mass Spectrom. Lett.* **2012**, *3* (3), 63–67.
- (128) Stubbins, A.; Spencer, R. G. M.; Chen, H.; Hatcher, P. G.; Mopper, K.; Hernes, P. J.; Mwamba, V. L.; Mangangu, A. M.; Wabakanghanzi, J. N.; Six, J. *Limnol. Oceanogr.* **2010**, *55* (4), 1467–1477.
- (129) Visser, S. A. *Environ. Sci. Technol.* **1983**, *17* (7), 412–417.
- (130) Waggoner, D. C.; Chen, H.; Willoughby, A. S.; Hatcher, P. G. *Org. Geochem.* **2015**, *82*, 69–76.
- (131) Stevens, D.; Shi, Q.; Hsu, C. S. *Energy & Fuels* **2013**, *27* (1), 167–171.
- (132) Hughey, C. A.; Hendrickson, C. L.; Rodgers, R. P.; Marshall, A. G.; Qian, K. *Anal. Chem.* **2001**, *73* (19), 4676–4681.
- (133) Stenson, A. C.; Marshall, A. G.; Cooper, W. T. **2003**, *75* (6), 1275–1284.
- (134) Sleno, L. *J. Mass Spectrom.* **2012**, *47* (2), 226–236.
- (135) Myers, A. L.; Jobst, K. J.; Mabury, S. a; Reiner, E. J. *J. Mass Spectrom.* **2014**, *49* (4), 291–296.
-

VII. References

- (136) Kilgour, D. P. A.; Mackay, C. L.; Langridge-smith, P. R. R.; Connor, P. B. O. *Anal. Chem.* **2012**, *84*, 7436–7439.
- (137) Bateman, K. P.; Castro-perez, J.; Wrona, M.; Shockcor, J. P.; Yu, K.; Oballa, R.; Nicoll-griffith, D. A. *Rapid Commun. Mass Spectrom.* **2007**, *21*, 1485–1496.
- (138) Chatel, G.; Rogers, R. D. *ACS Sustain. Chem. Eng.* **2014**, *2*, 322–339.
- (139) Dier, T. K. F.; Egele, K.; Fossog, V.; Hempelmann, R.; Volmer, D. A. *Anal. Chem.* **2016**, *88*, 1328–1335.
- (140) Dier, T. K. F.; Rauber, D.; Jauch, J.; Hempelmann, R.; Volmer, D. A. *ChemistrySelect* **2017**, *2* (2), 779–786.
- (141) Dier, T. K. F.; Fleckenstein, M.; Miltz, H.; Volmer, D. A. *Anal. Bioanal. Chem.* **2017**.
- (142) Jessome, L. L.; Volmer, D. A. *LCGC North Am.* **2006**, *24* (5), 498–510.
- (143) Remane, D.; Meyer, M. R.; Wissenbach, D. K.; Maurer, H. H. *Rapid Commun. Mass Spectrom.* **2010**, *24* (24), 3567–3577.
- (144) Van Hout, M. W. J.; Niederländer, H. A. G.; De Zeeuw, R. A.; De Jong, G. J. *Rapid Commun. Mass Spectrom.* **2003**, *17* (3), 245–250.
- (145) Banoub, J. H.; Delmas, M. *J. Mass Spectrom.* **2003**, *38* (8), 900–903.
- (146) Kind, T.; Fiehn, O. *BMC Bioinformatics* **2007**, *8*, 105.
- (147) Tsugawa, H.; Kind, T.; Nakabayashi, R.; Yukihiro, D.; Tanaka, W.; Cajka, T.; Saito, K.; Fiehn, O.; Arita, M. *Anal. Chem.* **2016**, *88* (16), 7946–7958.
- (148) Vaniya, A.; Fiehn, O. *TrAC - Trends Anal. Chem.* **2015**, *69*, 52–61.
- (149) Bourbonnais, R.; Leech, D.; Paice, M. G. *Biochim. Biophys. Acta* **1998**, *1379* (3), 381–390.
- (150) Kringstad, K. P.; Lindström, K. *Environ. Sci. Technol.* **1984**, *18* (8), 236A–248A.

VIII. Curriculum Vitae

Education

- 02/2014 – 04/2017** Saarland University (UdS), Saarbrücken, Germany
PhD student at the Institute of Bioanalytical Chemistry, topic of the doctoral thesis: “*Analysis and Characterization of Electrochemically Decomposed Lignin*” under supervision of Prof. Dr. Dietrich A. Volmer from Saarland University, Saarbrücken, Germany.
- 10/2011 – 12/2013** Saarland University (UdS), Saarbrücken, Germany
Topic of the master thesis: “*Investigation of Internal Standards for Quantitative Determination of Erlotinib by Imaging Mass Spectrometry*” under supervision of Prof. Dr. Dietrich A. Volmer from Saarland University, Saarbrücken, Germany.
Degree: *Master of Science – Chemistry*. Grade: 2.0 (gut)
- 10/2007 – 09/2011** Saarland University (UdS), Saarbrücken, Germany
Topic of the bachelor thesis: „*Simple fatty acid extraction with magnetic fluids*” under supervision of Prof. Dr. Dietrich A. Volmer from Saarland University, Saarbrücken, Germany.
Degree: *Bachelor of Science – Chemistry*. Grade: 3.1 (befriedigend)
- 06/2006** *Allgemeine Hochschulreife* (equivalent to High School Diploma) received from the Marienschule in Saarbrücken, Germany

Training

- 07/2016** Advanced training course “*Quality Control in Analytical Chemistry*” organized by the Bundesanstalt für Materialforschung und – prüfung (BAM), Berlin, Germany.
- 05/2015** Advanced training course/ short course “*LC-MS Practical Maintenance and Troubleshooting*” organized by Sue Abbatiello, Tom Blau and Will Thompson, St. Louis, Missouri, USA.
- 08/2014** Advanced training course/ short course “*Fundamentals of Mass Spectrometry*” organized by Jürgen H. Gross and David Sparkman, Geneva, Switzerland

VIII. Curriculum Vitae

Practical Experience

- 02/2013 – 04/2013** *Vertiefungsarbeit* in the research group of Prof. Dr. Gerhard Wenz, Saarland University, Saarbrücken, Germany.
- 09/2012** *Vertiefungsarbeit* in the research group of Prof. Dr. Rolf W. Hartmann, Saarland University, Saarbrücken, Germany.
- 05/2011 – 07/2011** *Vertiefungsarbeit* in the research group of Prof. Dr. Dietrich A. Volmer, Saarland University, Saarbrücken, Germany.
- 09/2010 – 11/2010** Internship at the Landesamt für Umwelt- und Arbeitsschutz, Saarbrücken, Germany.

IX. Scientific Contributions

Publications

M. Wirtz, A. Grüter, P. Rebmann, T. Dier, D.A. Volmer, V. Huch, G. Jung, Two-color emissive probes for click reactions, *Chem. Commun.*, **2014**, 50, 12694-12697

F.M. Kiss, D. Schmitz, J. Zapp, T.K.F. Dier, D.A. Volmer, R. Bernhardt, Comparison of CYP106A1 and CYP106A2 from *Bacillus megaterium*-identification of a novel 11-oxidase activity, *Appl. Microbiol. Biotechnol.*, **2015**, 99: 8495

F. Kern, T.K.F. Dier, Y Khatri, K.M. Ewen, J.P. Jacquot, D.A. Volmer, R. Bernhardt, Highly efficient CYP167A1 (EpoK) dependent epothilone B formation and production of 7-ketone epothilone D as a new epothilone derivative, *Sci. Rep.*, **2015**, 5: 14881

T.K.F. Dier, K. Egele, V. Fossog, R. Hempelmann, D.A. Volmer, Enhanced mass defect filtering to simplify and classify complex mixtures of lignin degradation products, *Anal. Chem.*, **2016**, 88 (2), 1328-1335

A.M. Huynh, J. Menges, M. Vester, T. Dier, V. Huch, D.A. Volmer, G. Jung, Monofluorination and Trifluoromethylation of BODIPY Dyes for Prolonged Single-Molecule Detection, *ChemPhysChem*, **2016**, 17 (3), 433-442

T.K.F. Dier, R. Rauber, J. Jauch, R. Hempelmann, D.A. Volmer, Novel Mixed-Mode Stationary Phases for Chromatographic Separation of Complex Mixtures of Decomposed Lignin, *ChemistrySelect*, **2017**, 2, 779-786

T.K.F. Dier, M. Fleckenstein, H. Militz, D.A. Volmer, Exploring the Potential of High Resolution Mass Spectrometry for the Investigation of Lignin-Derived Phenol Substitutes in Phenolic Resin Syntheses, *Anal. Bioanal. Chem.*, **2017**, DOI: 10.1007/s00216-017-0282-1

Oral presentation

“Analyse komplexer Gemische aus der elektrochemischen Spaltung von Lignin unter Verwendung verschiedener stationärer Phasen als Trennmedium und hochauflösender Massenspektrometrie”

26th Doctoral students seminar of the Society of German Chemists‘ (GDCh) expert group for separation science, **01/2016**, Hohenroda, Germany

Poster presentations

“Detailed Analysis of Lignin Cleavage Products from Electrochemical Degradation by High Resolution Mass Spectrometry”

20th International Mass Spectrometry Conference (IMSC), **08/2014**, Geneva, Switzerland

“Higher-order mass defect filtering to simplify and classify lignin depolymerization products”

63rd Annual Conference of the American Society of Mass Spectrometry (ASMS), **06/2015**, St. Louis, Missouri, USA

“Analysis and Characterization of Electrochemically Decomposed Lignin Using Liquid Chromatography and High Resolution Mass Spectrometry”

3rd Doctoral Students Day of Faculty 8, Saarland University, **11/2015**, Saarbrücken, Germany

“Characterization of Electrochemically Decomposed Lignin Using Liquid Chromatography and High Resolution Mass Spectrometry”

49th Annual Conference of the German Society of Mass Spectrometry (DGMS), **03/2016**, Hamburg, Germany

“Characterization of Electrochemically Decomposed Lignin Using Liquid Chromatography-High Resolution Mass Spectrometry”

64th Annual Conference of the American Society of Mass Spectrometry (ASMS),
06/2016, San Antonio, Texas, USA